Hadron reaction mechanisms

1982 Rep. Prog. Phys. 45 335

(http://iopscience.iop.org/0034-4885/45/4/001)

Rep. Prog. Phys., Vol. 45, 1982. Printed in Great Britain

Hadron reaction mechanisms

P D B Collins and A D Martin

Physics Department, University of Durham, South Road, Durham DH1 3LE, UK

Abstract

The mechanisms of hadron scattering at high energies are reviewed in an introductory fashion, but from a modern standpoint in which we try to combine the ideas of the parton model and quantum chromodynamics (QCD) with Regge theory and phenomenology. After a brief introduction to QCD and the basic features of hadron scattering data, we discuss scaling and the dimensional counting rules, the parton structure of hadrons, and the parton model for large momentum transfer processes, including scaling violations. Hadronic jets and the use of parton ideas in soft scattering processes are examined, and we then turn our attention to Regge theory and its applications in exclusive and inclusive reactions, stressing the relationship to parton exchange. The mechanisms of hadron production which build up cross sections, and hence the underlying Regge singularities, and the possible overlap of Regge and scaling regions are discussed. We conclude that the key to understanding hadron reaction mechanisms seems to lie in the marriage of Regge theory with QCD.

This review was received in September 1981.

0034–4885/82/040335+92$08.00

Contents

1. Introduction

1.1. Partons

The last decade has seen the discovery of a completely new branch of physics, the physics of the constituents of 'elementary' particles, which are usually called 'partons'. These partons come in two kinds; the quarks which have spin $\frac{1}{2}\hbar$ and carry such properties as charge, isospin, strangeness, etc, and the gluons which have spin $\hbar$. Quarks and gluons interact with each other because they carry a new sort of charge called 'colour'. The elementary particles of nuclear physics with which we have been familiar for much longer, like the proton, neutron, pi meson or Λ hyperon for example, are now regarded as composite particles constructed from these quarks and gluons.

This revelation of a new layer of the sub-structure of matter is, of course, in many respects a repetition of a familiar pattern in the history of physics. The 19th century saw the establishment of atoms as the basic elementary components from which chemical compounds (molecules) are constructed. Then came the discovery of the electron and the nucleus, and in the first 30 years of this century the quantum theory of the structure of atoms was developed; as bound states of negatively charged electrons and a positive nucleus held together by electromagnetic forces due to the exchange of virtual photons. During the 1930s and 1940s the theory of atomic nuclei, as composites of varying numbers of protons and neutrons bound by the nuclear (or strong) interaction force stemming from the exchange of mesons, was explored.

However, in the 1950s and 1960s experiments involving the scattering of these supposedly elementary particles at high energies produced very large numbers of other, similar, strongly interacting particles, and physicists were forced to recognise that protons and neutrons are simply the lightest members of a very large family of particles called 'baryons'. About 90 different species of baryon have been identified to date (Particle Data Group 1980), but most are highly unstable and decay after very short times (about 10^{-23} s) which is why they are not so well known. Similarly, since the postulation by Yukawa in 1935 of the 'meson' as the carrier of the nuclear force, and discovery of the pi meson in 1947, more than 70 additional mesons have been found (Particle Data Group 1980), and there is no reason to believe that their number has been exhausted. This very large group of particles which enjoy the strong interaction, the baryons and the mesons, are called 'hadrons' (from the Greek, meaning 'large').

Already in the early 1960s the suggestion had been made that hadrons could conveniently be regarded as composites of more basic objects called quarks which carry charge, isospin and strangeness (Gell-Mann 1964, Zweig 1964). At that time many physicists regarded these quarks as little more than a convenient mathematical device with which to model the properties of hadrons, since after all free quarks were not seen. However, it was not too surprising that, when experiments to probe the structure of the proton by scattering electrons began at Stanford in the late 1960s, it was revealed that protons did indeed contain point-like constituents. These were called 'parts' or 'partons' by Feynman (1969) and are now recognised as being the quarks of the original quark model. During the 1970s colliding-beam experiments

of the type $e^+e^- \to$ hadrons have revealed the existence of further types of quarks carrying new properties such as charm and beauty (see table 1), so we now know of quite a number of different partons.

Table 1. The flavour quantum numbers of quarks and leptons. Q, S, C, B, T are charge, strangeness, charm, beauty and truth. Free quarks are not seen and the mass represents the current quark mass felt via electromagnetic or weak interactions. All quarks and leptons have antiparticles (with opposite Q, S, ...). Each kind, or flavour, of quark comes in three colours.

Quarks							Leptons		
	Mass (GeV/c^2)	Q	S	C	B	T		Mass (GeV/c^2)	Q
Down, d	0.008	$-\frac{1}{3}$	0	0	0	0	e^-	0.0005	-1
Up, u	0.004	$+\frac{2}{3}$	0	0	0	0	ν_e	0	0
Strange, s	0.15	$-\frac{1}{3}$	-1	0	0	0	μ^-	0.105	-1
Charm, c	1.2	$+\frac{2}{3}$	0	1	0	0	ν_μ	0	0
Bottom, b	4.7	$-\frac{1}{3}$	0	0	-1	0	τ^-	1.8	-1
Top, t?	?	$+\frac{2}{3}$	0	0	0	1	ν_τ	0	0

This probing of the constitution of matter has been made possible by the development of accelerators of increased energy. A particle beam of momentum p has an associated wavelength $\lambda = h/p$ which, according to Heisenberg's uncertainty principle, determines the best spatial resolution which that beam can provide. For numerical estimates it is useful to recall that $\hbar c \equiv hc/2\pi \approx 2 \times 10^{-7}$ eV m = 0.2 GeV fm. Thus, to determine the electron distribution in an atom we are concerned with distances of the order of 1 Å = 10^{-10} m and hence need electron beams with energies about 10^3 eV, while to probe the charge distribution of a nucleus at distances of a few fm needs 0.1 GeV electrons, but to observe the parton structure of a proton at distances very much less than 1 fm requires electrons with at least 10 GeV energy.

Electron scattering experiments, and more recently muon scattering too, probe the charge structure of hadronic matter. Complementary information is obtained with neutrino beams which couple to matter via the weak interaction only, and hence probe its weak structure, while the scattering of hadrons by hadrons enables us to explore the strong interaction structure. The parton concept helps us to understand all three types of experiment. Our intention in this review is to try and illustrate how the parton sub-structure of hadrons determines the results of such experiments, but first we must introduce the various types of particles with which we shall be dealing, and the interactions which they undergo.

1.2. Leptons and quarks

Apart from gravity, which we shall not need to consider in this review, particles undergo three seemingly quite different types of interaction; the electromagnetic interaction of charged particles, the short-range weak interaction which is responsible for the β decays of nuclei for example, and the strong or hadronic force which, *inter alia*, binds nucleons into nuclei.

There is one group of particles, spin $\frac{1}{2}\hbar (\equiv \text{spin } \frac{1}{2})$ fermions called leptons, which do not experience the hadronic force but only electromagnetism and the weak interac-

tion (see table 1). The best known of these is the electron, e^-, and with it are associated its antiparticle the positron, e^+, and the electron's neutrino and antineutrino, ν_e, $\bar{\nu}_e$, which are produced along with the electron (or positron) in β decay (for example, $n \to p + e^- + \bar{\nu}_e$). A second family of leptons consists of the muon, μ^-, together with μ^+, ν_μ, $\bar{\nu}_\mu$ (ν_μ being a different kind of neutrino). The μ appears to be identical to e in most respects except that it is about 200 times heavier, and is unstable, decaying by $\mu^- \to e^- + \bar{\nu}_e + \nu_\mu$, with a lifetime $\approx 10^{-6}$ s. More recently the τ lepton family has been discovered (Perl *et al* 1975) in the experiment $e^+e^- \to \tau^+\tau^-$ and although the existence of its neutrino ν_τ is not quite firmly established the expected decays $\tau^- \to e^- + \bar{\nu}_e + \nu_\tau$ and $\tau^- \to \mu^- + \bar{\nu}_\mu + \nu_\tau$ do seem to occur (as well as $\tau^- \to$ hadrons $+ \nu_\tau$). No further charged leptons are known, up to a mass of 17 GeV/c^2 at least (Cords 1980).

All these leptons seem to be structureless points, i.e. they have no apparent size. This is deduced from scattering experiments such as $e^+e^- \to e^+e^-$ and $e^+e^- \to \mu^+\mu^-$ which attempt to probe their structure, but reveal none down to about 10^{-2} fm (Bohm 1980), but a more precise (if theoretically controversial) limit on the size of charged leptons ($<10^{-6}$ fm) can be deduced from the fact that their anomalous magnetic moments $(g-2)$ are in accord with the predictions of quantum electrodynamics (QED), to a few parts in 10^{-10} for the electron (Brodsky and Drell 1980). If the charge distribution occupied a finite volume this would obviously change the gyromagnetic ratio g from the Dirac value of 2. We thus regard the leptons as elementary (so far (!), but see Harari (1980) for a discussion of possibilities for composite leptons).

Hadrons, such as the proton, are not elementary however. The proton's gyromagnetic ratio is 5.56, not 2, indicating that its charge is distributed over a finite volume ($\simeq 1$ fm^3). This is because a proton is made up of more fundamental charged constituents, the quarks (see, for example, Close (1979) for a review of quark models).

Quarks are also spin-$\frac{1}{2}$ fermions with fractional electric charges, as shown in table 1, and are also point-like to the accuracy of present electron-scattering data (see § 3). In addition to the weak and electromagnetic interactions, quarks experience the strong colour force which, it is believed, is so strong as to confine them within hadrons. This is presumably why free quarks have not been found (see the next section). Certainly quarks cannot be knocked out of hadrons by any of the high-energy beams available at present, and the only positive evidence for free quarks is extremely controversial. Despite this the quarks are easily 'seen' in deep inelastic e, μ and ν scattering experiments on protons. But since the quarks cannot be taken out and weighed the evidence for their masses quoted in table 1 is somewhat indirect (see Weinberg 1977).

The quark composition of some of the lighter mesons ($q\bar{q}$) and baryons (qqq) is indicated in table 2. This (constituent) quark model has been remarkably successful in hadron spectroscopy (see, for example, Hey and Morgan 1978, Close 1979). Multiplets of the predicted spins and parities are found, and many members of the multiplets clearly identified. No states outside the quark model predictions, or multiquark states containing more than the minimal number of quarks (such as $qqqq\bar{q}$), have been established experimentally. The quarks shown in table 2 are the so-called 'valence' quarks which are needed to carry the quantum numbers (charge, strangeness, charm, etc) which are often referred to as 'flavours'.

There is one feature of table 2 which used to seem particularly puzzling. It will be noted that the Δ^{++}, for example, consists of three u quarks, all with their spins parallel to make a spin-$\frac{3}{2}$ state, with no orbital angular momentum. But quarks are fermions, and by the exclusion principle it should not be possible to have three identical quarks in the same state. (Compare the Li atom ground state where the two 1s

Table 2. The quark content of the lighter meson and baryon multiplets. The particle masses are listed in GeV/c^2. The hadrons made of n types (flavours) of quarks can be grouped into multiplets of SU(n). For the mesons ($q\bar{q}$) we show the members of the $15+1$ dimensional multiplets of SU(4) of spin, parity $J^P = 0^-, 1^-, 2^+$; while for the baryons (qqq) we just show the $\frac{1}{2}^+$ octet and $\frac{3}{2}^+$ decuplet of SU(3), although some charmed baryons have been identified. For u, d, s composites this is the famous SU(3) symmetry of Gell-Mann (1961) and Ne'eman (1961). The mass spread within a multiplet is indicative of symmetry breaking.

(a) Meson multiplets

	0^-	Mass	1^-	Mass	2^+	Mass
$u\bar{d}$, $d\bar{u}$	$\pi^{\pm}$	140	$\rho^{\pm}$	770	$A_2^{\pm}$	1317
$(u\bar{u}-d\bar{d})/\sqrt{2}$	π^0	135	ρ^0		A_2^0	
$u\bar{s}$, $s\bar{u}$	$K^{\pm}$	494	$K^{*\pm}$	892	$K^{*\pm}$	1434
$d\bar{s}$, $s\bar{d}$	K^0, $\bar{K}^0$	498	K^{*0}, $\bar{K}^{*0}$	898	K^{*0}, $\bar{K}^{*0}$	
$(u\bar{u}+d\bar{d})/\sqrt{2}$	η	549	ω	782	f	1273
$s\bar{s}$	η'	958	φ	1020	f'	1516
$c\bar{d}$, $d\bar{c}$	$D^{\pm}$	1868	$D^{*\pm}$	2009	$D^{*\pm}$	?
$c\bar{u}$, $u\bar{c}$	D^0, $\bar{D}^0$	1863	D^{*0}, $\bar{D}^{*0}$	2006	D^{*0}, $\bar{D}^{*0}$	?
$c\bar{s}$, $s\bar{c}$	$F^{\pm}$	2030	$F^{*\pm}$	2140	$F^{*\pm}$	?
$c\bar{c}$	η_c	2980	ψ	3097	χ	3551

(b) Baryon multiplets

	$\frac{1}{2}^+$	Mass	$\frac{3}{2}^+$	Mass
uuu, ddd			Δ^{++}, Δ^-	1232
uud, udd	p, n	939	Δ^+, Δ^0	
uus, uds, dds	$\Sigma^{+,0,-}$	1195	$\Sigma^{*+,0,-}$	1385
uds	Λ	1116		
uss, dss	Ξ^0, Ξ^-	1318	Ξ^{*0}, Ξ^{*-}	1533
sss			Ω^-	1672

electrons have opposite spin orientations while the third has $l = 1$ giving an overall $L = 1$, $S = \frac{1}{2}$ state.) The now generally accepted explanation for this apparent anomaly is that quarks possess an additional property, called 'colour', which can take three possible values, say red, green and blue (see, for example, Greenberg and Nelson 1977).

The hadrons are postulated to be colourless (white), i.e. they contain equal mixtures of red (R), green (G) and blue (B) quarks. Thus the Δ^{++} state is $u^R u^G u^B$ and so no longer contains identical fermions. More generally we write for a meson with the valence quark structure $q_1\bar{q}_2$ (table 2)

$$M = \frac{1}{\sqrt{3}}(q_1^R\bar{q}_2^R + q_1^B\bar{q}_2^B + q_1^G\bar{q}_2^G) \tag{1.1}$$

while a $q_1q_2q_3$ baryon becomes

$$B = \frac{1}{\sqrt{6}}\epsilon_{\alpha\beta\gamma}q_1^\alpha q_2^\beta q_3^\gamma \qquad \text{with } \alpha, \beta, \gamma = \text{R, G, B} \tag{1.2}$$

(where $\epsilon_{\alpha\beta\gamma}$ is the antisymmetric permutation tensor) ensuring overall antisymmetry.

The quarks are regarded as the fundamental triplets of an $SU(3)_C$ colour gauge symmetry group (Abers and Lee 1973, Politzer 1974, Iliopoulos 1976). There is now

abundant evidence for the existence of the three colour degrees of freedom for each flavour of quark, so the quarks appearing in tables 1 and 2 should really have colour labels R, G, B appended as above. The leptons, on the other hand, are colourless and hence not bound into hadrons.

It will be noted that we have associated quarks and leptons together to form different 'generations' in table 1. An extensive discussion of the justification for this will be found in Harari (1978). Quite apart from the obvious similarity of quarks and leptons, as point-like fermions having electromagnetic and weak interactions (though only the former participate in the strong interaction), there are theoretical reasons for believing that in order to ensure that a proper renormalisable field theory can be constructed the sum of the charges of all the fundamental fermions must vanish. It will be seen from table 1 that

$$Q_e + Q_\nu + 3(Q_u + Q_d) = 0 \tag{1.3}$$

(the factor of 3 stemming from the three colours of quarks) so the relation is satisfied by each generation of fermions separately.

1.3. The strong interaction

The most familiar type of force experienced by these particles is the electromagnetic interaction, which is due to the exchange of massless vector (i.e. spin 1) virtual photons (the quanta of the electromagnetic field) between charged particles (Bjorken and Drell 1964). The lowest-order diagram of QED involves the exchange of a single photon between an electron and a positron, as shown in figure 1(*a*). It gives rise to the Coulomb interaction potential

$$V(r) = -\alpha/r \tag{1.4}$$

where $\alpha \equiv e^2/4\pi\hbar c \simeq 1/137$ is the fine-structure constant. Higher-order contributions such as figure 1(*b*) involve more couplings and hence are smaller by further powers

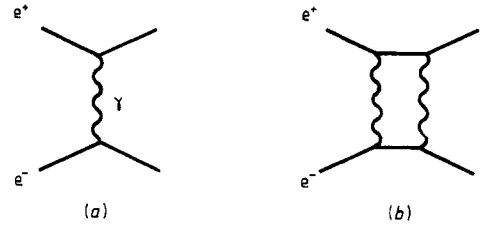

Figure 1. O(α) and O(α^2) photon exchange contributions to the e^+e^- QED interaction.

of α, and so can often be neglected. However, it is a very important matter of principle that the physical coupling increases with $Q^2 \equiv -q^2 > 0$ where q is the four-momentum of the virtual photon. This is due to vacuum polarisation effects that shield the bare charge. Including these diagrams, figure 2, gives the leading behaviour

$$\alpha(Q^2) \simeq \alpha\left[1 + \frac{\alpha}{3\pi}\log\left(\frac{Q^2}{\mu^2}\right) + \left(\frac{\alpha}{3\pi}\log\left(\frac{Q^2}{\mu^2}\right)\right)^2 + \ldots\right] \tag{1.5}$$

where μ is the arbitrary normalisation point at which α has been measured. In higher orders a whole series of $[\log(Q^2/\mu^2)]^n$ terms appears (for a simple account see Close

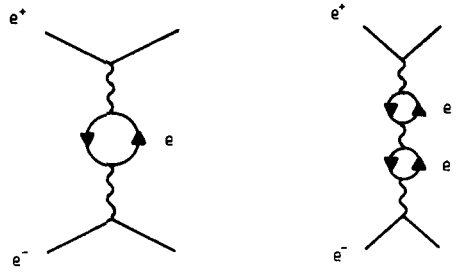

Figure 2. Vacuum polarisation corrections to the electric charge, see figure 1(*a*).

1982). These leading logs may be summed with the result

$$\alpha(Q^2) \simeq \frac{\alpha(\mu^2)}{1-[\alpha(\mu^2)/3\pi]\log(Q^2/\mu^2)} \tag{1.6}$$

for $Q^2 \gg \mu^2$. We thus have a 'running' coupling constant, not really constant at all, which changes (runs) with Q^2. As Q^2 increases the photon sees more and more of the bare charge, and at some very large, but finite, Q^2 the coupling $\alpha(Q^2)$ is infinite. The bare charge is thus ultraviolet-divergent, but this does not usually worry us since we expect that quantum gravity effects will have modified the theory long before such very large Q^2 (very short distances) are reached. In the infrared region of experimental QED the Q^2 dependence of α is essentially undetectable; a 10% effect requires a Q^2 range of $\exp(0.3\pi/\alpha) \simeq 10^{56}$. For all practically attainable Q^2, $\alpha \simeq (137)^{-1}$ and we can expect perturbation theory to be satisfactory.

The strong interaction is the result of the exchange of coloured massless vector gluons between coloured quarks (see Marciano and Pagels 1978). We noted in § 1.2 that three colours of quark are necessary (R, G, B) and that these are regarded as the fundamental triplet of an $SU(3)_C$ coloured gauge symmetry group. The emission of a gluon can change the colour of a quark and so there appears to be nine possible colours of gluons ($R\bar{R}, R\bar{G}, R\bar{B}, G\bar{G}, G\bar{R}, G\bar{B}, B\bar{B}, B\bar{R}, B\bar{G}$). However, the combination $(1/\sqrt{3})(R\bar{R}+B\bar{B}+G\bar{G})$ is colourless and so does not couple to the quarks (and hence if it existed would not be detectable). We thus have an octet of vector gluons in the adjoint representation of the $SU(3)_C$ group. The quark–gluon vertex coupling (figure 3(*b*)) may then be expressed as $\frac{1}{2}g_s\lambda^{\alpha}_{ij}$ where g_s is the strong coupling (analogous to the charge e of QED) and the λ^{α}_{ij} are Gell-Mann's SU(3) representation matrices.

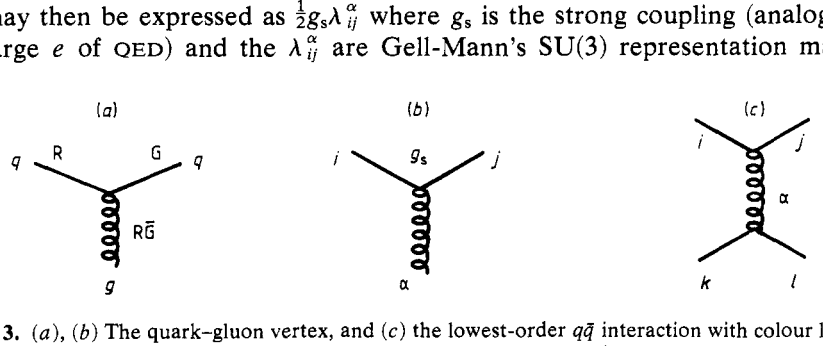

Figure 3. (*a*), (*b*) The quark–gluon vertex, and (*c*) the lowest-order $q\bar{q}$ interaction with colour labels.

There are eight of them, with $\alpha = 1, \ldots, 8$ for the gluon colours, while $i, j = 1, 2, 3$ for the quark colours.

Superficially this quantum chromodynamics (QCD) description of the strong interaction, with massless vector bosons exchanged between fermions, seems very similar to

QED in that the lowest-order diagram, figure 3(*c*), involving a single gluon exchanged between a quark and an antiquark gives

$$V_{ijkl}(r) = -\sum_{\alpha=1}^{8} \tfrac{1}{4}\lambda_{ij}^{\alpha}\lambda_{lk}^{\alpha}(\alpha_s/r) \tag{1.7}$$

where $\alpha_s \equiv g_s^2/4\pi$. For colourless initial and final states (when the q and $\bar{q}$ form a meson, for example), since

$$\sum_{\alpha} \lambda_{ij}^{\alpha}\lambda_{ji}^{\alpha} = 16/3 \tag{1.8}$$

we find

$$V(r) = -\tfrac{4}{3}(\alpha_s/r) \tag{1.9}$$

just like (1.4) except for the colour factor $\frac{4}{3}$. However, the effect of higher-order diagrams like figure 4 gives

$$\alpha_s(Q^2) \simeq \alpha_s\left\{1 - \frac{\alpha_s b_0}{4\pi}\log\left(\frac{Q^2}{\mu^2}\right) + \left[\frac{\alpha_s b_0}{4\pi}\log\left(\frac{Q^2}{\mu^2}\right)\right]^2 + \ldots\right\} \tag{1.10}$$

$$\simeq \frac{\alpha_s}{1 + (\alpha_s b_0/4\pi)\log(Q^2/\mu^2)} \equiv \frac{1}{(b_0/4\pi)\log(Q^2/\Lambda^2)}$$

$$\Lambda^2 \equiv \mu^2 \exp(-4\pi/\alpha_s b_0) \tag{1.11}$$

where μ^2 is the value of Q^2 at which α_s is measured, and $b_0 \equiv \frac{11}{3}N_c - \frac{2}{3}N_f$ where N_c is the number of colours ($=3$) and N_f is the number of flavours of quark ($=6$ in table 1). The N_c term stems from the gluon loop (figure 4(*b*)) which arises because gluons carry colour and hence couple to each other. There is no similar diagram in QED (figure 2) because photons do not carry the charge coupling. The N_f term arises from the quark loop (figure 4(*a*)) and is just the same as figure 2 of QED except that, of course, we must sum over all the flavours of quarks which can contribute.

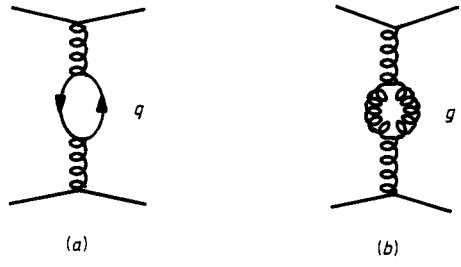

Figure 4. The lowest-order corrections to the quark–gluon coupling.

Thus, with $N_c = 3$ and $N_f = 6$ we have $b_0 = 7$, and as long as $N_f < 16$, we always find $b_0 > 0$ so that the sign in the denominator of (1.11) is opposite to that in (1.6). This has the important consequence that $\alpha_s(Q^2) \to 0$ as $Q^2 \to \infty$ which means that quarks and gluons appear like almost-free particles when looked at with very high-energy probes, which are sensitive to the short-distance structure of the hadron. This 'asymptotic freedom' (Politzer 1973, Gross and Wilczek 1973) will be an essential ingredient of the parton approach to the structure of hadrons which we shall explore in this review.

The other important consequence of (1.11) is that $\alpha_s(Q^2) \to \infty$ as $Q^2 \to \Lambda^2$ (which serves to define Λ) and so the perturbation series breaks down at small Q^2. Taking the Fourier transform of (1.11) we obtain

$$\alpha_s(r) = \frac{1}{(b_0/2\pi)\log(1/\Lambda r)} \tag{1.12}$$

and so the coupling becomes stronger as the separation between the q and $\bar{q}$ increases, and the perturbation series breaks down as $r \to \Lambda^{-1}$. This is because of the gluon self-coupling, which implies that the exchanged gluons will attract each other (unlike photons) and so the colour lines of force are constrained to a tube-like region between the quarks (unlike the Coulomb field in which the lines of force just spread out) (see figure 5). If these tubes have a constant energy density per unit length then the potential energy of the interaction will increase with the separation, $V(r) \sim \lambda r$, and so the quarks (and gluons) can never escape from the hadron. This so-called 'infrared slavery' is believed to be the origin of the confinement mechanism and explains why we do not observe free quarks (Mandelstam 1980, Dokshitzer *et al* 1980). They have very little chance of straying outside the confinement range $\sim \hbar c/\Lambda$. So the fact that hadrons have a size ~ 1 fm suggests that $\Lambda \simeq 0.2$ GeV.

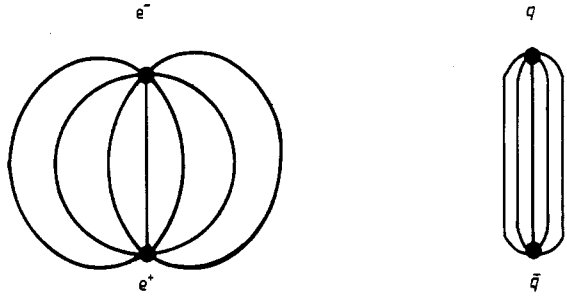

Figure 5. The e^+e^- Coulomb field with potential $V(r) \sim 1/r$, and the $q\bar{q}$ colour field with $V(r) \sim r$.

Unfortunately, practical calculations in field theory generally invoke perturbation methods which are clearly not applicable to the bound-state problem of QCD with $\alpha_s \gtrsim 1$, and so far it has not proved possible to demonstrate conclusively that confinement is a consequence of QCD. However, most physicists are now fairly confident that this is the right approach, partly because of the remarkable success of essentially non-relativistic models of hadrons based on these ideas.

Thus one might guess that the effective interaction potential between q and $\bar{q}$ in a meson could be approximated by a combination of a short-range asymptotic freedom contribution due to single-gluon exchange and a long-range confining potential which increases with r, such as

$$V(r) = -\tfrac{4}{3}\frac{\alpha_s}{r} + \lambda r. \tag{1.13}$$

This sort of potential, substituted into the Schrödinger equation, gives a very good account of the spectrum of mesons made of heavy quarks such as $\psi(c\bar{c})$ and its excited (charmonium) states, and of the $\Upsilon(b\bar{b})$ spectrum (Quigg and Rosner 1979, Isgur and Karl 1979, Eichten *et al* 1980). Indeed, if the usual non-relativistic reduction of the one-gluon exchange term is used to generate hyperfine spin–spin and spin–orbit interactions, just like the Fermi–Breit Hamiltonian of atomic physics but with 'colour

magnetic moments', many detailed features of both the meson and baryon spectrum can be explained with very few arbitrary parameters. The only unknowns are the quark masses and the couplings α_s, λ. We can thus take quite seriously the idea that hadrons are made of quarks bound together by a confining potential due to the exchange of gluons.

But this sort of approach only has theoretical plausibility for states which are made of heavy quarks like c and b, so that the binding energy is very small compared to the quark mass, and hence the internal motions are not too relativistic ($v/c \ll 1$). For particles which are composed entirely of u, d and s quarks, whose masses are $\leqslant \Lambda$, the QCD scale, the coupling α_s is $\geqslant 1$ and so the probability of creating additional virtual gluons and $q\bar{q}$ pairs within the hadron becomes very great. In these circumstances it seems better to regard the hadron as made up of three classes of constituent (Feynman 1972, Llewellyn-Smith 1972, Kogut and Susskind 1974):

(i) the 'valence' quarks q_v which carry its quantum numbers such as charge, strangeness, etc (for example, the proton consists of $u_v u_v d_v$ valence quarks according to table 2);

(ii) a 'sea' of virtual gluons, the quanta of the colour force field which are exchanged between the quarks, and between the gluons themselves;

(iii) a 'sea' of quarks and antiquarks, i.e. virtual $q_s\bar{q}_s$ pairs created by vacuum polarisation of the colour field as in figure 4.

Whereas the number of valence quarks is fixed by the quantum numbers of the particle, the number of virtual sea quarks and gluons is unlimited and rapidly fluctuating. As the gluons are massless there is no inhibition to the creation of large numbers of low-energy gluons and so the probability of finding such gluons can be expected to diverge as their energy tends to zero (the infrared divergence). One also expects large numbers of u and d sea quarks because they are very light compared to Λ (see table 1) but fewer s quarks, while the number of heavy c or b quarks is presumably quite small because of the high-energy 'cost' of creating them (virtually). More accurately, the uncertainty principle requires that a virtual state of mass M can exist only for times Δt such that $\Delta t < \hbar/Mc^2$ so high-mass $q\bar{q}$ pairs can only be present for a very small fraction of the time.

It is this essentially many-body nature of all relativistic bound-state systems which renders the perturbation methods of quantum field theory impotent. It might therefore seem that there is no hope of gaining any understanding of such complex structures, but fortunately this is not so. We can, in fact, obtain a good deal of experimental information about the structure of hadrons by probing them in various types of scattering experiment, and many features of the results can be explained through the parton model.

1.4. Deep inelastic scattering

Even though confinement prevents us from taking a quark out of a hadron for detailed examination, it is still possible to 'see' quarks, for example in lepton scattering experiments (Gilman 1972, Feynman 1972). The situation is perhaps somewhat analogous to the model 'ship in a bottle' which sailors used to make. One can readily see the ship because of the light it scatters, but one cannot get it out. If one wants to obtain a really detailed description of the ship one may need to make allowance for the refractive properties of the glass bottle which distorts its image—i.e. one needs to have an understanding of the confining mechanism.

One way of seeing the quarks in a hadron is by electron-scattering experiments. Electrons have been used for many years to probe the structures of atoms. As noted in § 1.1 one needs electrons of a few keV energy to resolve to better than 1 Å. A typical result is shown in figure 6(*a*) which gives the cross section as a function of the energy of the electron after scattering. There is a large elastic peak in which the electron has been scattered by the nucleus (with negligible loss of energy because the nucleus is so much heavier and barely recoils) and then a smaller 'quasi-elastic' peak in which the electron has hit one of the electrons in the atom, and lost on average half its energy in the process. However, because the atomic electron is confined to move in orbit round the nucleus, this peak has a width determined by the dispersion of the momentum of the bound electron, and hence, through the uncertainty principle, by the size of the atom.

To discover the structure of the nucleus one needs to scatter electrons having energies of a few hundred MeV, to give a resolution of the order of a fermi; see figure 6(*b*). There is an elastic peak due to scattering off the nucleus as a whole, and a quasi-elastic peak, in which the electron has been scattered by an individual proton, whose width indicates the dispersion of the proton's Fermi momentum.

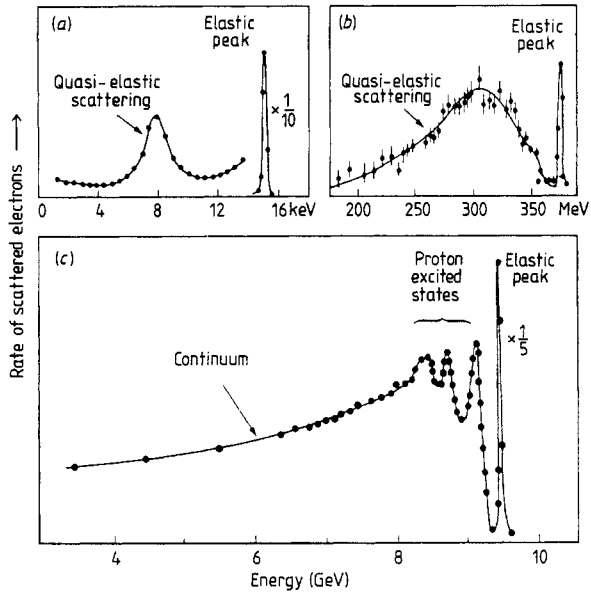

Figure 6. Electron scattering data, in different energy regimes, compiled by Amaldi (1979). (*a*) $e^- +$ carbon, $E = 15$ keV, $\theta = 45°$; (*b*) $e^- +$ helium, $E = 400$ MeV, $\theta = 60°$; (*c*) $e^- +$ proton, $E = 10$ GeV, $\theta = 10°$, showing the energy of the scattered electron.

Similarly one can probe the structure of an individual proton by scattering electrons of a few GeV energy. Again there is an elastic peak in which the proton recoils as a whole, some subsidiary peaks due to the excitation of the proton to various higher-mass N* resonant states, and then a continuum distribution of those electrons which have been scattered by the constituents of the proton, i.e. the quarks. This is the so-called 'deep inelastic scattering' (DIS). As we shall see in § 3 the size of this continuum cross section, and its variation with energy, scattering angle, etc, is just what one would expect if the scattering were due to free, point-like, spin-$\frac{1}{2}$, charged particles. The

quarks appear to be free (i.e. there is rather little effect of the strong force which binds the quarks into the hadron) because we are using a large momentum probe, and $\alpha_s(Q^2) \to 0$ as $Q^2 \to \infty$. The success of the parton model depends crucially on this asymptotic freedom.

Similar experiments can be carried out using neutrino beams (Llewellyn-Smith 1972) instead of electrons, probing the weak interaction structure rather than the charge distribution, and entirely consistent results are obtained (see § 4). The gluons have no electromagnetic or weak interaction and so are not seen directly in these DIS experiments, but their properties can be inferred indirectly, as we shall see.

But what happens to the quarks after they have been struck hard by the electron or neutrino? In the corresponding atomic (or nuclear) scattering experiments the constituent electrons (or protons) are knocked out of the composite system and so can be detected as free particles in the final state. However, we do not obtain free quarks as a result of DIS. The reason for this is, of course, confinement, which we believe operates something like figure 7 (Bjorken 1973, Dokshitzer *et al* 1980).

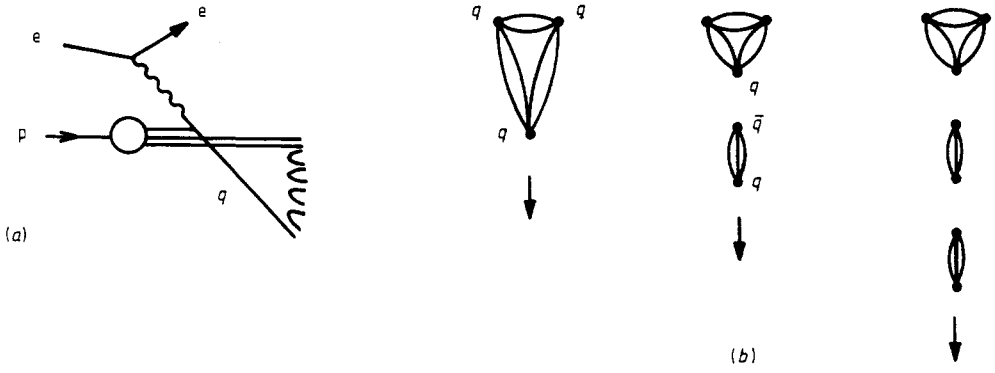

Figure 7. Deep inelastic electron–proton scattering. Diagram (*b*) shows, at successive time intervals, the struck quark leaving the proton. The hadronisation, or creation of $q\bar{q}$ pairs, which is sketched in diagram (*a*) in the form of a chain, neutralises the colour in the final state.

The struck quark in figure 7(*a*) attempts to leave the proton, but in so doing it stretches the colour lines of force into a tube (cf figure 5) until the potential energy of the colour field is sufficient to create a $q\bar{q}$ pair. These can act as the end points for the lines of force, which thus break into two shorter tubes with lower net energy (despite the extra $q\bar{q}$ mass) than the single extended tube (figure 7(*b*)). The outgoing quark continues on its way, stretching the lines of force, and further $q\bar{q}$ pairs are produced, until eventually all its kinetic energy has been degraded into clusters of quarks and gluons, each of which has zero net colour and low internal momentum. These clusters can (indeed must) form hadrons since now $\alpha_s(Q^2) \gtrsim 1$, and so the energy given to the struck quark finally manifests itself as a 'jet' of hadrons travelling more or less in the direction of that quark (Konishi *et al* 1979). The quark thus escapes from its parent hadron, but only into another, newly created, faster moving hadron. The price of asymptotic freedom is infrared slavery!

Hence DIS is followed by a process of 'hadronisation' in which the energy lost by the electron during the scattering process is converted, via colour polarisation of the vacuum, into new hadrons. We shall be examining these jet phenomena in more detail in § 5.

1.5. Exchange forces

We have seen that fundamentally the strong interaction seems very similar to QED in that the basic interaction, massless vector gluon exchange between coloured quarks, is very like massless vector photon exchange between charged electrons. The crucial difference is that gluons carry colour and hence couple to each other, whereas photons do not carry charge. This means that the strong coupling constant 'runs' in the opposite direction to the electromagnetic coupling, and becomes very large at low momenta, ensuring that the coloured quarks and gluons are confined within colourless hadrons. Any attempt to knock them out simply produces more hadrons.

The strong interaction which we observe most directly, therefore, is not that between the quarks themselves, but between the composite hadrons. The nuclear force which binds protons and neutrons into nuclei, for example, is the residual colour polarisation force between these colourless hadrons. This is analogous to molecular binding forces, which can be regarded as the residual electromagnetic polarisation effects between neutral composite atoms. Its principal manifestation is an exchange force, involving the exchange of electrons between the atoms. Similarly the nuclear force involves the exchange of coloured quarks and gluons between the hadrons.

By the uncertainty principle the range of an exchanged particle of mass m is given by $r = \hbar/mc$ and so the longest-range part of the p–n force is provided by the exchange of the lightest colourless composite object which can be made up from quarks and gluons. From table 2 we see that this is the pion. This is just what Yukawa suggested in 1935, except that we now regard it as the exchange of a $q_v\bar{q}_v$ valence pair with attendant sea quarks and gluons (figure 8(a)), not of an elementary particle.

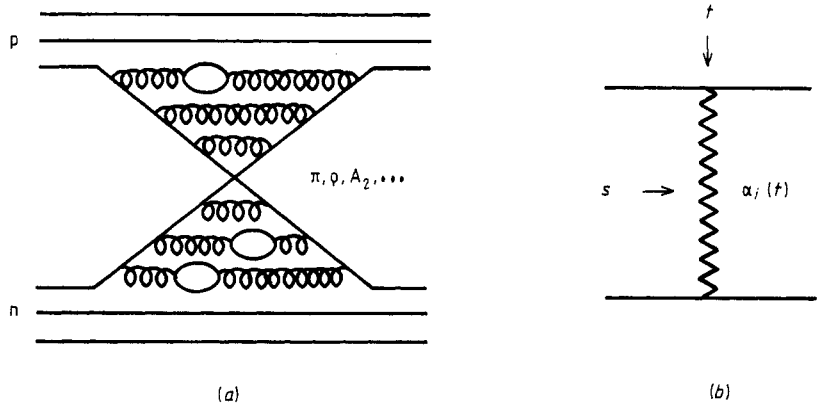

Figure 8. Proton–neutron scattering at small angles, illustrating (a) the complicated parton exchange structure and (b) the equivalent, but more useful, Regge trajectory exchange, $\alpha_i(t)$ with $i = \pi, \rho, A_2 \ldots$.

But of course the $q\bar{q}$ pair need not be in a pion, but in any of the other more massive meson states which can be made with these quarks (see table 2) such as the ρ or A_2. These heavier states provide shorter-range forces of course. This partly explains why the short-range part of the nuclear force is so complicated—there are so many massive mesons which can be exchanged. In fact, if we are interested in high-energy hadron scattering we are forced to take into account the exchange of all these particles together. A way of doing this was discovered (in a quite different context) by Regge in 1959 (see Collins 1977).

If one regards the mesons as $q\bar{q}$ bound states produced by an effective gluon exchange potential $V(r)$ like (1.13) (see figure 5), then the radial Schrödinger equation contains the effective potential

$$V_{\text{eff}}(r) = V(r) + l(l+1)/r^2 \tag{1.14}$$

where the second term on the right-hand side is the repulsive centrifugal barrier term, which increases with the orbital angular momentum l, and represents the fact that it is harder to bind high l states because of the centrifugal repulsion. This is why high l states are generally heavier than low l ones. In fact, one can solve Schrödinger's equation (or for a more relativistic problem the Bethe–Salpeter equation) for arbitrary values of l, and the mass eigenvalue, m, varies continuously along a trajectory in the l plane. m increases with l, connecting the various physically meaningful solutions which exist for $l = n\hbar$ (n integer ≥ 0). So we anticipate that hadrons will lie on so-called 'Regge trajectories' $l = \alpha(m^2)$ such that if m_i is the mass of meson i, and S_i is its spin, then $S_i = \alpha(m_i^2)$ with $S_i = 0, \hbar, 2\hbar, \ldots$. An example of such a trajectory connecting some of the lighter meson states is shown in figure 9.

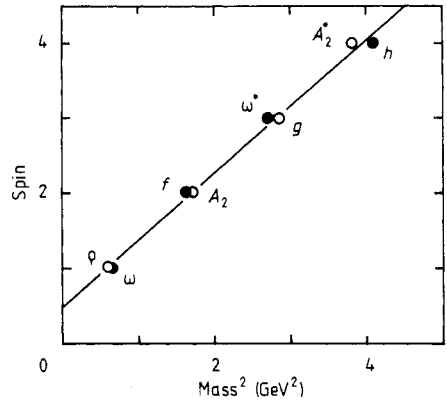

Figure 9. Chew–Frautschi plot of (approximately exchange-degenerate) meson Regge trajectories. ○, $I = 1$; ●, $I = 0$.

As we shall find in § 7, Regge theory also predicts that the high-energy behaviour of a hadron scattering amplitude at small angles will take the form $A(s,t) \sim s^{\alpha(t)}$ (where s is the square of the centre-of-mass energy, and $-t$ is the square of the momentum transferred) if $\alpha(t)$ is the trajectory of the particles which can be exchanged (figure 8(b)). This is the modern generalisation of Yukawa's meson exchange hypothesis, and is very successful in explaining hadron scattering cross sections. Regge theory thus incorporates many of the most complicated confinement aspects of QCD and hence is an essential tool of particle physics. Its relation to parton ideas will be explained in §§ 7–9.

1.6. Outline of the review

Our aim is to give a fairly elementary review of hadron reaction mechanisms from a modern viewpoint, incorporating the ideas invoked in this introduction.

In the next section we review briefly the main features of hadron scattering data which we want to try and understand. Then in § 3 we examine in more detail processes

in which hadrons are produced with a large transverse momentum (p_T) in which the effects of the point-like quark and gluon interactions are seen rather directly. Section 4 is concerned with the corrections which are necessary to make the simple parton picture more compatible with QCD and confinement, while in § 5 we look at the jets of hadrons which occur in such processes. In § 6 we explore the application of parton ideas to low p_T hadron scattering, while in the following section we show how the successes of Regge theory may be incorporated into the picture. This theory is used to explore inclusive hadron production and diffractive scattering in §§ 8 and 9, respectively, and we attempt to bring out the relation between the older Regge theory and the newer parton model approach. We conclude with a summary in § 10.

Because we are trying to cover a very large field of physics our discussion is necessarily somewhat superficial, but this seems appropriate for an introductory survey aimed at readers who are not particularly familiar with the recent developments in particle physics. We have made no attempt to give credit for particular discoveries, but have concentrated on providing useful references, mainly to review articles, which not only contain much more detailed accounts of the individual topics, but also references to the original literature.

2. High-energy hadron scattering

Most of our information about the structure and properties of hadrons and their constituent partons is based on the analysis of high-energy scattering data. Lepton–hadron scattering is used to probe the weak and electromagnetic structure of hadrons, while hadron–hadron collisions tell us about the more complicated strong interaction properties. In this section we want to review, very briefly, the basic features of hadron scattering experiments. Readers requiring more detailed information might look at, for example, Barger (1974), Irving and Worden (1977), Rushbrooke and Webber (1978), Giacomelli and Jacob (1980), Darriulat (1980), Ganguli and Roy (1980) and McCubbin (1981).

2.1. Hadron scattering data

Hadron scattering experiments are performed in two main types of facilities. There are fixed-target experiments in which high-energy beams of hadrons—usually consisting of p, $\bar{\text{p}}$, $\pi^{\pm}$ or $\text{K}^{\pm}$ but also, less commonly, n, K^0, Σ or Λ—strike particles in a fixed material target (usually protons). If we call the beam particle A, while B is the target particle, their four-momenta will be (setting $c \equiv 1$)

$$P_{\text{A}_\text{L}} = (E_\text{L}, \boldsymbol{p}_\text{L}) \qquad p_{\text{B}_\text{L}} = (m_\text{B}, \mathbf{0})$$

where E_L and $\boldsymbol{p}_\text{L}$ are the laboratory-frame energy and momentum of A and where B, which is at rest, has mass m_B. As a Lorentz-invariant measure of the energy available in the scattering process we introduce

$$s \equiv (p_\text{A} + p_\text{B})^2 = (E_\text{L} + m_\text{B}, \boldsymbol{p}_\text{L})^2 = m_\text{A}^2 + m_\text{B}^2 + 2m_\text{B}E_\text{L} \tag{2.1}$$

where in the last step we have used the mass-shell relation

$$E^2 = \boldsymbol{p}^2 + m^2. \tag{2.2}$$

Also there are colliding-beam facilities in which two stored beams of stable hadrons (usually p, but sometimes $\bar{p}$, d, etc) can be made to collide head on. In this case, if A and B have equal and opposite momenta, so that their four-momenta are

$$p_A = (E_A, \boldsymbol{p}) \qquad p_B = (E_B, -\boldsymbol{p}) \tag{2.3}$$

then the invariant

$$s = (E_A + E_B, \boldsymbol{p} - \boldsymbol{p})^2 = (E_A + E_B)^2 \tag{2.4}$$

is just the square of the total centre-of-mass energy. A comparison of (2.1) and (2.4) indicates the energy ($\sqrt{s}$) gain of colliding beams as compared to fixed-target machines. Their disadvantage is the much lower collision rates achieved with two comparatively tenuous beams.

The accelerators now available range from the older fixed-target machines with E_L of a few GeV to the CERN intersecting storage rings (ISR) in which p beams with energies up to about 30 GeV collide permitting $s \simeq (2 \times 30\ \text{GeV})^2 = 3600\ \text{GeV}^2$. The newly-constructed CERN $\bar{p}p$ collider is beginning to yield data at energies up to about $\sqrt{s} = 540$ GeV, and colliders are being designed at other laboratories to reach $\sqrt{s} =$ 2000 GeV($\equiv 2$ TeV) or more.

At the high energies so far available it is found that the total scattering cross section σ_T (for $pp \to X$ where X represents all types of particles) varies very little with energy, and that $\sigma_T(pp) \simeq 40\ \text{mb} = (2\ \text{fm})^2$ just as one would expect on geometrical grounds for particles of size about 1 fm (see figure 10). This constancy is an example of 'scaling', i.e. the magnitude of σ_T is independent of the energy scale. However, we see from figure 10 that most total cross sections fall a bit with increasing energy at low energies, and rise slowly at high energies. We shall explore the reasons for this in § 9.

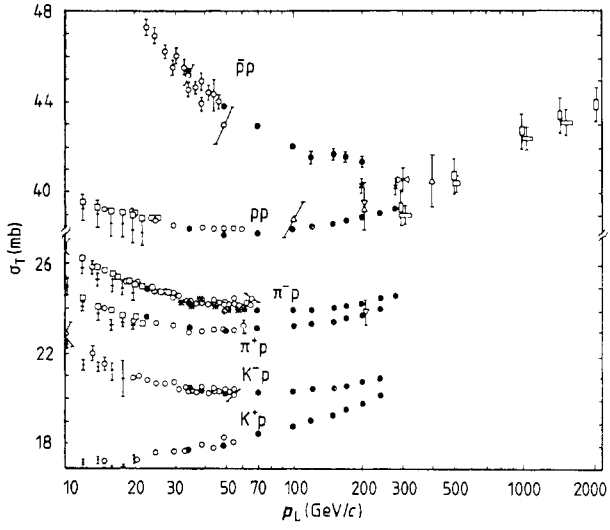

Figure 10. The total cross sections for scattering on protons, taken from Carroll *et al* (1976).

At high energies the final state is often quite complicated, several particles being produced in a collision, some of which are likely to miss any detectors which have been set up. It has thus become common to measure the so-called 'inclusive' single-

particle production cross section, for say $AB \to CX$, where C is the detected particle and X symbolises all the other particles which may have been produced but which have not been observed. The invariant single-particle distribution is defined by

$$f(AB \to CX) \equiv E_C \frac{d^3\sigma}{d^3\boldsymbol{p}_C} = \frac{E_C}{\pi} \frac{d^2\sigma}{dp_L\, dp_T^2} \tag{2.5}$$

where $d^3\sigma/d^3\boldsymbol{p}_C$ is the differential cross section (i.e. the probability per unit incident flux) for detecting particle C within the phase-space volume element $d^3\boldsymbol{p}_C$. E_C is included in (2.5) to ensure the Lorentz invariance of f (see, for example, Collins 1977, p327); p_L and p_T are the components of $\boldsymbol{p}_C$ along and transverse to the beam direction, respectively.

A comparatively small fraction of the incident energy goes into making new particles. Thus even at the highest CERN ISR energies the average number of charged particles produced in pp collisions is $\langle n_{ch}\rangle \simeq 12$, 90% of which are pions. The variation with s (in GeV^2) is very approximately (see figure 11(a))

$$\langle n_{ch}\rangle = 2 \log s - 4 \tag{2.6}$$

whereas if a fixed fraction of the energy went into particle production we would find $\langle n_{ch}\rangle \sim s^{1/2}$.

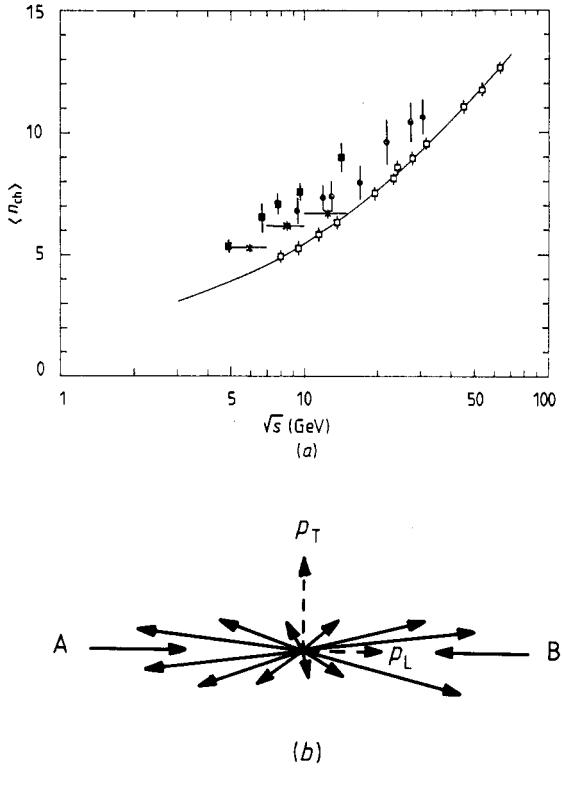

Figure 11. (a) The energy dependence of the averaged charged multiplicity for pp collisions, compared with that for e^+e^- annihilations, $\bar{p}p$ annihilations and νp interactions, taken from Berger *et al* (1980). ●, e^+e^-(PLUTO), $K_s^0 \to \pi^+\pi^-$ excluded; □, pp interactions; ■, $\bar{p}p$ annihilation; *, νp interactions. (b) Schematic drawing of AB scattering producing a two-jet event and showing the limited transverse momentum of the produced particles.

Instead, most of the incident energy emerges as the kinetic energy of the outgoing particles, many of which are found to be travelling in two jets with only a rather small deviation from the directions of the incoming particles. Figure 11(*b*) shows a typical plot of the momenta of the outgoing particles and it will be evident that whereas the longitudinal momentum component, p_L, takes a wide range of values, the transverse momentum, p_T, is generally quite small (<1 GeV/c). The production cross section falls with increasing p_T roughly like (figure 12(*a*))

$$\frac{d\sigma}{dp_T} \sim \exp(-6p_T) \tag{2.7}$$

giving an average p_T of only about 0.35 GeV/c, though this does increase slowly with energy.

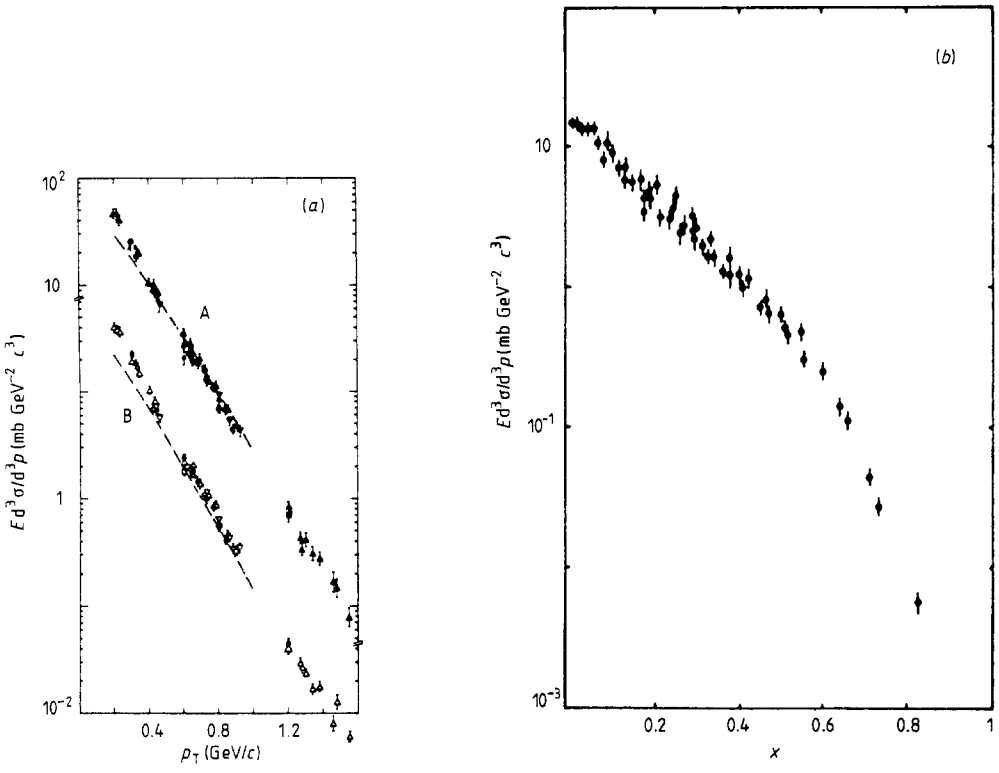

Figure 12. The invariant inclusive cross section as a function of (*a*) p_T at fixed x ($y_{lab} = 1.5$) (A, $p+p \rightarrow \pi^+ + \cdots$; B, $p+p \rightarrow \pi^- + \cdots$), and (*b*) x at fixed p_T (0.4 GeV/c) (see Giacomelli and Jacob 1979).

It is convenient to introduce the dimensionless variable

$$x \equiv p_L/p \tag{2.8}$$

which measures, in the centre-of-mass frame, the fraction of the beam's momentum (p) which is contained in the longitudinal momentum component (p_L) of the detected particle. Clearly x varies from -1 to 1. A typical example of a cross section plotted as a function of x is shown in figure 12(*b*), from which it will be seen that a fairly large number of slow particles is produced (x near 0), but that the distribution decreases

rapidly to zero as $x \to 1$, like $(1-x)^n$. The shape of this x distribution is found to be essentially independent of energy, an effect which is generally known as 'Feynman scaling' (Feynman 1969). The value of the exponent, n, in these distributions will be of great interest to us in § 6.

Another variable which is often used to display the p_L dependence of the cross section is the rapidity, y, defined by (De Tar 1971)

$$y = \tfrac{1}{2} \log \left(\frac{E + p_L}{E - p_L} \right). \tag{2.9}$$

Clearly y depends on the choice of frame, but it has the advantage of being simply additive under Lorentz boosts along the z axis. Thus if we consider a frame boosted by velocity u, so that

$$E \to \gamma(E + up_L) \qquad p_L \to \gamma(p_L + uE)$$

where $\gamma = (1-u^2)^{-1/2}$, then we see that

$$y \to y + \tfrac{1}{2} \log \left(\frac{1+u}{1-u} \right) \equiv y + y_{\text{boost}}.$$

In the non-relativistic limit $(v \ll 1) E \to m$, $p \to mv$, and thus $y \to v$.

The cross section for inclusive particle production as a function of the centre-of-mass rapidity is shown in figure 13, which exhibits a central plateau at small y and falling cross sections in the fragmentation regions where $y \to \pm y_{\max}$. The magnitude of the central region cross section changes only rather slowly with energy, indicating an approximate scaling, which we will discuss further in § 8.

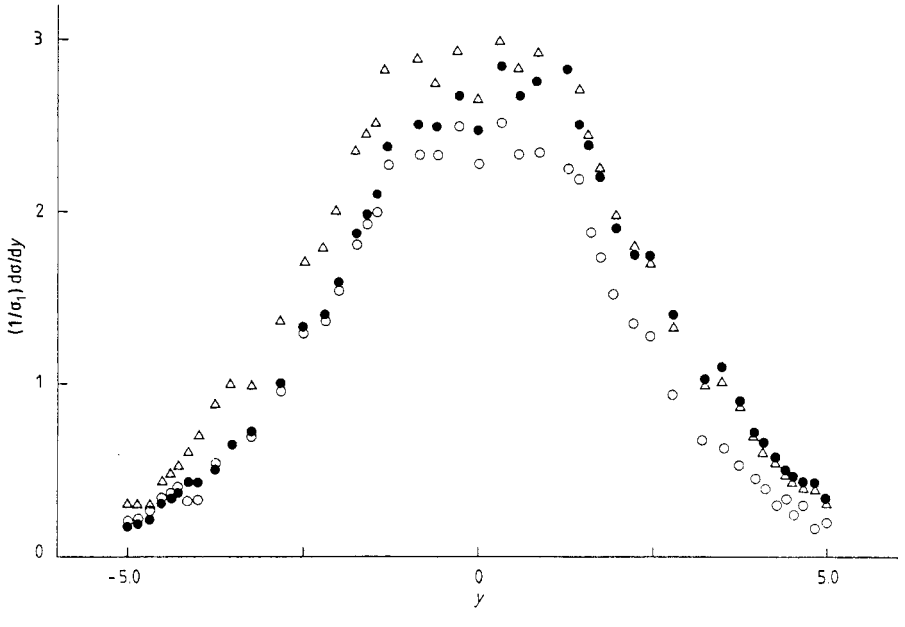

Figure 13. The inclusive rapidity distribution in pp collisions. ○ p_{ISR} 15.4 GeV/c, △ p_{ISR} 26.7 GeV/c, ● beam 1 15.4 GeV/c, beam 2 26.7 GeV/c.

Sometimes experiments are designed to detect all the particles in the final state (such as $AB \to CD$, $AB \to CDE$, etc). These are called 'exclusive' experiments because care is taken to ensure, using energy, momentum and quantum number conservation arguments, that the detected particles were indeed the only ones produced in the event. As the energy increases any particular exclusive final state contributes only a diminishing fraction of the total cross section.

For future convenience we introduce here the kinematic invariants needed to describe two-body final-state processes of the form $AB \to CD$, shown in figure 14.

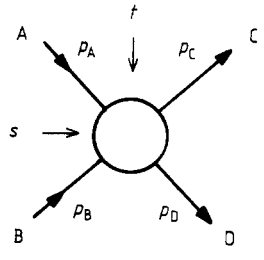

Figure 14. Kinematic variables for the process $AB \to CD$.

We have already introduced ((2.1))

$$s \equiv (p_A + p_B)^2$$

the total centre-of-mass energy squared. We shall also need the momentum transfer variable:

$$\begin{aligned} t &\equiv (p_A - p_C)^2 \\ &= m_A^2 + m_B^2 - 2p_A \cdot p_C \\ &= m_A^2 + m_B^2 - 2E_A E_C + 2|\boldsymbol{p}_A||\boldsymbol{p}_C| \cos\theta \end{aligned} \tag{2.10}$$

where $p_A \equiv (E_A, \boldsymbol{p}_A)$ is the four-momentum of particle A (and similarly for C) and θ is the scattering angle in the centre-of-mass frame. It is also useful to define

$$u \equiv (p_A - p_D)^2 \tag{2.11}$$

but four-momentum conservation requires that

$$s + t + u = m_A^2 + m_B^2 + m_C^2 + m_D^2 \tag{2.12}$$

so only two of s, t and u are independent variables. A more complete discussion of all these variables can be found, for example, in Collins (1977) or Ganguli and Roy (1980).

2.2. Scattering processes from a parton viewpoint

Nowadays we regard hadrons as clusters ('bags') of confined partons (i.e. quarks, antiquarks and gluons). The scattering of two hadrons, A and B, may thus be viewed as in figure 15. Though each cluster is colourless overall, within it there will be a distribution of colour charge, and the approach of the other cluster will induce a redistribution (polarisation) of this colour charge (just like the polarisation of an atom's electron distribution which is induced by a passing charged particle).

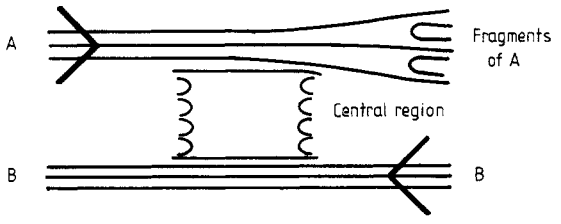

Figure 15. The parton description of a two-jet event, showing the fragmentation of A, central production, and a fast moving particle B little affected by the interaction. In a typical two-jet event B would also fragment, as in figure 11(*b*).

Some of the partons will presumably be rather little affected, so in the figure many of A's partons travel more or less straight on, but because of the excitation they form into new colourless hadrons, which we call the fragments of A. Some of these hadrons may be carrying a significant fraction of the momentum of A and so appear at large positive values of x (near 1). The incoming partons may be so little influenced that they recombine into the same hadron, as with B in figure 15. In this case we will find in the final state a 'leading particle' with x near -1, which is in fact just the incident hadron B with slightly reduced momentum. Or the incoming hadron may be excited to a more massive state with the same quantum numbers which subsequently decays, such as $p \to N^* \to p\pi$. This is called 'diffraction scattering', and the π is a fragment of the incoming p.

Those partons in A and B which happen to slow down, or to be travelling very slowly in the centre of mass at the moment of collision, may combine to produce new hadrons, nearly at rest. It is this central particle production (at $x \simeq 0$, or $y_{cm} \simeq 0$) which populates the central region plateau. Because most of these particles are pions (the pion is the lightest hadron and hence it occurs in the decay products of most hadrons) this is sometimes called the 'pionisation' region (in analogy with the ionisation produced in the scattering of charged particles).

These high-energy hadron scattering events thus mostly result in two jets of fast moving particles; one containing the fragments of A and the other the fragments of B, together with a central region of low momentum particles not particularly associated with A or B.

This gives us an intuitive understanding of the scaling exhibited by hadron cross sections. The total cross section depends mainly on the geometrical size of the clusters since the effective range of the colour polarisation force does not change much with energy. Similarly, the inclusive cross section for producing a particle in one of the fragmentation regions depends on how the excited parton clusters turn into jets of hadrons, which is essentially independent of the energy of the scattering process. In the central region the cross section increases roughly proportionally to the available rapidity ($y \sim \log s$, hence $\langle n \rangle \sim \log s$) but the cross section per unit rapidity interval remains almost constant at about two charged particles per unit of y (see (2.6)).

Elastic scattering is the special case in which both the incoming clusters of partons retain their integrity and are not broken up to form new hadrons. This is clearly only likely if the collision is rather soft, i.e. there is very little momentum transferred by the energy-independent colour polarisation force. We can therefore expect that the elastic differential cross section, $d\sigma/dt$, will change only slowly with energy and will fall off rapidly with increasing $|t|$. Both of these expectations are vindicated by the

data, as we shall find in § 9. Very similar remarks apply to quasi-elastic diffractive processes such as $\pi N \to \pi N^*$. The differential cross section does not change much with energy and has a similar t dependence to elastic scattering.

More interesting are two-body final-state processes in which there is an exchange of flavour quantum numbers, such as $\pi^- p \to \pi^0 n$ or $\pi^- p \to K^0 \Lambda$. In the former there is an exchange of charge between the incoming particles, while the latter requires the exchange of both charge and strangeness. Unlike the processes we have been discussing so far, this clearly cannot be achieved just by colour polarisation but, since the flavour quantum numbers are carried by quarks, it is necessary for quarks to pass from one cluster to another, thus reversing their directions of motion. This is hard to achieve at high energies and it is not surprising therefore that the cross section for such processes should fall with increasing energy $\sim s^{-n}$ with typically $n = 1$–2.

As we mentioned in § 1 the two exchanged valence quarks can carry with them a sea of virtual gluons and $q\bar{q}$ pairs, which together comprise a Regge trajectory of hadrons, and we shall find in § 7 that the differential cross section has the asymptotic behaviour with energy:

$$d\sigma/dt \sim s^{2\alpha(t)-2} \tag{2.13}$$

where $\alpha(t)$ is the exchanged trajectory, as in figure 8. Again, the occurrence of just two hadrons in the final state is unlikely if the momentum transfer is large and so $d\sigma/dt$ falls rapidly with $|t|$ for this type of process too.

It will be evident from figure 16 that the exponential fall, (2.7), of the inclusive cross section with p_T changes at $p_T \simeq 1$ GeV/c and that although the cross section for large p_T is very small (only about 1 particle in 10^5 has $p_T > 2$ GeV/c) it is much larger than one would expect if one simply extrapolated the small p_T behaviour. This change suggests that a different process is involved in large p_T particle production.

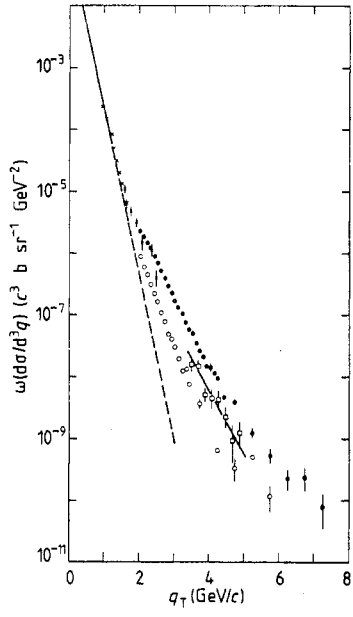

Figure 16. The pioneer ISR data, shown at the 1972 Chicago Conference, on the inclusive production of π^0 mesons at 90° in pp collisions. The broken line is the extrapolation of exp $(-6p_T)$ which describes the $p_T \leqslant 1$ GeV/c data. × $s = 2850$ GeV^2, ● $s = 2850$ GeV^2, ○ $s = 950$ GeV^2, □ $s = 2000$ GeV^2.

The transverse momentum, p_T, is the conjugate variable to the impact parameter of the collision b (figure 17(a)) so the large p_T implies that the basic scattering process has occurred at small b. In the parton picture this means that two of the partons have passed very close to each other and so have been scattered at wide angles. These partons attempt to leave the confinement region and in so doing produce jets of hadrons as described in § 1. The remaining partons continue almost undisturbed, and so large p_T hadrons will occur in four-jet events, like figure 17. There are the forward and backward jets from the fragmentation of the unscattered partons (similar to those in small p_T scattering) and a pair of almost back-to-back wide-angle jets stemming from the hadronisation of the scattered partons. (The way jets originate from wide-angle parton scattering is discussed in detail in § 5.)

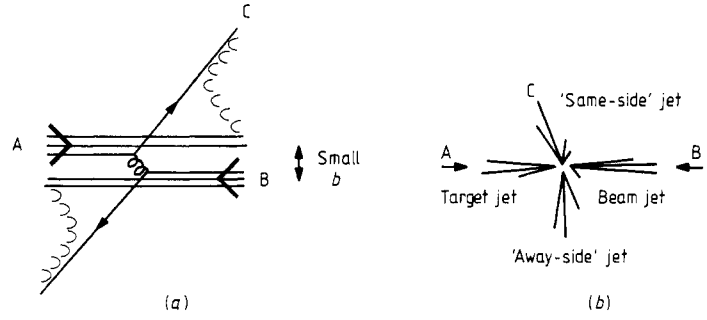

Figure 17. (a) A parton–parton interaction leading to a large p_T AB→CX event, and (b) an idealised picture showing the wide-angle jets arising from the fragmentation of the partons.

Though comparatively rare this type of event is very important because it can give a rather direct insight into the fundamental parton interaction, unlike the more commonplace small p_T events which involve the whole clusters of partons. It is for this reason that we shall begin our detailed examination of hadron scattering mechanisms in the next section with a discussion of large p_T processes.

First, however, we wish to look more closely at the scaling predictions of the parton model.

2.3. Scaling

As an example of a process which exhibits scaling we consider first the QED reaction $e^+e^- \to \mu^+\mu^-$ (figure 18(a)). In the lowest-order single-photon-exchange approximation the cross section for unpolarised electrons at high energies ($s \equiv (p_{e^+} + p_{e^-})^2 \gg m_e^2$)

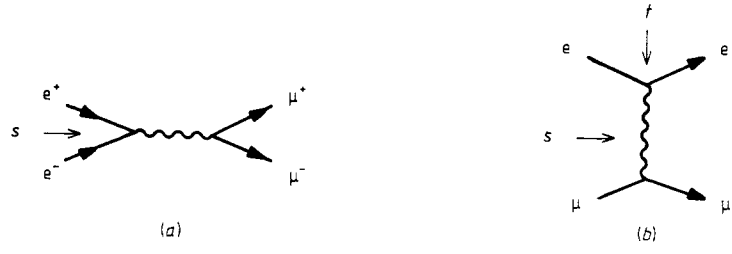

Figure 18. Lowest-order diagrams for (a) $e^+e^- \to \mu^+\mu^-$ and (b) $e\mu \to e\mu$.

is (Jauch and Rohrlich 1955, Bjorken and Drell 1964, Itzykson and Zuber 1980)

$$\sigma(e^+e^- \to \mu^+\mu^-) = \frac{1}{s}\left(\frac{4\pi\alpha^2}{3}\right)\left(1-\frac{4m_\mu^2}{s}\right)^{1/2}\left(\frac{2m_\mu^2+s}{s}\right) \tag{2.14}$$

$$\xrightarrow[s\gg m_\mu^2]{} \frac{4\pi\alpha^2}{3s}. \tag{2.15}$$

In this expression the first factor s represents the flux of electrons (remember $\sigma \equiv$ the scattering probability per unit flux), the first bracket gives the basic strength of the interaction in first order ($\propto \alpha^2$), the second bracket contains the threshold behaviour and vanishes at the threshold energy $s = 4m_\mu^2$, while the final bracket represents the helicity structure and contains two terms because the outgoing μ may have parallel or antiparallel spins. At high energies these last two factors become irrelevant, however, and we see from (2.15) that

$$s\sigma \to 4\pi\alpha^2/3 \tag{2.16}$$

independent of s. That is to say, $s\sigma$ is 'scale-invariant', or 'scales'. Since the cross section has the dimensions of an area, and we are working in units where $\hbar c = 0.197\,\text{GeV fm} \equiv 1$, an area in fm^2 must be expressed in GeV^{-2}. In (2.15) this dimensional factor comes from the flux factor, s^{-1}, while the interaction appears just through the dimensionless α (though there is scale-breaking s dependence at lower energies in (2.14)).

Similarly for $e\mu \to e\mu$ scattering of figure 18(b) the differential cross section is, for $s, t \gg m_\mu^2$ (Close 1979),

$$\frac{d\sigma}{dt} = \frac{4\pi\alpha^2}{s^2}\tfrac{1}{2}\left(\frac{s^2+u^2}{t^2}\right) \tag{2.17}$$

where $s+t+u = 2m_e^2 + 2m_\mu^2$ from (2.12) and where the t^{-2} arises from the photon propagator. We thus find that

$$s^2\frac{d\sigma}{dt} = 2\pi\alpha^2\left(\frac{s^2+u^2}{t^2}\right) \xrightarrow[s,t\to\infty]{} f\left(\frac{t}{s}\right) \tag{2.18}$$

is a function only of the dimensionless ratio t/s, and is scale-invariant. Again the flux factor s^{-2} carries the dimensions of $d\sigma/dt$ in (2.17).

There is no scale factor in these expressions because electrons and muons are point-like fundamental particles which have no charge radius to introduce a size scale into the problem. If it were possible to scatter electrons off free quarks we would expect the cross section to be identical to (2.17) (but with $\alpha \to \alpha e_q$ where e_q is the quark charge in units of e) because a quark is also a point-like fundamental particle.

However, if we scatter an electron off a meson with a large transfer of momentum, t, the simplest parton diagram we can draw is figure 19(a) in which the electron scatters off one of the quarks. We then have a $q\bar{q}$ system in which the constituents are moving apart rapidly, and the chances of them pulling back together via gluon exchange to re-form the meson is obviously quite small. In fact, the probability amplitude should be proportional to the meson form factor, $F_M(t)$, which goes like t^{-1} at large t, since $t = q^2$ represents the amount by which the struck quark is off its mass shell after the electron has hit it. To see this recall that in Feynman perturbation theory a particle of mass m and four-momentum k has a propagator $\sim(k^2 - m^2)^{-1}$,

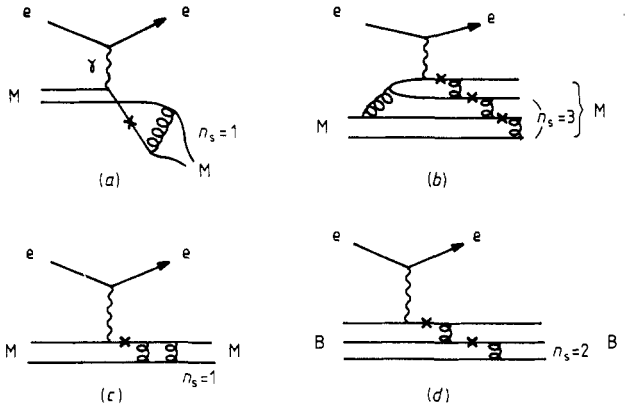

Figure 19. Parton diagrams for large momentum transfer electron–meson (*a*), (*b*), (*c*) and electron–baryon (*d*) elastic scattering. Internal quark lines far off mass shell are indicated with a cross. In (*a*) there is one spectator quark to the electron quark scattering, while in (*b*) there are three, and two in (*d*).

and k^2-m^2 is the amount by which the particle is off its mass shell (2.2). In figure 19(*a*) the quark line is off its mass shell as it travels between the photon vertex and the gluon vertex (the amplitudes for photon and gluon exchange between fermions are scale-invariant as in (2.18) so the internal quark line is the only one that matters; see Sivers *et al* (1976) for a more detailed discussion).

Hence for eM→eM we have at large s and $t(\gg m_M^2)$

$$s^2\frac{d\sigma}{dt}=4\pi\alpha^2\tfrac{1}{2}\frac{us}{t^2}F_M^2(t)\xrightarrow[s,t\to\infty]{}f\left(\frac{t}{s}\right)F_M^2(t)\sim f\left(\frac{t}{s}\right)t^{-2}. \tag{2.19}$$

The different angular factors in (2.18) and (2.19) ($1+u^2/s^2$ and u/s) simply arise because the electron is scattering on a spin-$\frac{1}{2}$ muon as compared to a spin-0 meson. The form factor, $F_M(t)$, is a measure of the non-point-like structure of the meson. It is found that, for example, the pion form factor is well represented by

$$F_\pi(t)=\left(1-\frac{t}{m_\rho^2}\right)^{-1}\underset{t\to\infty}{\sim}t^{-1} \tag{2.20}$$

where m_ρ, the mass of the ρ meson, introduces a mass scale into the problem. Form (2.20) is expected according to the vector dominance hypothesis in which the photon couples through the lightest available vector mesons (see Gilman 1972, Gourdin 1974).

We must, of course, also consider many other types of diagram, such as figure 19(*b*) for example, in which the electron scatters off a sea quark rather than a valence quark. But in this case the number of off-shell propagators, and hence the number of gluons needed to pull the meson back together again, is greater and the amplitude behaves like $\sim t^{-N}$ where N is the number of such propagators. The simpler figure 19(*a*) will thus be the dominant diagram at large t. There are also multi-gluon exchange diagrams like figure 19(*c*), but these produce only log (t) modifications to figure 19(*a*), at least at large t where QCD perturbation theory should be reliable (see Brodsky and Lepage 1979a,b).

For electron–baryon scattering the simplest diagram is figure 19(*d*) in which again the electron strikes one of the quarks, but now a minimum of two gluons is needed to pull the three quarks back together again. There are thus two off-shell quark

propagators and so the baryon's form factor should behave like $F_B(t) \sim t^{-2}$. In fact, the spin-$\frac{1}{2}$ proton has two independent form factors, $G_E(t)$ and $G_M(t)$, which represent its electric and magnetic couplings respectively (see Gourdin 1974, Close 1979) but both are found to behave like

$$G_{E,M}(t) \simeq \left(1 - \frac{t}{0.71}\right)^{-2} \sim t^{-2}. \tag{2.21}$$

Again, more complicated diagrams either give non-leading contributions as $t \to \infty$ or produce only logarithmic modifications to this leading power behaviour.

These arguments are readily generalised, and the rule is that any form factor should have the leading power behaviour as $t \to \infty$

$$F(t) \sim (t)^{-n_s} \tag{2.22}$$

where n_s is the minimum possible number of 'spectator' partons which are not involved in the initial electron–parton interaction. n_s is equal to the minimum number of gluons required to hold the hadron together, and hence gives the number of far off-shell quark propagators. For mesons $n_s = 1$ while for baryons it is 2. Hence for electron–hadron scattering we have the 'dimensional counting rule' (Sivers *et al* 1976) that

$$s^2 \frac{d\sigma}{dt} \underset{s,t\to\infty}{\sim} f\left(\frac{t}{s}\right)(t)^{-2n_s} \tag{2.23}$$

where $f(t/s)$ is a dimensionless function of the dimensionless ratio t/s, while the factor $(t)^{-2n_s}$ gives the degree of breaking of the scaling law (2.18) for point-like particles, and is characteristic of the composite structure of the hadron.

It should be noted that it is only because we are interested in those unusual events where just a single meson or baryon is found in the final state that we obtain the suppression in (2.23). If instead we consider the total cross section for, say, $ep \to eX$ where X is any number of hadrons then, as we shall discover in § 3, one again finds scaling. This is because no far-off-mass-shell propagators are required as the excess energy can be radiated away into hadrons a bit at a time as sketched in figure 20.

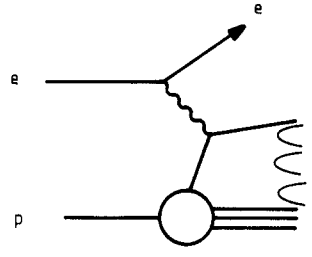

Figure 20. Parton diagram for $ep \to eX$.

Next we look at hadron–hadron scattering. The basic process is qq scattering, and the simplest single-gluon exchange diagram (figure 21), results in (Cutler and Sivers 1978)

$$\frac{d\sigma}{dt}(qq \to qq) = \tfrac{2}{9} \frac{4\pi\alpha_s^2}{s^2} \tfrac{1}{2}\left(\frac{s^2+u^2}{t^2}\right) \underset{s,t\to\infty}{\sim} f\left(\frac{t}{s}\right)\frac{1}{s^2} \tag{2.24}$$

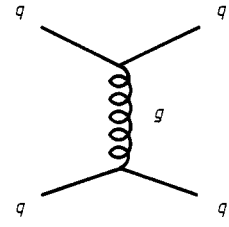

Figure 21. Lowest-order diagram for qq scattering.

just like (2.17) except that $\alpha \to \alpha_s$ and we have acquired a factor $\frac{2}{9}$ from summing over all possible colours of the exchanged gluon (compare (1.7) to (1.9)). At large t where $\alpha_s(t)$ becomes small (see (1.11)) we expect this to be the dominant contribution, but of course in the absence of free quarks it is impossible to check directly this scaling prediction stemming from the point-like nature of the quarks.

If instead we consider meson–meson scattering the simplest diagram is figure 22 in which the basic qq scattering is followed by the same sort of recombination

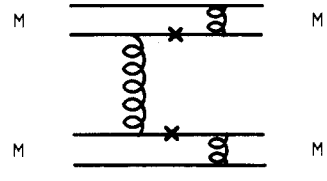

Figure 22. Parton diagram for large momentum transfer MM→MM scattering. The crosses indicate far-off-mass-shell quarks. Of course, the basic hard gluon exchange between the mesons must be supplemented by further soft gluons to ensure that the final mesons are colour singlets.

mechanism as figure 19(a), and so we expect that (Sivers *et al* 1976)

$$\frac{d\sigma}{dt}(MM \to MM) \underset{s,t\to\infty}{\sim} \frac{d\sigma}{dt}(qq \to qq) F_M^4(t) \tag{2.25}$$

$$\sim \frac{1}{s^2} f\left(\frac{t}{s}\right)\left(\frac{1}{t}\right)^4 \tag{2.26}$$

which $\sim s^{-6}$ at fixed values of t/s, i.e. at fixed angle. In this expression we have ignored the contributions of the soft gluons which must also be exchanged to keep the final state M colourless, but which are expected to produce at most logarithmic modifications. Similarly for meson–baryon and baryon–baryon scattering we have

$$\frac{d\sigma}{dt}(MB \to MB) \underset{s,t\to\infty}{\sim} \frac{d\sigma}{dt}(qq \to qq) F_M^2(t) F_B^2(t) \sim \frac{1}{s^2} f\left(\frac{t}{s}\right)\left(\frac{1}{t}\right)^6 \tag{2.27}$$

$$\frac{d\sigma}{dt}(BB \to BB) \underset{s,t\to\infty}{\sim} \frac{d\sigma}{dt}(qq \to qq) F_B^4(t) \sim \frac{1}{s^2} f\left(\frac{t}{s}\right)\left(\frac{1}{t}\right)^8 \tag{2.28}$$

so that at fixed angle these processes should behave like s^{-8} and s^{-10}, respectively.

These predictions seem to work rather well for $|t| \geqslant 2.5\ (\mathrm{GeV}/c)^2$. We are thus led to the more general dimensional counting rule that

$$s^2 \frac{\mathrm{d}\sigma}{\mathrm{d}t}(\mathrm{AB} \to \mathrm{CD}) \underset{\substack{s,t\to\infty \\ s/t \text{ fixed}}}{\sim} f\left(\frac{t}{s}\right) s^{-2n_s} \tag{2.29}$$

where n_s is the minimum of spectator partons in the basic parton scattering process (which in turn is equal to the number of off-shell quark propagators, or the number of gluon propagators required over and above the scaling gluon exchange of the initial qq scattering). As before lowest-order parton model predictions will acquire logarithmic corrections from higher-order diagrams with further gluon exchanges like those of figure 19(c) (Brodsky and Lepage 1979a,b).

The breakdown of strict scaling in (2.29) stems from the fact that we are demanding the re-formation of a specific two-body final state at wide angles. If instead we allow the struck quarks' energy to be freely radiated away through hadron production we expect that the inclusive production process $\mathrm{AB} \to \mathrm{CX}$, where C is the detected large p_T hadron and X represents everything else produced, will take the asymptotic form

$$f(\mathrm{AB} \to \mathrm{CX}) \underset{s,p_\mathrm{T}\to\infty}{\sim} f\left(\frac{p_\mathrm{T}}{\sqrt{s}}, \theta_\mathrm{cm}\right) p_\mathrm{T}^{-4} \tag{2.30}$$

where f is some dimensionless function of the dimensionless variables $p_\mathrm{T}/\sqrt{s}$ and the centre-of-mass scattering angle, and the p_T^{-4} behaviour arises from the natural scale of the basic qq scattering process (2.24). In other words we anticipate that $p_\mathrm{T}^4 f(\mathrm{AB} \to \mathrm{CX})$ will be scale-invariant. We shall review the success of this prediction in some detail in §§ 3 and 4 (see Jacob and Landshoff 1978).

Finally we must look again at the total cross section $\mathrm{AB} \to \mathrm{X}$. We have said that this will be dominated by small p_T processes in which the incoming partons deviate rather little from their initial directions of motion. If we suppose that first a gluon is exchanged between the hadrons, and then particle production occurs to try and neutralise the colour, the optical theorem can be used to perform the sum over all the possible final states as in figure 23. Since the gluon exchange amplitude at fixed t behaves like s as $s \to \infty$ (cf (2.24)) we obtain

$$\sigma_\mathrm{T}(\mathrm{AB} \to \mathrm{X}) \underset{s\to\infty}{\sim} (1/s)s = \text{constant} \tag{2.31}$$

i.e. the total cross section should be invariant as $s \to \infty$. We can anticipate $\log s$ modifications to this result due to multiple gluon exchange, but this rather constant behaviour of total cross sections is certainly in accord with figure 10.

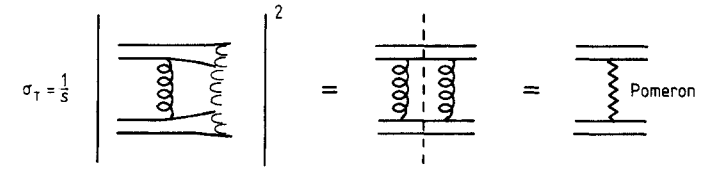

Figure 23. Diagrammatic representation of the optical theorem. The first equality indicates that the AB total cross section is the sum over all possible multiparticle production cross sections. The second equality expresses this as an amplitude product where the broken line implies the sum over all possible intermediate states. Via unitarity, this product is equal to the imaginary part of the forward $\mathrm{AB} \to \mathrm{AB}$ amplitude (which at high energy is dominated by Pomeron exchange).

Long ago Pomeranchuk (1958) predicted (from entirely different considerations) that total cross sections would approach a constant asymptotic limit, and the Regge trajectory whose exchange ensures this behaviour became known as the Pomeron, with $\alpha_P(t=0)=1$. In the parton model the Pomeron is identified as a colourless, flavourless multiple (two and more) gluon exchange. We shall pursue this identification further in § 9.

3. Large p_T processes

As we remarked in the previous section large momentum transfer processes provide an insight into the fundamental parton interactions. Here we introduce the naive parton model, which provides a useful first approximation for such processes.

3.1. The parton model for large p_T scattering

If hadrons are made up of more fundamental parton constituents (i.e. quarks and gluons) it must be possible to describe any hadronic reaction in terms of the interactions of these constituents. But this viewpoint will obviously be most useful for those reactions in which the basic parton scattering process is fairly well separated in time from the more complex confinement effect, which prevents the partons from escaping as free particles and causes them to re-assemble in hadrons. The production of hadrons which have a large momentum component ($\boldsymbol{p}_T$) transverse to the beam direction is a good example of such a reaction (Feynman 1972, Sivers *et al* 1976, Jacob and Landshoff 1978, Close 1979).

The basic diagram for $AB \to CX$, where C is the hadron with large $|\boldsymbol{p}_T|$ (say $p_T > 2\ \mathrm{GeV}/c$) while X represents all the other particles in the final state, is shown in figure 24. The incoming particles A and B contain, *inter alia*, partons a and b (respectively) which scatter, producing partons labelled c and d (which may often be the same as a and b) which have a large transverse momentum component q_T. Subsequently hadron C is produced from c via the confinement mechanism. Since k_T is the conjugate variable to the impact parameter of the parton scattering process, large q_T implies that the partons have scattered at a small distance where, according to the arguments of § 1.3, α_s is small. Hence we may reasonably hope that perturbation theory will be applicable.

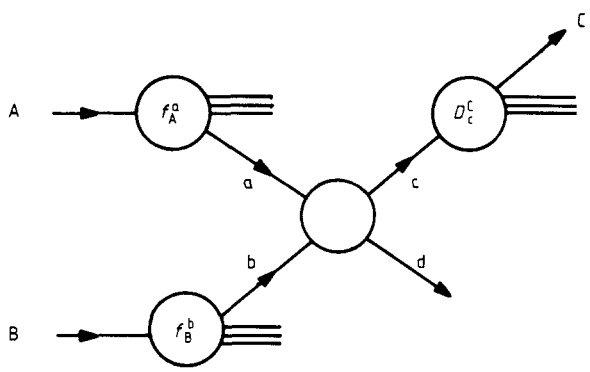

Figure 24. The hadronic interaction $AB \to CX$ at large p_T in terms of the parton sub-process $ab \to cd$, the structure functions f_A^a, f_B^b, and the fragmentation function D_c^C.

The uncertainty principle tells us that the time interval τ within which parton scattering occurs is rather short ($\tau \sim \hbar/q_T c$). Partons c and d then fly apart until the confinement mechanism causes hadron production, including the production of C. If we suppose that R is the characteristic distance within which confinement occurs (probably $R \sim 0.5$ fm, a typical hadron 'size') then the time taken for C to be produced will be of the order of $T \sim Rq_T/mc^2$ (q_T/mc being the Lorentz dilation in transforming from the C rest frame to the AB centre-of-mass frame). Thus as q_T increases the processes of parton scattering and hadron production become separated by longer times ($T \gg \tau$) and the description given in figure 24 becomes more plausible.

We can in fact use figure 24 to try and estimate the cross section for the inclusive process AB → CX. Let $f_A^a(x_a)$ be the probability that hadron A contains a parton a which is carrying a fraction $x_a = q_a/p_A$ of its momentum, $0 \leqslant x_a \leqslant 1$. For the time being we neglect any momentum a may have in directions transverse to the beam direction (the z axis), and also neglect the masses of both hadrons and partons as being small compared to the momenta we are considering, so the four-momenta may be approximated as

$$\begin{aligned} p_A &\simeq (p_A, \mathbf{0}, p_A) \\ q_a &\simeq (q_a, \mathbf{0}, q_a) = x_a(p_A, \mathbf{0}, p_A) \end{aligned} \tag{3.1}$$

since $p_A \gg m_A$, etc. The functions $f_A^a(x_a)$ are called the 'structure functions' of A. Similarly we introduce the 'fragmentation function' $D_c^C(z_c)$ representing the probability that the outgoing parton c produces a hadron C carrying a momentum fraction $z_c = p_C/q_c$, where $0 \leqslant z_c \leqslant 1$. We are assuming that C is produced colinearly with c and that the fragmentation depends only on z_c and is independent of the nature of the initial state.

If we neglect the particle masses, the invariant variables for AB → CX are

$$\begin{aligned} s &= (p_A + p_B)^2 \simeq 2p_A \cdot p_B \\ t &= (p_A - p_C)^2 \simeq -2p_A \cdot p_C \end{aligned} \tag{3.2}$$

where $\sqrt{s}$ is the total centre-of-mass energy and $\sqrt{-t}$ is the invariant momentum transfer from A to C. The corresponding variables for the parton sub-process, ab → cd, are

$$\begin{aligned} \bar{s} &\equiv (q_a + q_b)^2 \simeq 2q_a \cdot q_b = 2x_a x_b p_A \cdot p_B \simeq x_a x_b s \\ \bar{t} &\equiv (q_a - q_c)^2 \simeq -2q_a \cdot q_c = -2x_a p_A \cdot p_C/z_c \simeq x_a t/z_c. \end{aligned} \tag{3.3}$$

We can express the invariant cross section for AB → CX as the weighted sum of differential cross sections, $d\sigma/d\bar{t}$, of all possible parton scatterings that can contribute:

$$E_C \frac{d\sigma}{d^3 p_C}(AB \to CX) = \sum_{abcd} \int_0^1 dx_a \int_0^1 dx_b f_A^a(x_a) f_B^b(x_b) \frac{1}{\pi z_c} \frac{d\sigma}{d\bar{t}}(ab \to cd) D_c^C(z_c) \tag{3.4}$$

as shown in detail, for example, in the review by Sivers *et al* (1976); see also Feynman and Field (1977). So we can predict the cross section if we know the structure functions, the fragmentation functions and the cross sections for all the parton sub-processes.

3.2. The structure functions

The best probes for determining the structure functions of nucleons are deep inelastic lepton–nucleon scattering processes such as $eA \to eX$, $\mu A \to \mu X$, $\nu_\mu A \to \mu^- X$ and $\bar{\nu}_\mu A \to \mu^+ X$ with a large momentum transferred between the lepton and the nucleon, A. Thus in electron scattering (figure 25) the cross section for electron–quark scattering is well known (apart from the quark charge it is the same as for $e\mu \to e\mu$) and we can write formally (Gilman 1972)

$$\frac{d^2\sigma}{dx\,dy}(eA \to eX) \propto \sum_q f_A^q(x) \frac{d\sigma}{dt}(eq \to eq). \tag{3.5}$$

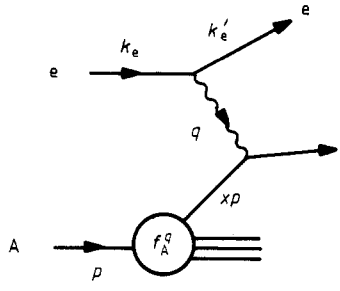

Figure 25. Deep inelastic lepton–nucleon scattering, $eA \to eX$, via photon exchange between the electron and a quark of nucleon A. The particle four-momenta are shown.

Of course the electron 'sees' only the charged partons, i.e. the quarks. In place of the invariant variables $Q^2 \equiv -q^2$ and $\nu \equiv p \cdot q$ we have introduced dimensionless quantities

$$x = Q^2/2p \cdot q \qquad y = p \cdot q/p \cdot k_e \tag{3.6}$$

where the particle four-momenta are defined in figure 25. x is the fraction of the hadron's momentum carried by the quark (which is assumed to be moving colinearly with A), as can be seen from the mass shell condition for the outgoing quark, $(xp+q)^2 = 0$. We neglect particle masses. Note that

$$1 - y = p \cdot k_e'/p \cdot k_e \simeq -u/s \simeq \tfrac{1}{2}(1 + \cos\theta^*) \tag{3.7}$$

where θ^* is the centre-of-mass scattering angle. The allowed kinematic region for $eA \to eX$ is therefore $0 \leqslant x, y \leqslant 1$.

In the rest frame of the nucleon, $p = (M, 0, 0, 0)$, we have

$$\begin{aligned} Q^2 &\equiv -q^2 = -(k_e - k_e')^2 = 4EE' \sin^2\theta/2 \\ \nu &\equiv p \cdot q = M(E - E') \\ y &= (E - E')/E. \end{aligned} \tag{3.8}$$

Thus for a given incident electron energy E, a measurement of the outgoing electron energy, E', and scattering angle θ determines precisely the x value of the quark from which the electron has scattered, as well as y, which is simply the fraction of the electron's energy transferred to the nucleon.

If quarks have spin $\frac{1}{2}$ and a point-like coupling to the photon (just like the electron or muon, except for e_q) then it is straightforward to show that the precise form of

(3.5) is (Gilman 1972)

$$\frac{d^2\sigma}{dx\,dy}(eA \to eX) = \frac{2\pi\alpha^2}{Q^4} s[(1-y)^2+1]\sum_q e_q^2 x f_A^q(x). \tag{3.9}$$

The most important feature of this prediction is the scaling behaviour, i.e. $f_A^q(x)$ depends on the ratio $x = Q^2/2\nu$ and not on Q^2 and ν individually. This is known as Bjorken scaling. If the quarks were not point-like but had a spatial distribution of charge, the eq interaction would depend on the quark's form factor $F(Q^2)$ and so in (3.9) $f_A^q(x)$ would be replaced by $F_A^q(x, Q^2)$. It was the observation of scaling in deep inelastic scattering which provided the principal motivation for the introduction of the parton model.

A similar analysis can be made for deep inelastic neutrino scattering (Llewellyn-Smith 1972) with the obvious modifications due to the short range and parity violation of the weak interaction, and the occurrence of the weak Fermi coupling constant G instead of e^2. For example, for neutrino scattering on a target which contains an equal number of neutrons and protons, the cross section per nucleon is

$$\frac{d^2\sigma}{dx\,dy}(\nu A \to \mu^- X) = \frac{G^2 s}{2\pi} x \sum_{q,\bar{q}} [f_p^q(x) + (1-y)^2 f_p^{\bar{q}}(x)] \tag{3.10}$$

while for $\bar{\nu}$ scattering the proton structure functions are interchanged $f_p^q \leftrightarrow f_p^{\bar{q}}$. The y distribution follows directly from the helicity structure of the neutrino–quark interaction. There are only left-handed q and ν charged-current weak interactions, so the helicities of the interacting particles are both $-\frac{1}{2}$, giving a total spin of the νq system $S_z = 0$. This results in an isotropic (y-independent) cross section. However, the $\bar{q}$ is right-handed (helicity $+\frac{1}{2}$) so the $\nu\bar{q}$ system has $S_z = -1$. For backward scattering this would have to change to $S_z = 1$, which is impossible as the z component of the spin must be conserved, and so we get a $(1-y)^2$ distribution which vanishes for $\theta^* = \pi$ (see (3.7)). The electromagnetic current has no 'handedness' and so both terms appear with equal weight in (3.9).

Another type of process in which hadron structure functions can be studied is high-mass lepton-pair production such as $AB \to \mu^+\mu^- X$. This is known as the Drell–Yan process (Drell and Yan 1971). In the parton model (figure 26) the cross section is (see Stroynowski 1981)

$$\frac{d\sigma}{dm^2}(AB \to \mu^+\mu^- X) = \left(\frac{4\pi\alpha^2}{3m^2}\right)\frac{1}{3}\sum_q e_q^2 \int_0^1 dx_a \int_0^1 dx_b\,[f_A^q(x_a) f_B^{\bar{q}}(x_b) + f_A^{\bar{q}}(x_a) f_B^q(x_b)]\delta(m^2 - x_a x_b s) \tag{3.11}$$

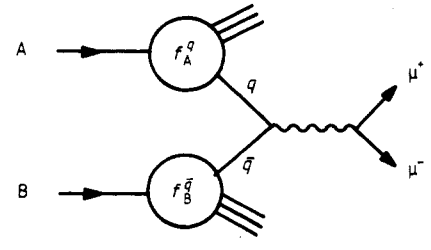

Figure 26. The basic $q\bar{q} \to \gamma \to \mu^+\mu^-$ parton model interaction for the Drell–Yan process $AB \to \mu^+\mu^- X$.

where m is the mass of the lepton pair. The first factor in brackets is the high-energy QED cross section for $e^+e^- \to \mu^+\mu^-$, since $q\bar{q} \to \mu^+\mu^-$ is the same apart from the quark charge. The extra factor $\frac{1}{3}$ accounts for the fact that all three colours of q and $\bar{q}$ occur with equal probability but only a q and $\bar{q}$ of the same colour can annihilate to form a colourless photon.

The same quark structure functions should appear in all the above processes and it is an important test of the parton idea that all these types of data can be accounted for by an identical parametrisation of the structure functions (Fox 1977, Buras and Gaemers 1978, Buras 1980). An example of the resulting fits is given in figure 27.

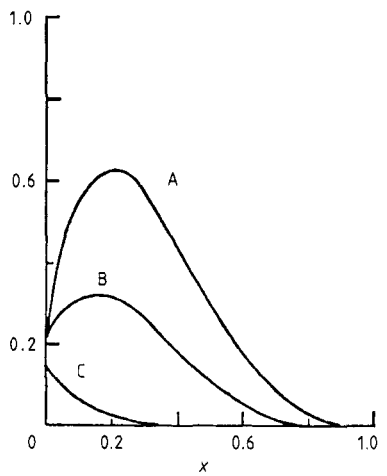

Figure 27. The quark structure functions of the proton, $q(x) \equiv f_p^q(x)$, taken from Barger and Phillips (1974). A, $xu(x)$; B, $xd(x)$; C, $x\bar{u}(x) = x\bar{d}(x) = x\bar{s}(x)$.

Several aspects of these distributions can be deduced from quite elementary considerations. First, the structure functions must be consistent with the quantum numbers of the hadron (charge, isospin, strangeness, . . .). Thus for a proton, whose quantum numbers are those of the *uud* combination of 'valence' quarks, we have the sum rules

$$\int_0^1 [f_p^u(x) - f_p^{\bar{u}}(x)]\,dx = 2 \qquad \int_0^1 [f_p^d(x) - f_p^{\bar{d}}(x)]\,dx = 1 \qquad \int_0^1 [f_p^s(x) - f_p^{\bar{s}}(x)]\,dx = 0. \tag{3.12}$$

The 'sea' quarks appear in $q\bar{q}$ pairs which do not affect the net quantum numbers. Furthermore, between them the partons, each with momentum fraction xp_A, must carry all the momentum of the hadron, p_A, so

$$\sum_a \int_0^1 x f_A^a(x)\,dx = 1. \tag{3.13}$$

In fact, if one inserts the observed quark distributions in a proton into (3.13) one obtains only about 0.5 on the RHS of (3.13) (CHARM 1981) from which it is concluded that the gluons, which are not seen by the weak or electromagnetic probes, are carrying about half the proton's momentum.

In the limit as $x \to 1$ we would have a single parton carrying all the momentum of the hadron, but this is clearly impossible and so the structure functions must vanish. The dimensional counting rules (Brodsky and Farrar 1973) lead us to expect that (2.23)

$$f(x) \underset{x\to 1}{\sim} (1-x)^{2n_s-1} \tag{3.14}$$

where n_s is the minimum number of other (spectator) partons whose momentum would have to vanish in this limit. Thus a valence quark (q_v) in a meson must be accompanied by at least $\bar{q}_v$ so $n_s = 1$ and $f_M^v(x) \sim (1-x)$, while a sea quark (q_s) has at least three spectators and $f_M^s(x) \sim (1-x)^5$. Similarly a gluon has at least two spectators ($q_v\bar{q}_v$, see figure 28) and $f_M^g \sim (1-x)^3$. These counting rules are discussed in more detail in § 6.2.

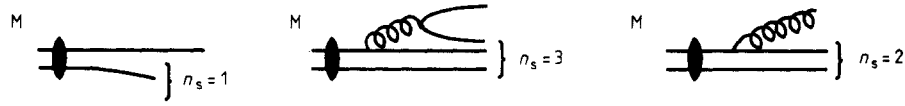

Figure 28. The minimum number of spectators, n_s, accompanying a valence, a sea quark and a gluon in a meson.

From (3.6) we see that as $x \to 0$, $\nu \to \infty$ for fixed q^2, and so in this limit we are in the regime of high-energy virtual-photon–hadron scattering. In this so-called 'Regge' regime it is found that (Gilman 1972) the total γA cross section has the form (cf (7.22))

$$\sigma_T(\gamma A) \underset{\nu\to\infty}{\longrightarrow} \beta_P \nu^{\alpha_P - 1} + \beta_R \nu^{\alpha_R - 1} \tag{3.15}$$

(modulo log ν factors) where β_P and β_R are coefficients, the constant $\alpha_P = 1$ behaviour being independent of the quantum numbers of A, while $\alpha_R(<1)$ is the leading Regge trajectory (i.e. particle exchange) contribution, which does depend on the flavour of A. From (3.9) we deduce that

$$\sigma_T(\gamma A) \propto \sum_q e_q^2 x f_A^q(x) \tag{3.16}$$

assuming that the high-energy region ($\nu \to \infty$ at fixed Q^2) overlaps the scaling region ($\nu, Q^2 \to \infty$ at fixed $x = Q^2/2\nu$). Thus identifying the first term on the RHS of (3.15) with the sea quarks (flavour-independent) contribution, and the second with the valence quarks, we obtain

$$\begin{aligned} f_A^s(x) &\underset{x\to 0}{\longrightarrow} x^{-\alpha_P} \qquad (\alpha_P \simeq 1) \\ f_A^v(x) &\underset{x\to 0}{\longrightarrow} x^{-\alpha_R} \qquad (\alpha_R \simeq \tfrac{1}{2} \text{ for } u \text{ and } d \text{ quarks}). \end{aligned} \tag{3.17}$$

Thus the sea quarks have a bremsstrahlung-like spectrum at small x (gluons creating $q\bar{q}$ pairs) and the number increases logarithmically as $x \to 0$. This behaviour is borne out by comparing ep → eX and en → eX data. At small x the parton multiplicity is high and isospin-independent giving the observed $\sigma_p \simeq \sigma_n$. At large x there are few partons and the difference of the p, n valence quark composition means $\sigma_p \neq \sigma_n$, as shown by the data.

Combining (3.14) and (3.17) we arrive at the approximate form of the structure function:

$$f_A^a(x) = C_A^a x^{-\alpha}(1-x)^{2n_s-1} \tag{3.18}$$

though of course this is only the leading behaviour as $x \to 0$ and 1. The normalisation C_A^a can be fixed by the sum rules (3.12) and (3.13). We thus have quite a good idea of what the structure functions should look like, and figure 27 clearly bears out these expectations.

3.3. The fragmentation functions

The final stage of figure 24, the conversion of the high momentum parton c into the hadron C, is supposed to be independent of how c was produced. Hence we can obtain the fragmentation function $D_c^C(z)$ rather directly from the process $e^+e^- \to CX$ (see figure 29) in which the initial state has no hadrons to confuse matters (see Wiik and Wolf 1979).

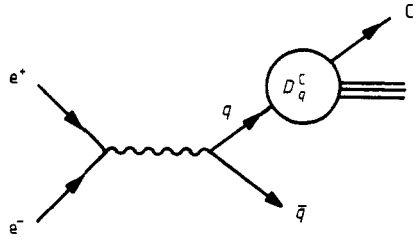

Figure 29. Determination of the fragmentation function, $D_q^C(z)$, from $e^+e^- \to CX$. Hadron C has a fraction z of the quark's momentum.

In the parton model the cross section is given by

$$\begin{aligned}\frac{d\sigma}{dz}(e^+e^- \to CX) &= \sum_q \sigma(e^+e^- \to q\bar{q})[D_q^C(z) + D_{\bar{q}}^C(z)] \\ &= \left(\frac{4\pi\alpha^2}{3s}\right) 3 \sum_q e_q^2 [D_q^C(z) + D_{\bar{q}}^C(z)]\end{aligned} \tag{3.19}$$

where the first bracket is the QED cross section for $e^+e^- \to \mu^+\mu^-$ via the one-photon intermediate state, the additional factor of 3 stems from three different colours of quarks which can be produced, and e_q is the charge of the quark. Clearly C may have been produced from either the q or the $\bar{q}$. Note that

$$z \equiv p_C/q_q \simeq p_C/E \tag{3.20}$$

where E is the electron's centre-of-mass energy, since initially the $q\bar{q}$ pair must carry the full e^+e^- energy.

Similarly, in deep inelastic hadron production $lA \to l'CX$ (where l and l′ are leptons) the cross section is given by

$$\frac{d^3\sigma}{dx\,dy\,dz} = [(3.9) \text{ or } (3.10)]D_c^C(z) \tag{3.21}$$

provided that C is a fragment of the struck quark c and not of the spectators in figure 25.

The form of the $D_c^C(z)$ is partially determined by sum rules, and by the limiting behaviour as $z \to 0$ and 1.

Thus, since the energy of all the hadrons which fragment from a given quark must equal the initial energy of that quark we have

$$\sum_C \int_0^1 z D_q^C(z)\, dz = 1 \tag{3.22}$$

while charge conservation requires

$$\sum_C e_C \int_0^1 [D_q^C(z) - D_{\bar{q}}^C(z)]\, dz = e_q. \tag{3.23}$$

The average multiplicity of hadrons of type C is given by

$$\langle n_C \rangle = \sum_q \int_{z_{\min}}^1 D_q^C(z)\, dz \tag{3.24}$$

where $z_{\min}$ is the lowest value of z possible for a hadron of mass m_C. As $z \to 1$ the hadron takes all of the parton's momentum so any other partons which are left behind in the hadronisation must have negligible momentum. Hence dimensional counting leads us to expect that

$$D_q^C(z) \underset{z \to 1}{\sim} (1-z)^{2n_s - 1} \tag{3.25}$$

where n_s is the minimum possible number of spectators. Thus for a quark q fragmenting into a meson we have $n_s = 1$ if M contains q and $n_s = 3$ if it does not; see figure 30.

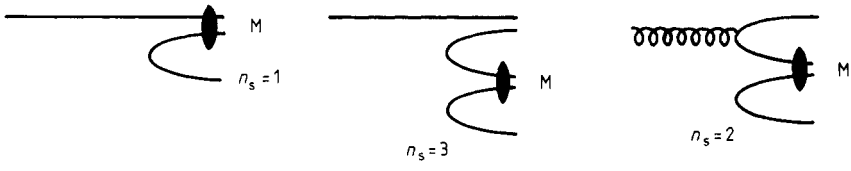

Figure 30. The minimum number of spectators, n_s, accompanying the fragmentation of partons into a meson M.

As $z \to 0$ the essentially massless hadrons are taking none of the parton's momentum and so we expect $D(z) \sim z^{-1}$, which gives a logarithmic increase of $\langle n_C \rangle$ with energy in (3.24). It is thus convenient to approximate

$$D_q^C(z) = D_q^C z^{-1} (1-z)^{2n_s - 1} \tag{3.26}$$

with the normalisation D_q^C bounded by the sum rules (3.22) and (3.23).

3.4. Parton scattering cross sections

The leading-order QCD diagrams for the basic ab → cd sub-process of figure 24 are shown in figure 31. They are very similar to QED diagrams (for example, $qq \to qq$ via gluon exchange is like ee → ee via photon exchange) except for the replacement of α by α_s multiplied by the appropriate SU(3) colour factor. The results are given in table

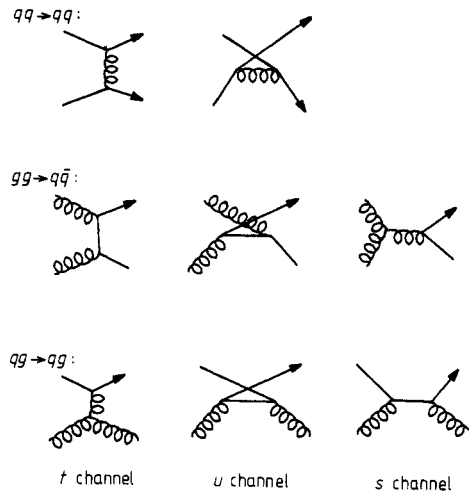

Figure 31. Basic QCD diagrams. Quarks, q, and gluons, g, are shown by straight and curly lines, respectively. The process $q\bar{q} \to q\bar{q}$ has an s channel, but no u channel contribution. In addition there are $gg \to gg$ diagrams.

Table 3. Parton–parton differential cross sections, $d\sigma/dt = \pi\alpha_s^2|A|^2/s^2$, in lowest order, where here s, t, u are the sub-process variables $\bar{s}$, $\bar{t}$, $\bar{u}$ of (3.3). The initial (final) colours and spins have been averaged (summed). The subscripts 1, 2 denote distinct quark flavours. The table is from Combridge *et al* (1977).

Subprocess	$\lvert A\rvert^2$
$q_1q_2 \to q_1q_2$ $q_1\bar{q}_2 \to q_1\bar{q}_2$	$\frac{4}{9}\left(\frac{s^2+u^2}{t^2}\right)$
$q_1\bar{q}_1 \to q_2\bar{q}_2$	As above with $s \leftrightarrow t$
$q_1q_1 \to q_1q_1$	$\frac{4}{9}\left(\frac{s^2+u^2}{t^2}+\frac{s^2+t^2}{u^2}\right)-\frac{8}{27}\frac{s^2}{ut}$
$q_1\bar{q}_1 \to q_1\bar{q}_1$	As above with $s \leftrightarrow u$
$q\bar{q} \to gg$	$\frac{32}{27}\left(\frac{u^2+t^2}{ut}\right)-\frac{8}{3}\left(\frac{u^2+t^2}{s^2}\right)$
$gg \to q\bar{q}$	$\frac{1}{6}\left(\frac{u^2+t^2}{ut}\right)-\frac{3}{8}\left(\frac{u^2+t^2}{s^2}\right)$
$qg \to qg$	$-\frac{4}{9}\left(\frac{u^2+s^2}{us}\right)+\left(\frac{u^2+s^2}{t^2}\right)$
$gg \to gg$	$\frac{9}{2}\left(3-\frac{ut}{s^2}-\frac{us}{t^2}-\frac{st}{u^2}\right)$

3 (see Combridge *et al* 1977, Cutler and Sivers 1978). The value of α_s is known to be $\simeq 0.2$ for $Q = 3$ GeV (e.g. from the charmonium spectrum) so higher-order corrections involving higher powers of α_s should not be very important.

With these cross sections, and the results of the previous subsections, we have all the ingredients needed to obtain the cross section for the hadronic process AB → CX

based on (3.4). But even without a detailed knowledge of the structure and fragmentation functions we can predict the basic form of this cross section. Both f and D are dimensionless functions of dimensionless variables (x and z respectively), so the only scale-dependent factors in (3.4) are the parton differential cross sections of table 3, all of which have the fixed-angle form

$$\frac{d\sigma}{d\hat{t}}(ab \to cd) \sim \frac{1}{\hat{s}^2} = \text{GeV}^{-4}. \tag{3.27}$$

Hence we anticipate that

$$E_C \frac{d^3\sigma}{d^3p_C}(AB \to CX; s, p_T; \theta_{cm}) = F(\theta_{cm}, x_T) p_T^{-4} \tag{3.28}$$

where $x_T \equiv 2p_T/\sqrt{s}$ is dimensionless (as of course is θ_{cm}) and F is a scale-invariant function. But we have already remarked that the $pp \to \pi^0 X$ cross section behaves like p_T^{-8} for $2 < p_T < 6$ GeV/c, bending to perhaps p_T^{-6} for $p_T > 10$ GeV/c (see figure 16). Clearly the parton model which worked so well for lepton scattering processes has failed us. However, a more general scaling parametrisation

$$E_C \frac{d^3\sigma}{d^3p_C} \sim p_T^{-n}(1 - x_T)^m$$

with n and m arbitrary, can account for much of the data on large p_T scattering (Sivers *et al* 1976). This is indicative of an underlying hard scattering process and suggests that it would be premature to discard the whole idea.

4. Scaling violations

As the basic framework outlined in the previous section seems so plausible it is natural to hope that the incorrect prediction, (3.28), is due to the inadequacy of the approximations rather than the fundamental ideas. The next step is thus to try and include higher-order corrections in α_s, the strong coupling constant, to see if these can assist us to better agreement with experiment.

4.1. The coupling constant

We already know one source of violation of the scaling behaviour. We mentioned in § 1 that α_s is not a constant but a logarithmically decreasing function of Q^2 due to the (anti-) shielding of the colour charge. The result, (1.11),

$$\alpha_s(Q^2) = \frac{4\pi}{b_0 \log(Q^2/\Lambda^2)}$$

depends on a free parameter, Λ, which determines the scale at which α_s becomes large, and hopefully results in the confinement of quarks within hadrons. Experiments suggest that $0.1 \leqslant \Lambda \leqslant 0.5$ GeV^2 so α_s should certainly be decreasing with $Q^2 = \hat{t}$. It is claimed that this can reduce the effective power of p_T by as much as one unit in the range $2 < p_T < 6$ GeV/c, though this is critically dependent on the value chosen for Λ within the allowed range (Feynman *et al* 1978). The replacement $\alpha_s \to \alpha_s(Q^2)$ is actually required by the factorisation theorem which we discuss in the next subsection.

4.2. The evolution of the structure and fragmentation functions

In the parton model of § 3 we supposed that each hadron had some definite fixed parton structure described by the structure functions $f_A^a(x)$, which depend only on x. But in QCD each parton can radiate other partons, as in figure 32, so the actual number of partons we see depends on the 'resolving power' of the observing system we employ.

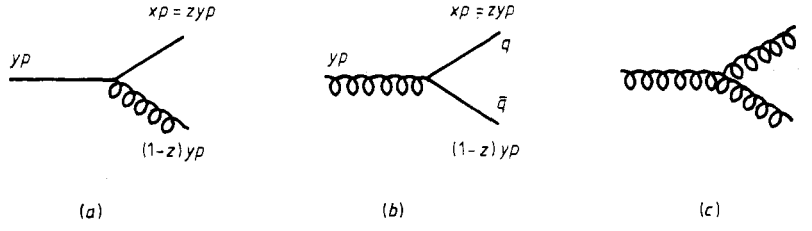

Figure 32. Basic parton processes described by the 'splitting' probability functions (*a*) $P_{q\to q}(z)$ (or $P_{q\to g}(1-z)$), (*b*) $P_{g\to q}(z)$ and (*c*) $P_{g\to g}(z)$.

In electron–proton scattering, for example, the uncertainty principle tells us that the distance resolution is $\Delta x \simeq \hbar/\sqrt{Q^2}$ where $\sqrt{Q^2}$ is the invariant mass of the virtual photon. Thus at low $Q^2(\ll 1\text{GeV}^2)$ an ep scattering experiment will do little more than determine that the proton has a charge and magnetic moment (figure 33(*a*)). At higher Q^2 ($\lesssim 1$ GeV^2) a photon 'sees' the virtual pion cloud (figure 33(*b*)), and the

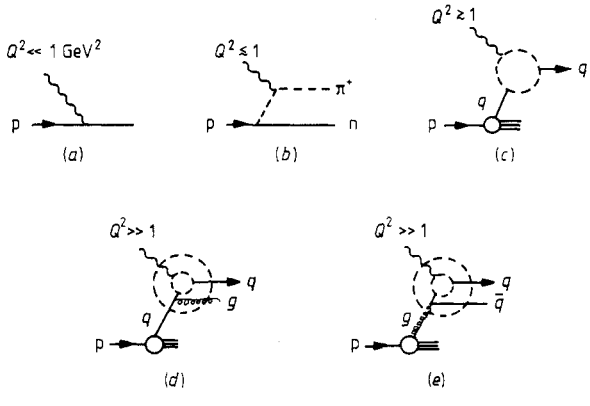

Figure 33. The proton as seen by a virtual photon as Q^2 increases, (*a*)→(*d*), (*e*).

proton appears as an extended composite object described by the form factors $G_{E,M}(Q^2)$. At $Q^2 \gtrsim 1$ GeV^2 we begin to see evidence for the three point-like valence quarks (figure 33(*c*)). If the quarks were non-interacting no further structure would be resolved as Q^2 increased and exact scaling (described by $f_p^q(x)$) would set in. However, due to the basic QCD vertices of figure 32, on increasing the resolution ($Q^2 \gg 1$ GeV^2) we find that each quark is itself surrounded by a gluon cloud and a sea of $q\bar{q}$ pairs. Hence the number of partons which share the hadron's momentum increases with Q^2. There is an increased probability of finding a quark at small x, and a decreased chance of finding one at high x, because the high-momentum quarks

lose momentum by radiating gluons. Hence the structure functions evolve with Q^2 as sketched in figure 34, the total area under the curve remaining fixed to ensure that momentum is conserved.

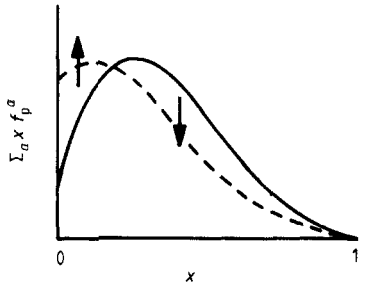

Figure 34. Qualitative pattern of the change of the proton's structure functions with increasing Q^2. Note the increase in the sea quark contribution to xf_p^a at $x = 0$ as Q^2 increases. The area under the two curves is the same. ——, Q_0^2; – – –, Q^2 $(Q^2 > Q_0^2)$.

To determine the Q^2 evolution of structure functions from QCD we follow the physically intuitive approach developed by Altarelli and Parisi (1977). The alternative more formal approach, based on renormalisation group techniques, can be found, for example, in the reviews by Buras (1980) and Reya (1981).

We begin by supposing that the proton consists of valence quarks only, with structure functions $f_p^q(x)$ which give the probability of finding a quark with a fraction x of the proton's momentum, p. Next we consider the possibility that a quark carrying momentum yp emits a gluon, leaving itself with momentum xp $(x \leqslant y \leqslant 1)$ as in figure 32(a). The probability for this is

$$\frac{\alpha_s(Q^2)}{2\pi} P_{q\to q}\left(\frac{x}{y}\right) \log\left(\frac{Q^2}{Q_0^2}\right) \tag{4.1}$$

to first order in the colour coupling α_s. The splitting function $P_{q\to q}(z)$ is similar to that for $e \to e\gamma$ in the QED theory of bremsstrahlung, and can be calculated from the Feynman rules (Altarelli and Parisi 1977) to be

$$P_{q\to q}(z) = \frac{4}{3}\,\frac{1+z^2}{1-z}. \tag{4.2}$$

The divergence as $z \to 1$ is cancelled when virtual gluon contributions are included. The log Q^2 arises because the transverse momentum within the proton is no longer bounded, as it was in the parton model. When one integrates the quark propagator over the available phase space one obtains the integral

$$\int_{Q_0^2}^{\sim Q^2} \frac{\mathrm{d}p_T^2}{p_T^2} \simeq \log\left(\frac{Q^2}{Q_0^2}\right) \tag{4.3}$$

where Q_0 is an arbitrary normalisation mass. Now α_s only decreases like $(\log Q^2)^{-1}$ and so (4.1) does not decrease as $Q^2 \to \infty$ as it stands. However, it is possible to restore perturbation theory by absorbing the log Q^2 term into the definition of the structure function (see, for example, Field 1979). Similarly a gluon with a momentum fraction y may produce a $q\bar{q}$ pair, the resulting quark having a momentum fraction

x, figure 32(b). The splitting function is

$$P_{g\to q}(z)=\tfrac{1}{2}[z^2+(1-z)^2].$$

The evolution of the quark structure function with Q^2 is thus given by

$$\frac{\mathrm{d}f_{\mathrm{p}}^{q}(x,Q^2)}{\mathrm{d}\log Q^2}=\frac{\alpha_{\mathrm{s}}}{2\pi}\int_x^1\frac{\mathrm{d}y}{y}\left[P_{q\to q}\left(\frac{x}{y}\right)f_{\mathrm{p}}^{q}(y,Q^2)+P_{g\to q}\left(\frac{x}{y}\right)f_{\mathrm{p}}^{\mathrm{g}}(y,Q^2)\right]. \tag{4.4}$$

In the same way we can express the Q^2 evolution of the gluon distribution within the proton as

$$\frac{\mathrm{d}f_{\mathrm{p}}^{g}(x,Q^2)}{\mathrm{d}\log Q^2}=\frac{\alpha_{\mathrm{s}}}{2\pi}\int_x^1\frac{\mathrm{d}y}{y}\left[\sum_q P_{q\to g}\left(\frac{x}{y}\right)f_{\mathrm{p}}^{q}(y,Q^2)+P_{g\to g}\left(\frac{x}{y}\right)f_{\mathrm{p}}^{\mathrm{g}}(y,Q^2)\right] \tag{4.5}$$

where the sum is over the different flavours of quarks. As before the 'splitting' probability functions can be calculated from the QCD Feynman rules, and are found to be

$$\begin{aligned}P_{q\to g}(z)&=\frac{4}{3}\left(\frac{1+(1-z)^2}{z}\right)\\ P_{g\to g}(z)&=6\left(\frac{z}{1-z}+\frac{1-z}{z}+z(1-z)\right).\end{aligned} \tag{4.6}$$

Although we can not determine the structure functions, $f(x,Q^2)$, from first principles, we see from (4.4) and (4.5) that, once we have measured them for one value of Q^2, we do know how they will change with Q^2. In practice these equations are not very easy to use because the gluon distributions have to be inferred indirectly (though they cancel from the evolution of the structure function difference $q-\bar{q}$), and because of the effects of higher orders of perturbation theory. The interested reader may like to consult the review by Reya (1981) for a comparison of this theory of scale breaking with the data on deep inelastic scattering. It seems that the scaling violations which occur are at least consistent with QCD.

Precisely similar considerations apply to the fragmentation functions, i.e. $D_{\mathrm{c}}^{\mathrm{C}}(z)\to D_{\mathrm{c}}^{\mathrm{C}}(z,Q^2)$, where the change in D due to the emission of partons (as in figure 35) is given by

$$\begin{aligned}\frac{\mathrm{d}D_q^{\mathrm{C}}(z,Q^2)}{\mathrm{d}\log Q^2}&=\frac{\alpha_{\mathrm{s}}}{2\pi}\int_z^1\frac{\mathrm{d}y}{y}\left[P_{q\to q}(y)\,D_q^{\mathrm{C}}\left(\frac{z}{y},Q^2\right)+P_{g\to q}(y)\,D_g^{\mathrm{C}}\left(\frac{z}{y},Q^2\right)\right]\\ \frac{\mathrm{d}D_g^{\mathrm{C}}(z,Q^2)}{\mathrm{d}\log Q^2}&=\frac{\alpha_{\mathrm{s}}}{2\pi}\int_z^1\frac{\mathrm{d}y}{y}\left[\sum_q P_{q\to g}(y)\,D_q^{\mathrm{C}}\left(\frac{z}{y},Q^2\right)+P_{g\to g}(y)D_g^{\mathrm{C}}\left(\frac{z}{y},Q^2\right)\right].\end{aligned} \tag{4.7}$$

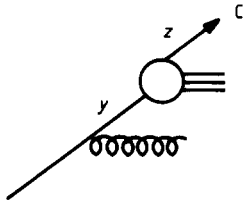

Figure 35. A scaling violation contribution to the fragmentation function D_q^{C}.

There are also parton emission corrections to the basic parton scattering processes of figure 31.

Clearly it is important to know if the structure and fragmentation functions, $f_A^a(x, Q^2)$ and $D_c^C(z, Q^2)$, are process-independent. Then the parton distributions determined from one process (like $ep \to eX$) could be used to help predict hadronic processes (like $pp \to \pi^0 X$), just as in the simple parton model of § 3. Indeed it has been shown that all divergent perturbative contributions to the processes can be summed, factored off and absorbed into universal quark and gluon distributions; and that only the Born approximation diagrams of figure 31 need be included, provided that $\alpha_s \to \alpha_s(Q^2)$. A discussion of, and references to, this powerful factorisation result can be found, for example, in Ellis and Sachrajda (1979) and Reya (1981).

To leading order the scaling violations to the hadronic process $AB \to CX$ can therefore be included in an elegant and simple way. All we have to do is to replace (3.4) by

$$E_C \frac{d\sigma}{d^3 p_C} = \sum_{abcd} \int_0^1 dx_a \int_0^1 dx_b f_A^a(x_a, Q^2) f_B^b(x_b, Q^2) \frac{1}{\pi z_c} \frac{d\sigma}{d\hat{t}}(ab \to cd) D_c^C(z_c, Q^2) \tag{4.8}$$

where the parton distributions are those measured in deep inelastic lepton scattering and where the Born diagrams of figure 31 are used, with $\alpha_s(Q^2)$, to calculate the hard-scattering sub-process $ab \to cd$. There remains, however, a problem as to what to take for Q^2 in α_s. For different diagrams $Q^2 = \hat{s}, \hat{t}, \hat{u}$, or some combination thereof might seem appropriate. A common practice is to employ a symmetrical combination such as $Q^2 = \hat{s}\hat{t}\hat{u}/(\hat{s}^2 + \hat{t}^2 + \hat{u}^2)$. Such substitutions make no difference to the leading log Q^2 term, but leave a significant ambiguity in the low p_T prediction.

It is found that with these changes the cross section is predicted to behave like p_T^{-6} approximately at large p_T (Field 1979). This is certainly better than the p_T^{-4} behaviour of the naive parton model, and seems fairly satisfactory for the $p_T > 6$ GeV/c data of figure 37, but does not account for the higher powers of p_T observed for $p_T < 6$ GeV/c in so many processes.

4.3. Intrinsic parton k_T

A rather serious defect of the parton model of § 3 is that the partons are assumed to be travelling colinearly with their parent hadron with no motion in sideways directions. In fact, this cannot be correct because the partons are confined within the radius of the hadron (typically of the order of 0.5 fm) and so by the uncertainty principle must have a momentum spread ('Fermi motion') $\Delta k \simeq \hbar/(0.5\text{ fm}) \simeq 0.4$ GeV/c transverse to the hadron's direction. This has the consequence that the p_T of the observed hadron, C, may in part be due to the fact that partons a and b already had a net sideways motion, as in figure 36(a), even before scattering occurred. We denote this transverse momentum of the initial state by

$$\boldsymbol{k}_T = \boldsymbol{k}_{aT} + \boldsymbol{k}_{bT}. \tag{4.9}$$

Furthermore the partons may acquire transverse momentum by parton emission before scattering. Thus in figure 36(b) parton a recoils from a radiated gluon before hitting b. This effect can be calculated perturbatively, at least for large k_T. It is often added to the Fermi motion, though it is not clear that these are entirely separate

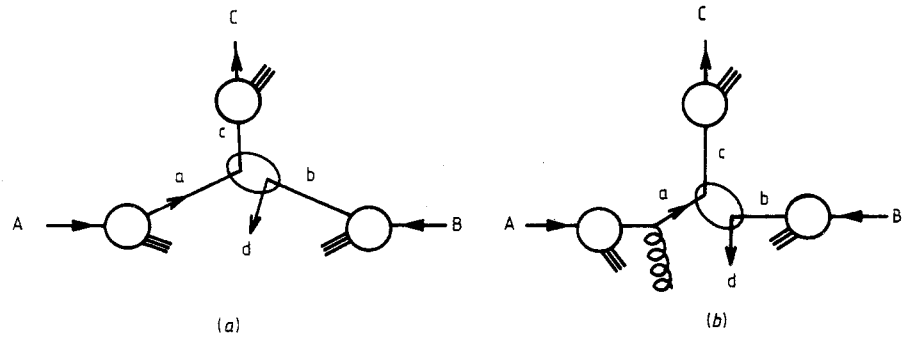

Figure 36. A sketch of (*a*) the intrinsic k_T due to sideways motion of partons a and b and (*b*) the 'effective' k_T due to bremsstrahlung, of partons before the hard scattering sub-process ab→cd. The effect of the bremsstrahlung contributions can be calculated using perturbative QCD, but only at large k_T; diagram (*b*) shows a lowest-order α_s contribution to the k_T of parton a.

effects since if the gluon is reabsorbed by the other fragments of A it obviously constitutes part of the binding of a into A which creates the Fermi motion.

This intrinsic k_T can be observed rather directly in the Drell–Yan process AB→$\mu^+\mu^-$X. If only the lowest-order diagram, figure 26, is considered then the $\mu^+\mu^-$ pair should have no net transverse momentum, i.e. $\boldsymbol{p}_T \equiv \boldsymbol{q}_{T\mu^+} + \boldsymbol{q}_{T\mu^-} = 0$, but in practice $p_T \neq 0$ because quarks a and b have transverse momentum, and $\boldsymbol{p}_T = \boldsymbol{k}_T$. The p_T distribution is found to be approximately Gaussian $[\exp(-p_T^2/\langle p_T^2\rangle)]$ with $\langle p_T^2\rangle \simeq 1.9\ (\mathrm{GeV}/c)^2$, roughly independent of s and Q^2, corresponding to an effective $\langle k_T\rangle \simeq 0.85\ \mathrm{GeV}/c$ per parton.

The inclusion of this effect in large p_T hadron production is not straightforward. The difficulty stems from the fact that the tail of the Gaussian k_T distribution permits particle C to be produced with $\boldsymbol{p}_T = \boldsymbol{k}_T$, i.e. its transverse momentum stems entirely from the intrinsic k_T of the partons, so $\bar{t} = 0$ in the parton scattering process ab→cd. However, the Born approximations of table 3 contain an IR divergence for $\bar{t} = 0$ and so the cross section for C production is predicted to be infinite! This nonsensical conclusion stems from the fact that we are still trying to use table 3 for small $\bar{t}$ where $\alpha_s(\bar{t})$ is very large, and the perturbation expansion in α_s, of which these results are just the first term, breaks down.

It is possible to circumvent this difficulty by some such device as replacing $\bar{t} \to \bar{t} - t_0 (t_0 > 0)$ in table 3, or by setting $\mathrm{d}\sigma/\mathrm{d}\bar{t} = 0$ for $|\bar{t}| < t_0$ in (4.8), but then the final result is quite sensitive to the method adopted and the choice of t_0, which becomes an arbitrary free parameter. Moreover, the interacting partons are off their mass shell by an amount which depends on k_T, and if the correct off-shell kinematics are used in (4.8) this intrinsic transverse momentum does not make so much difference.

It has been found that by including all the above corrections to the naive parton model of § 3 the data on pp→π^0X (which has the greatest range of p_T of any process so far measured) can be fitted successfully. An example is shown in figure 37. Very roughly the p_T^{-n} behaviour is changed from $n = 4$ in the naive parton model to 5 with $\alpha_s(Q^2)$, $n \simeq 6$ when f, D are functions of Q^2, and $n \simeq 8$ for $2 < p_T < 6\ \mathrm{GeV}/c$ when intrinsic k_T is included. However, quite apart from the reservations one must feel as to whether the intrinsic k_T has been incorporated correctly, explaining the data in this way leads one to expect a similar behaviour, with only minor changes due to different f and D, for all large p_T cross sections. At least for moderate $p_T (2 < p_T <$

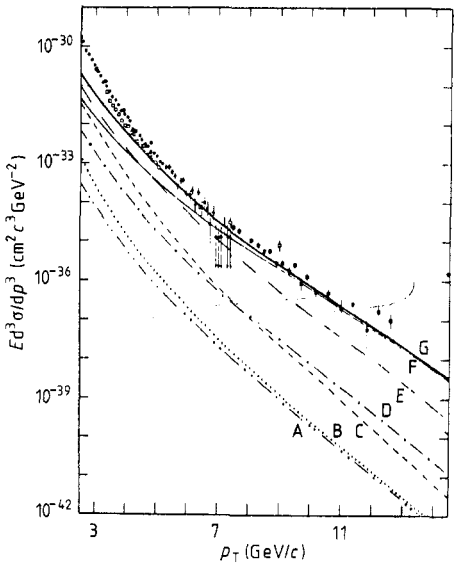

Figure 37. A fit to $pp \to \pi^0 X$ data at large p_T by Owens *et al* (1978) showing the individual sub-process contributions. The agreement at small p_T can be somewhat improved by including intrinsic k_T effects. A, $q\bar{q} \to gg$; B, $gg \to q\bar{q}$; C, $gg \to gg$; D, $q\bar{q} \to q\bar{q}$; E, $gq \to gq$; F, $qq \to qq$; G, total.

6 GeV/c) this is not borne out by experiment, so some further corrections are clearly necessary.

4.4. Other contributions

The corrections which we have included so far should be sufficient in the leading log approximation, i.e. for $\log(p_T^2/\Lambda^2) \gg 1$ where Λ is the QCD mass scale parameter ($\Lambda \lesssim 1$ GeV). However, there are many other corrections of the form $p_T^{-m}(m > 4)$ which may be important at moderate values of p_T. These arise if more than the minimal number of partons are involved in the scattering process.

For example, in inclusive meson production $AB \to M'X$, instead of the basic $qq \to qq$ process and similar processes of figure 31, we might have the sub-process $qM \to qM'$ where M is a $q\bar{q}$ cluster of fixed mass and M′ is the detected 'trigger' particle (see figure 38). Comparing the two competing types of sub-process we have

$$\frac{d\sigma/d\hat{t}\,(qM \to qM')}{d\sigma/d\hat{t}\,(qq \to qq)} \sim F_M^2(p_T^2) \sim p_T^{-4} \tag{4.10}$$

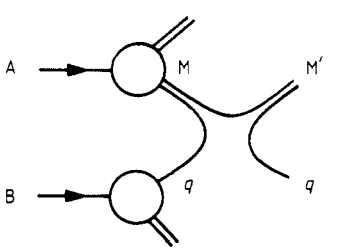

Figure 38. The $qM \to qM'$ contribution to $AB \to M'X$ drawn as in the constituent interchange model (CIM).

where F_M is the meson transition form factor. Obviously the $qM \to qM'$ contribution is not as important as $qq \to qq$ at large p_T, but it may be quite significant at moderate values of p_T. There is, after all, a large probability of finding the meson M in the incoming hadron (recall the meson 'cloud' of the proton) and if M′ of the sub-process is the 'trigger' particle there is no further diminution of the cross section due to a final $q \to M'$ fragmentation. For $qq \to qq$ the outgoing quark gives only a part of its momentum to the trigger particle M′, so the sub-process occurs at an effectively higher p_T where the cross section is much smaller. We speak of 'trigger bias' since the fragmentation needed to produce a single particle reduces the cross section as compared to that for jet production.

Basic processes of the type $qM \to qM'$ often involve the exchange of quarks and are called 'constituent interchange mechanisms', or CIM for short (Sivers *et al* 1976) as in figure 38. According to the dimensional counting rules of § 2.3 each CIM diagram gives a $(p_T^2)^{2-n}$ contribution to the inclusive cross section, where n is the number of partons taking part in the sub-process. Thus for $qM \to qM'$ we have $n = 6$ leading to a p_T^{-8} behaviour, as expected from (4.10). The process $\bar{q}q \to \bar{M}M'$ also has $n = 6$, whereas $MM \to MM'$ has $n = 8$ and so on. Similarly we expect the structure functions will have corrections of the form $f_A'^a(x)(Q^2)^{-m}$ with $m = 2, 4, \ldots$, due to internal gluon exchanges, etc, as in figure 39. For technical reasons these are called 'higher

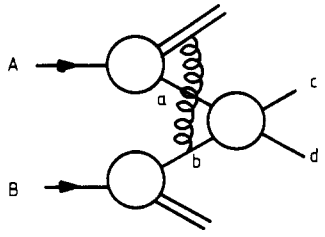

Figure 39. A higher twist diagram which involves an interaction with a 'spectator' parton.

twist' effects (see Buras 1980) and though clearly irrelevant for large Q^2 the fact that their magnitude is unknown makes the precise determination of the logarithmic scaling violations of the leading term ($n = 4$) difficult.

One thus ends up with a sequence of terms:

$$E_C \frac{d^3\sigma}{d^3p_C}(AB \to CX) = F_1(\theta_{cm}, x_T)p_T^{-4} + F_2(\theta_{cm}, x_T)p_T^{-6} + \cdots \tag{4.11}$$

each of which should enjoy logarithmic scaling corrections. Some fairly satisfactory fits to the data along these lines have been made (Jones and Gunion 1979), but the presence of arbitrary normalisation parameters makes their significance hard to assess. In $pp \to \pi^0 X$ the p_T^{-4} parton scattering mechanism does not seem to dominate until $p_T > 10\ \text{GeV}/c$, and instead for $2 < p_T < 6\ \text{GeV}/c$ the p_T^{-8} $qM \to qM$ contribution is the most significant. This is also true in $pp \to \pi^{\pm} X$, whereas in $pp \to pX$ the behaviour is p_T^{-12} as expected for $qB \to qp$.

These CIM processes involve the exchange of quarks and hence of flavour quantum numbers. This can be tested by comparing the quantum numbers of the trigger particle, C, with those of the particles X which have the opposite sign for p_T and which presumably result from the fragmentation of d (Brodsky 1979a, b). With gluon

exchange there will be no quantum number correlations between the two sides whereas with quark exchange the opposite-side particles are likely to have the opposite sign of charge (and other additive quantum numbers) to C. Some such correlation is in fact observed at moderate p_T (see figure 40) and argues in favour of CIM contributions. On the other hand, it is found that the cross sections for $\pi^- p \to \pi^- X$ and $\pi^- p \to \pi^+ X$ are almost equal for $2 < p_T < 6$ GeV/c, as one would expect for the flavour-blind gluon exchange, but quite contrary to CIM which predicts the π^- should predominate due to hard scattering of the incident π^-.

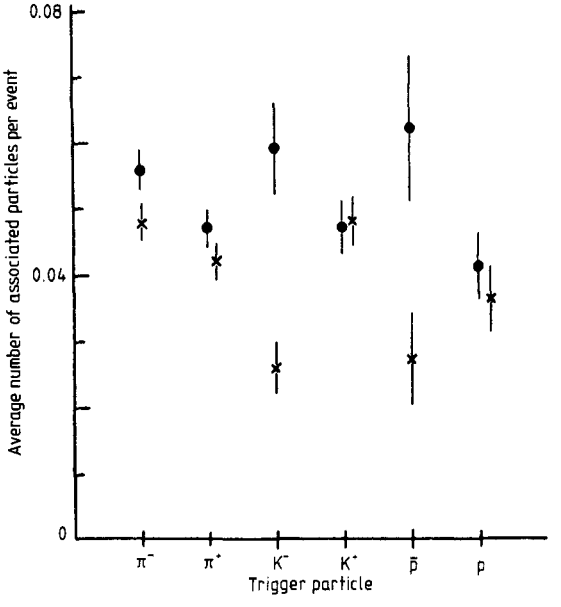

Figure 40. Charge correlations for various types of trigger taken from Albrow *et al* (1978). The dots and crosses are the average number of fast positive and negative particles, respectively, on the side away from a 90° trigger. $3 < p_{trig} < 4.5$ GeV/c, $p_T > 1.5$ GeV/c, $|y| < 1$, $|\varphi| < 30°$.

The intermediate p_T region (2–6 GeV/c) is thus rather confusing, and neither parton scattering nor CIM seems able to explain all aspects of the data, but at larger p_T the parton model with QCD corrections does seem to be in quite good agreement with the admittedly modest quantity of data available to date.

5. Jets

5.1. Introduction

After a hard scattering process such as figure 24 there will be partons flying apart with a large relative momentum, but carrying a colour charge, which we believe to be a confined quantity. The partons must thus dispose of their momentum by radiating colourless hadrons. It is this process which we have parametrised by the fragmentation functions $D_c^C(z, Q^2)$ in the preceding sections. We now want to look at the way this actually happens in a bit more detail (see, for example, Dokshitzer *et al* 1980, Webber 1982).

It is convenient to consider first $e^+e^- \to$ hadrons since in this process there are no coloured partons in the initial state to complicate matters (see, for example, Wiik and Wolf 1979, Wolf 1980). The parton model description is shown in figure 41(*a*) in

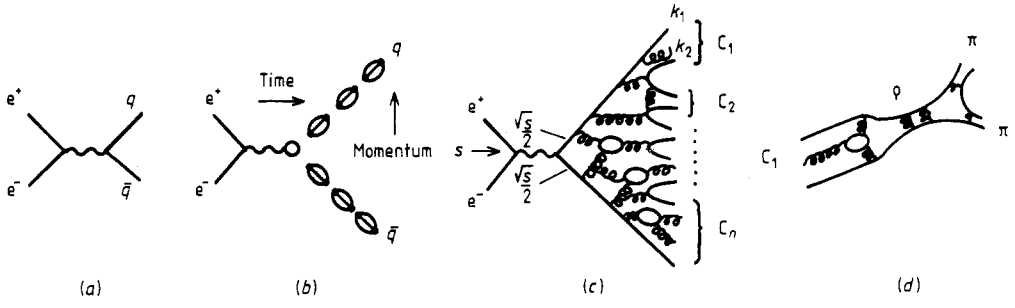

Figure 41. The process $e^+e^- \to$ hadrons.

which initially there is a quark and an antiquark, each carrying colour charge and trying to leave the interaction region. The colour lines of force thus get stretched and so the force between the quarks increases, rather as if they were attached to the two ends of an elastic band. One might at first suppose that this $q\bar{q}$ pair would therefore be compelled to remain as a single $(q\bar{q})$ hadron, at rest in the e^+e^- centre-of-mass system but with a very large internal energy (i.e. $\sqrt{s}$ = hadron mass). However, as we noted in § 1, it is energetically more favourable for the 'string' to break by the formation of additional $q\bar{q}$ pairs (i.e. colour polarisation of the vacuum occurs) leaving a collection of colourless states with only rather short lines of force (~ 1 fm) which are, of course, low-mass hadrons, mainly pions.

The way in which these hadrons may develop with time is shown in figure 41(*b*) and a typical Feynman-like diagram representing such an event in figure 41(*c*) (Konishi *et al* 1979). At the photon vertex there is a q and a $\bar{q}$, each with momentum $\simeq \sqrt{s}/2$, but confined and hence having a virtual mass k given by $k^2 = s$. They are thus far off the quark mass shell $k^2 = m_q^2 \simeq 0$. But each successive branching (gluon emission, $q\bar{q}$ creation, etc) reduces the momentum of the individual partons until clusters can be found with $k_C^2 = (k_1 + k_2 + \cdots)^2 = m_C^2$ in which $m_C^2 = m_h^2$, the mass of some hadron. If such a cluster has zero net colour it is likely to combine to form this hadron (since $\alpha_s(m_C^2)$ is large), which is then free to leave the interaction region (figure 41(*d*)). In this way we expect two back-to-back jets of hadrons to occur (figure 42), sharing between them the momentum of the initial q or $\bar{q}$, and each having only a small momentum component transverse to the quark's direction of motion, $p_T \lesssim \Lambda$ (Amati and Veneziano 1979).

As we shall see later, it is also possible for one of the quarks to emit a 'hard' gluon (which has a large transverse momentum component, $k_T \gg \Lambda$), in which case there will be a three-jet event, as in figure 43.

In the initial stages of this evolution all the virtual parton masses are large, $k_i^2 \gg \Lambda^2$, and so $\alpha_s(k_i^2)$ is small and the diagrams can be evaluated by the usual rules of Feynman perturbation theory (Ellis *et al* 1976). In fact, the probability of a particular branching process occurring is given by (4.1) and (4.6) and hence a perturbative 'jet calculus' can be derived (Konishi *et al* 1979). But in the final stages where the partons are combining into hadrons (figure 41(*d*)) α_s is not small and so they are not amenable

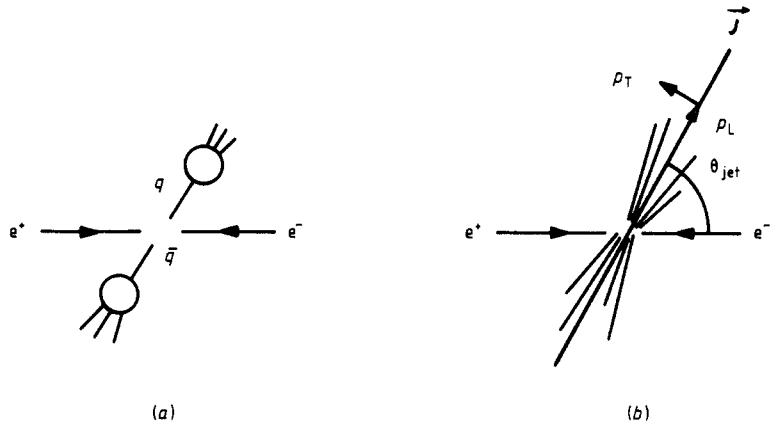

Figure 42. The process $e^+e^- \rightarrow$ two jets.

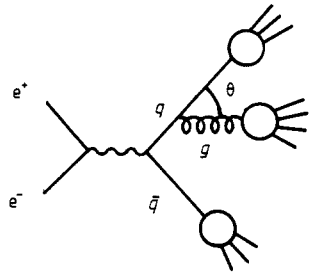

Figure 43. The process $e^+e^- \rightarrow$ three jets.

to QCD calculations so far. Despite this we can reasonably expect that the sum of the momenta of the hadrons in a jet will correspond (to an accuracy $\simeq \Lambda$) to the momentum of the parent parton.

5.2. Jets in $e^+e^- \rightarrow$ hadrons

To test whether such jets are in fact occurring experimentally it is useful to define a measure of the degree of 'jettyness' exhibited by the hadrons produced in an event (Wiik and Wolf 1979). In the centre-of-mass system the q and $\bar{q}$ are initially moving with equal and opposite momentum along some jet axis $\boldsymbol{J}$ (figure 42). We expect the hadrons in the jets to be travelling more or less in this direction too, and so to find the direction of $\boldsymbol{J}$ we look for the axis such that the magnitudes of the particles' momentum components, p_T, transverse to $\boldsymbol{J}$ are minimised, while their longitudinal components (p_L) are maximised. Two such jet measures are (Bjorken and Brodsky 1970, Farhi 1977)

$$\text{sphericity} \qquad S \equiv \min_{\boldsymbol{J}} \left(\frac{3}{2} \frac{\Sigma_i p_{T_i}^2}{\Sigma_i p_i^2} \right) \tag{5.1}$$

$$\text{thrust} \qquad T \equiv \max_{\boldsymbol{J}} \left(\frac{\Sigma_i |p_{L_i}|}{\Sigma_i p_i} \right) \tag{5.2}$$

where the sum runs over all the particles i in the event, and the extrema are chosen by varying the direction of $\boldsymbol{J}$. If there were no jets and all momentum directions were equally probable, then $S=1$ and $T=\frac{1}{2}$, irrespective of the choice of $\boldsymbol{J}$. For perfect jets all the hadrons would be travelling along a given axis and so the extrema would be $S=0$ and $T=1$ when $\boldsymbol{J}$ is along that axis.

Figure 44 illustrates the way in which the average sphericity and thrust of $e^+e^- \to$ hadrons events vary as a function of the energy and it will be seen that $\langle S\rangle$ and $1-\langle T\rangle$ do indeed become quite small at high energies. They do not vanish, however, indicating that some hadrons always have a finite p_T.

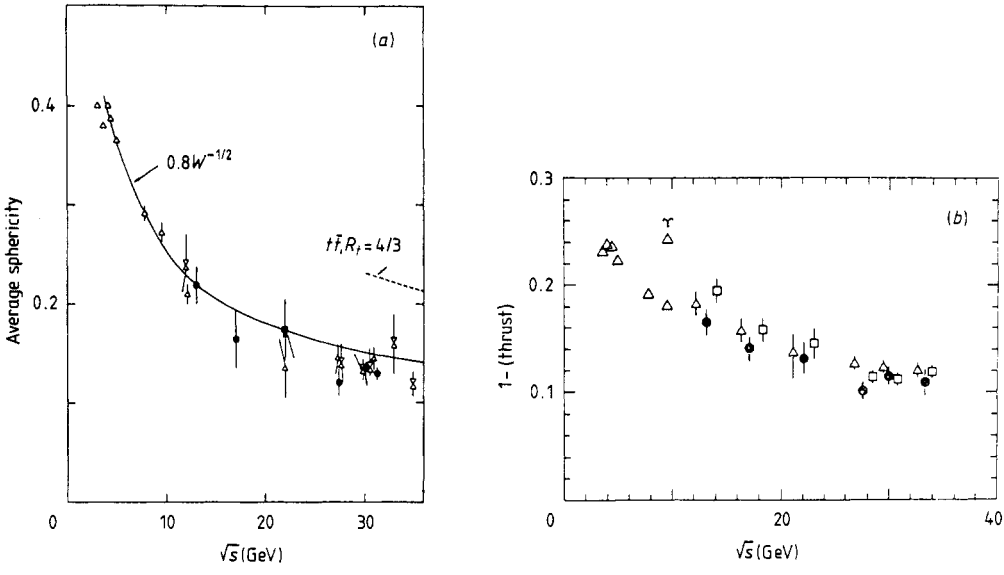

Figure 44. The average sphericity (a) and $1-$thrust (b) as a function of the e^+e^- CM energy (Wolf 1980). ⧖ JADE, △ PLUTO, ● TASSO, □ MARK-J.

In part this is presumably due to the confinement mechanism. We have noted in § 4 that partons which are confined within hadrons have a Fermi momentum component perpendicular to the hadron's direction of motion, with $\langle k_T^2\rangle \simeq 0.3\ \text{GeV}^2$. We must thus expect that any hadrons radiated from a parton will have a complementary $\langle p_T^2\rangle \simeq 0.3\ \text{GeV}^2 (\simeq \Lambda^2)$ and this is borne out by figure 45. The jet direction thus becomes better defined as the jet energy ($\frac{1}{2}\sqrt{s}$), and hence the average p_L, increases, and the jet opening angle decreases with energy roughly like

$$\theta \sim \frac{\langle p_T\rangle}{\langle p_L\rangle} \sim \frac{1}{\sqrt{s}}. \tag{5.3}$$

However, it will be seen that $\langle p_T^2\rangle$ increases slowly with energy. This behaviour is also expected in QCD because we must also consider diagrams such as figure 43, for example, in which one of the quarks radiates a gluon. If we denote the energy fractions carried by the three final-state partons as

$$x_i = 2E_i/\sqrt{s} \qquad i = q, \bar{q}, g \tag{5.4}$$

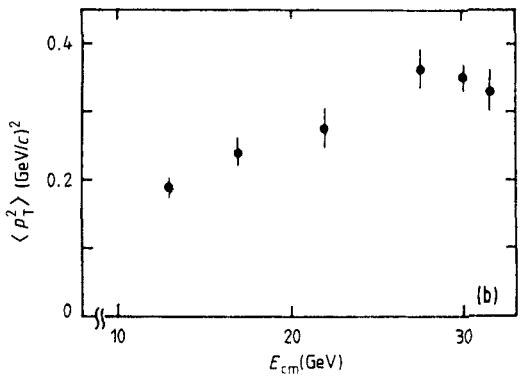

Figure 45. The average transverse momentum squared of hadrons with respect to the jet axis (Wolf 1980).

then for massless partons the differential cross section for the process $e^+e^- \to q\bar{q}g$ is

$$\frac{d^2\sigma}{dx_q\, dx_{\bar{q}}} = \frac{2\alpha_s}{3\pi}\sigma(e^+e^- \to q\bar{q})\frac{x_q^2 + x_{\bar{q}}^2}{(1-x_q)(1-x_{\bar{q}})}. \tag{5.5}$$

This expression introduces one of the principal problems of using QCD perturbation theory, for it diverges as x_q or $x_{\bar{q}} \to 1$. Now by four-momentum conservation

$$s(1-x_{\bar{q}}) = (p_q + p_g)^2 = 2p_q \cdot p_g = 2E_qE_g(1-\cos\theta) \tag{5.6}$$

where θ is the angle between the outgoing quark and the gluon. So $x_{\bar{q}} \to 1$ if either $E_g \to 0$, i.e. if the gluon carries no energy, or if $\theta \to 0$, i.e. if the gluon travels along the direction of its parent quark. These are known as the infrared (IR) and colinear divergences, respectively, and plague any theory containing massless particles (including QED) (Dokshitzer *et al* 1980, Webber 1982). Indeed we have already met the IR divergence in §§ 4.2 and 4.3.

For small E_g, θ (5.5) gives

$$\frac{d^2\sigma}{dE_g\, d\theta} \sim \frac{\alpha_s}{E_g\theta}\sigma(e^+e^- \to q\bar{q}) \tag{5.7}$$

and so the average transverse momentum of the gluon is

$$\langle k_T \rangle \sim \frac{\alpha_s\sigma}{\sigma}\int \frac{E_g \sin\theta}{E_g\theta}\, dE_g\, d\theta \sim \alpha_s\sqrt{s} \sim \frac{\sqrt{s}}{\log s}. \tag{5.8}$$

If this is reflected in the transverse momentum of the hadrons then (5.3) suggests that the jet opening angle will decrease only like $(\log s)^{-1}$ at very high s. This is presumably the origin of the observed slow increase of $\langle p_T^2 \rangle$ with s in figure 45.

If E_g and θ are not small we can expect to see a third (gluon) jet, in addition to the two quark jets, and such events have indeed been observed in high-energy e^+e^- annihilation experiments. Since in (5.5) the relative probability of $q\bar{q}g/q\bar{q}$ is of the order of α_s (see Wiik and Wolf 1979), the magnitude of the three-jet cross section relative to that for two jets can be used to determine that $\alpha_s \simeq 0.18$ for $\sqrt{s} \simeq 30$ GeV (Wiik 1980).

The divergence in (5.5) will obviously give a divergent contribution to the total cross section for $e^+e^- \to$ hadrons. However, we know that real massless gluons are not seen, and this divergence can be 'regularised' away by giving the gluon a finite

mass, m_g (see, for example, Field 1979a,b), in which case the $x_{\bar{q}} \to 1$ region of the integration of (5.5) over the x gives

$$\sigma(e^+e^- \to q\bar{q}g) \simeq \sigma(e^+e^- \to q\bar{q}) \frac{2\alpha_s}{3\pi} \log\left(\frac{m_g^2}{s}\right). \tag{5.9}$$

This dependence on the gluon mass looks unpleasant, but in fact it can be shown that this term is precisely cancelled by the corresponding $O(\alpha_s)$ correction to $\sigma(e^+e^- \to q\bar{q})$ shown in figure 46(c), and that the sum of the diagrams in figure 46 leaves us with the $O(\alpha_s)$ correction:

$$\sigma(e^+e^- \to \text{hadrons}) = \sigma(e^+e^- \to \mu^+\mu^-) \sum_q e_q^2 \left(1 + \frac{\alpha_s}{\pi}\right) \tag{5.10}$$

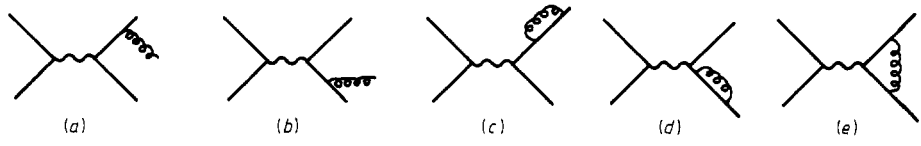

Figure 46. Lowest-order contributions to $e^+e^- \to q\bar{q}g$ (a), (b) and corrections to $e^+e^- \to q\bar{q}$ (c), (d), (e).

where $\sigma(e^+e^- \to \mu^+\mu^-)$ is the cross section (2.15), and the final answer, (5.10), is independent of m_g despite (5.9).

The total hadron cross section is thus IR-safe (certainly to first order in α_s and presumably to all orders), i.e. it has no singularities as $m_g \to 0$. This is because the total cross section is independent of the number of partons produced: it does not make any difference whether we regard the gluon in figure 43 as part of the quark jet, or as providing a separate jet. Similarly a quantity such as thrust, which depends linearly on the momenta, and hence by momentum conservation is independent of the number of partons in the final state, is IR-safe and can be calculated in perturbation theory. To first order (De Rujula *et al* 1978)

$$1 - \langle T \rangle = 1.57 \frac{2}{3} \frac{\alpha_s}{\pi}. \tag{5.11}$$

But the sphericity, being quadratic in the momenta, is not IR-safe, and cannot be predicted by perturbative QCD. The number of partons produced in an event is not experimentally observable since whenever off mass-shell partons find themselves in clusters having an invariant mass of order Λ, $\alpha_s \to 1$ and hadronisation occurs as described above.

Another example of how to overcome these IR problems has been given by Sterman and Weinberg (1977) (see also Webber 1982). In the naive parton model of figure 41(a) one expects that the angular distribution of the quark jet axis $\boldsymbol{J}$ in $e^+e^- \to q\bar{q}$ will be the same as that of the μ distribution in $e^+e^- \to \mu^+\mu^-$, viz

$$\frac{d\sigma}{d\Omega} = \frac{\alpha^2}{4s}(1 + \cos^2\theta) \tag{5.12}$$

where θ is the angle between the direction of motion of the muons and the direction of the electron beam in the centre-of-mass system. However, if one tries to calculate the corrections caused by higher-order processes such as $e^+e^- \to q\bar{q}g$ one again runs into divergence problems due to the massless gluons. Instead Sterman and Weinberg define an event as a two-jet event if all but a fraction $\epsilon (\ll 1)$ of the total energy of

the event falls within two back-to-back cones of opening angle δ. They then use perturbative QCD to calculate the cross section in the form

$$\frac{d\sigma}{d\Omega_{jet}}(\epsilon, \delta) = \frac{d\sigma}{d\Omega_0} \sum_q e_q^2 f(\delta, \epsilon) \tag{5.13}$$

where $d\sigma/d\Omega_0$ is the QED cross section of (5.12) which has to be modified by the charges of the produced quarks, and f contains QCD corrections which in first order in α_s include terms such as $\alpha_s \log(1/\delta) \log(1/\epsilon)$ which diverge if we try to define the jets too closely by making δ or ϵ small.

Very similar jets to those in $e^+e^- \to$ hadrons are also seen in the current fragmentation region of deep inelastic scattering, such as $ep \to eX$, where the struck quark fragments seemingly independently of the spectator partons (see Di Lella 1979, Darriulat 1980).

5.3. Jets in hadron scattering

As we noted in § 2, large p_T hadron scattering processes are predominantly four-jet events, as in figure 17. Two of the jets contain fragments of the incoming hadrons and hence continue more or less in the forward direction, while the two wide-angle back-to-back jets, stemming from the hard scattered partons, contain particles with large p_T. Thus, accompanying the large p_T particle which has triggered the detectors to tell us that a large p_T event has occurred, there are other particles, travelling in essentially the same direction, forming a 'same-side' jet, and in the opposite hemisphere an 'away-side' jet. Figure 47 shows that large p_T particles whose rapidities are closely correlated with that of the trigger particle are found on both the same and the opposite sides. The longitudinal jets appear to be the same as those observed in ordinary hadron scattering when no large p_T particle is produced. These will be the subject of the next section.

This type of triggering on a single high p_T particle, though very convenient experimentally, greatly reduces the probability of observing jets because the fragmentation functions depress the likelihood of a single particle carrying a significant fraction of the jet's momentum (Jacob and Landshoff 1978).

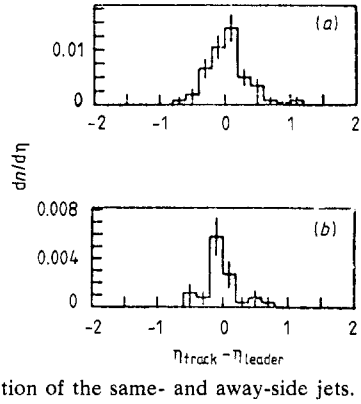

Figure 47. The rapidity correlation of the same- and away-side jets. The data are the charged particles associated with a π^0 with $p_T \geq 7$ GeV/c that is produced in the opposite hemisphere. The rapidity ($\eta = y$) is referred to that of the 'hardest' away particle (the leader), and we see that the collimation increases with the p_T of the leader. (*a*) $3 < p_T < 4$, (*b*) $4 < p_T < 5$ GeV/c.

To illustrate this suppose that the cross section for producing a parton jet with large P_T behaves as

$$\frac{d\sigma(\text{jet})}{dP_T} = \frac{A}{P_T^N} \tag{5.14}$$

and that the jet then fragments into hadrons carrying a longitudinal fraction z of the jet's momentum with probability $D(z)$, then

$$\begin{aligned}\frac{d\sigma(\text{particle})}{dp_T} &= \int_0^1 dz \int dP_T \frac{A}{P_T^N} D(z)\delta(p_T - zP_T) \\ &= \frac{A}{p_T^N}\int_0^1 D(z)\, z^{N-1}\, dz.\end{aligned} \tag{5.15}$$

So if we take $D(z) = (1-z)^m/(m+1)z$, corresponding to the form (3.26) with the normalisation satisfying the momentum sum rule (3.22), then

$$\left.\frac{d\sigma(\text{particle})/dp_T}{d\sigma(\text{jet})/dP_T}\right|_{P_T = p_T} = \frac{(N-2)!\,m!}{(m+1)(N+m-1)!}. \tag{5.16}$$

Thus for π production from a quark jet with $m = 2n_s - 1 = 1$ and $N = 8$, as observed, the ratio is $1/112$. So single-particle cross sections should be suppressed with respect to jet cross sections by at least two orders of magnitude (three with larger m, N). The two types of cross section should show the same dependence on p_T, however. Both these expectations are borne out by figure 48, though of course much depends on how the jet cross section is defined experimentally, i.e. which particles are included in the jet and which, because they are moving too slowly or at too large an angle to the jet axis, are excluded. Nowadays jet cross sections can be obtained using calorimeters which trigger whenever sufficient total hadron energy is deposited at a large angle to the beam direction, but of course it is still not possible to be sure that the calorimeter has caught all the jet particles, and no others.

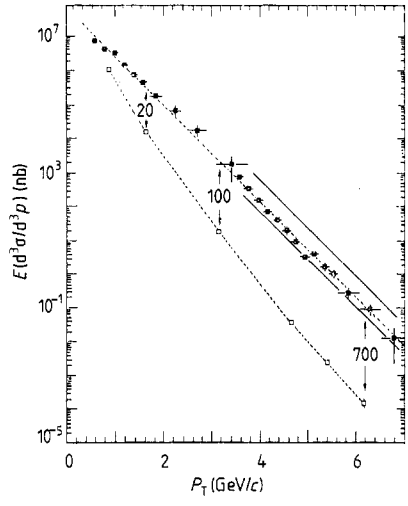

Figure 48. The inclusive jet production cross section (■) compared to inclusive single π production (□) taken from the review by Darriulat (1980).

The best way to remove any such bias is to look at the away-side jet opposite to a high p_T trigger. Since the quark fragmentation functions are suppressed at large z less than those describing gluon fragmentation (see (3.25) and figure 30) it is more likely that the large p_T trigger particle is from a quark jet, but the opposite side may quite often be a gluon jet. If there were great differences between quark and gluon jets we might expect that these away-side jets in large p_T hadron scattering would look somewhat different from the jets in $e^+e^- \rightarrow$ hadrons and DIS. In fact, the data show that the average multiplicity (figure 49), the shape of the fragmentation functions

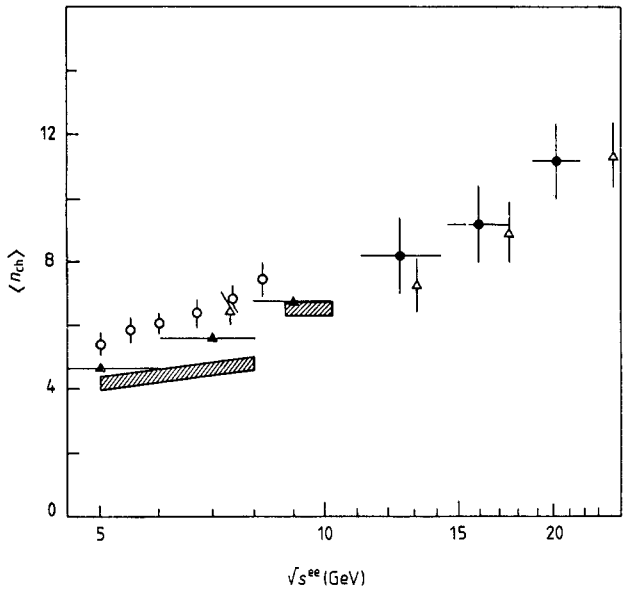

Figure 49. The mean charged multiplicity of hadron jets measured in large p_T hadronic processes (○), in νp interactions (▲), and in e^+e^- annihilations (shaded zones and △), taken from Darriulat (1980). All data are referred to the equivalent e^+e^- energy.

(figure 50), and the average transverse momentum of the particles with respect to the jet axis, are all consistent in the three types of process. The modest accuracy of the data, and the uncertainty as to which particles should be included in the jets, obscure any differences there may be between quark and gluon jets. There should also be higher-order, five and more jet events when the quarks radiate hard gluons, etc, but as yet these have not been clearly distinguished.

A very interesting problem is the extent to which the flavour quantum numbers of the particles produced in a jet reflect the flavour of the parent parton. If we adopt a simple model such as figure 51(a) in which all the particles produced above the broken line are regarded as having large p_T, and hence are included in the quark jet, while those below it are slow particles and not part of the jet, then the average charge of the jet will be (Brodsky and Weiss 1977)

$$\langle Q_{\text{jet}} \rangle = Q_q + \langle Q_{\bar{q}} \rangle \tag{5.17}$$

where Q_q is the charge of the quark and the second term on the right-hand side represents the average charge of the $\bar{q}$ line, which must also be cut by the broken line if only colour neutral particles are to appear in the jet final state.

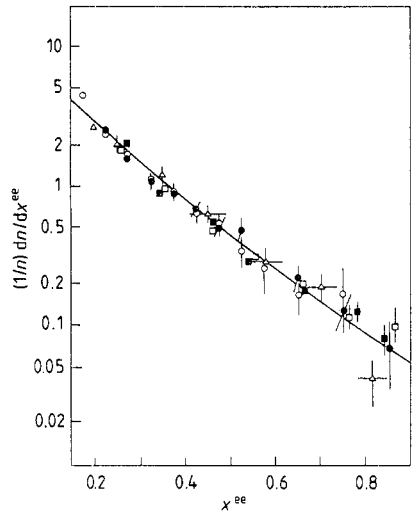

Figure 50. The jet fragmentation functions measured in pp collisions (○●□■), in νp interactions (△) and in e^+e^- annihilations (——), taken from Darriulat (1980).

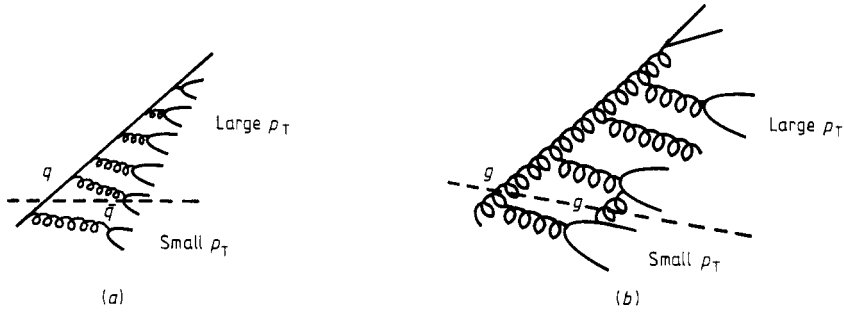

Figure 51. Colour flow in (*a*) quark and (*b*) gluon jets.

If we suppose that $\bar{u}$ and $\bar{d}$ antiquarks can be created with equal probability (and similarly for the heavier pairs $(\bar{c}, \bar{s})$ and $(\bar{t}, \bar{b})$) then

$$\langle Q_{\bar{q}} \rangle = \tfrac{1}{2}(Q_{\bar{u}} + Q_{\bar{d}}) = \tfrac{1}{2}(-\tfrac{2}{3} + \tfrac{1}{3}) = -\tfrac{1}{6}. \tag{5.18}$$

Alternatively, if we suppose that only those antiquarks with masses less than Λ, the QCD mass scale, are easily produced (i.e. $\bar{u}$, $\bar{d}$ and $\bar{s}$) while the heavier $\bar{c}$, $\bar{b}$, etc, appear only very infrequently, one might expect that instead

$$\langle Q_{\bar{q}} \rangle = \tfrac{1}{3}(Q_{\bar{u}} + Q_{\bar{d}} + Q_{\bar{s}}) = \tfrac{1}{3}(-\tfrac{2}{3} + \tfrac{1}{3} + \tfrac{1}{3}) = 0. \tag{5.19}$$

The truth probably lies somewhere between (5.18) and (5.19) in which case we find

$$\begin{aligned} &\langle Q_{u,\text{jet}} \rangle = \tfrac{2}{3} + (-\tfrac{1}{6} \text{ to } 0) = \tfrac{1}{2} \text{ to } \tfrac{2}{3} && \text{(and for } c, t \text{ jets)} \\ &\langle Q_{d,\text{jet}} \rangle = -\tfrac{1}{3} + (-\tfrac{1}{6} \text{ to } 0) = -\tfrac{1}{2} \text{ to } -\tfrac{1}{3} && \text{(and for } s, b \text{ jets).} \end{aligned} \tag{5.20}$$

These conclusions are best tested in deep inelastic ν scattering which (neglecting sea quarks and the Cabibbo weak mixing angles) selects almost a unique quark flavour.

Thus in $\nu p \to \mu^- X$ ($\simeq u$ jet only) it is found that $\langle Q_{jet} \rangle = 0.61 \pm 0.09$, while in $\bar{\nu} p \to \mu^+ X$ ($\simeq d$ jet only) $\langle Q_{jet} \rangle = -0.15 \pm 0.21$, in good agreement with (5.20) (Berge *et al* 1980).

For gluon jets (figure 51(*b*)) the cutoff line must cross two gluon lines to ensure colour neutrality and a similar analysis suggests that $\langle Q_{g,jet} \rangle \simeq 0$, but this is much harder to test experimentally.

The above arguments are readily extended to other conserved flavour quantum numbers, such as strangeness or charm. If it is the case that hadron production proceeds mainly by ordered $q\bar{q}$ creation as in figure 51 then one would expect an anticorrelation between the flavours of adjacent particles in the jet. Such an anti-correlation between the charges of the leading and next-leading particles in jets has in fact been observed (Darriulat 1980).

The gluon exchange mechanism of figure 31 suggests that there should be no correlation between the flavours of particles in opposite-side jets as we noted in § 4. Figure 40 shows the average numbers of + and − charge particles in the away-side jets opposite to various large p_T triggers. A significant anticorrelation of the charges is evident, though not in all experiments. If true this suggests that quark exchange (as in the CIM model, for example) is making a significant contribution to the cross section (Brodsky 1979a, b).

Obviously, much remains to be understood about the parton fragmentation process and the properties of jets in hadron collisions. So far all the evidence points to a strong similarity between these jets and those found in e^+e^- annihilation and deep inelastic scattering experiments. It is expected that much more will be learned when really high-energy hadron colliding-beam facilities such as the CERN $p\bar{p}$ collider produce results because then jets with really large $p_T (\sim 50\ \text{GeV}/c)$ will be produced at a significant rate, and jet identification should then be less of a problem.

6. Parton ideas for low p_T hadronic interactions

The success of the parton approach in hard scattering processes prompts the question of its relevance to hadronic processes at small momentum transfer. It might be thought that phenomena in the low p_T regime would be too complicated to be explained in terms of partons. There appears to be no large Q^2 in the problem to justify the use of perturbative QCD. However, in the last few years there has been much activity, particularly in trying to explain the longitudinal momentum (or x) distribution of fast hadrons at low p_T in terms of the quark structure and fragmentation functions. There is a variety of different dynamical models, among which are the quark chain model (Capella *et al* 1979), quark fragmentation model (Andersson *et al* 1977), quark recombination model (Das and Hwa 1977, Hwa 1980) and a dual topological unitarisation approach (Cohen-Tannoudji *et al* 1980). The confusion is increased in that many of these models seem to have very different bases and yet all claim success in describing the data.

As long ago as 1972 a simple additive quark model was used to estimate the hadron yields in the central region of hadron–hadron collisions (Anisovich and Shekhter 1973). For a meson–nucleon collision the idea is shown in figure 52. The interaction, shown as a blob, involves a single q (or $\bar{q}$) from each hadron. At high energies many quarks and antiquarks are produced, and the hadron production has no memory of the initial state. In other words, the number of $q\bar{q}$ pairs in the hadron sea is so large in the small x region that the influence of the initial quantum numbers

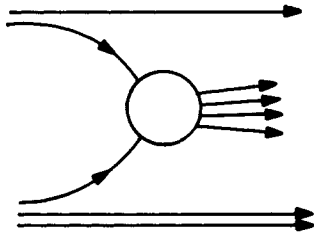

Figure 52.

is negligible. The distribution of particles in the central region should therefore be independent of the incident hadrons.

To make a hadron an outgoing quark at small x must pick up at least one neighbouring quark. At high energies there should be a 50% chance of a q grabbing a $\bar{q}$ to make a meson; in the other half of cases a qq system is formed which must combine again, and is equally likely to form qqq (baryon) or $qq\bar{q}$, etc. The particle yields are calculated assuming the statistical equality of all possible q and $\bar{q}$ combinations. Due to the relative scarcity of observed hadrons containing strange quarks a suppression factor λ is introduced for each strange quark produced (presumably due to its greater mass). The dominant production is taken to be 0^-, 1^- mesons and $\frac{1}{2}^+$, $\frac{3}{2}^+$ baryons and antibaryons. The effect of resonance decays on the particle yields is included; in fact most of the π arise via the decay of resonances, such as the ρ. This simple model, with $\lambda \simeq 0.3$, successfully explains the relative meson yields, and the universal x dependence, in the central region (see, for example, Kittel 1981). In particular, since quarks and antiquarks are assumed to be produced with uncorrelated spin projections, the number of $q\bar{q}$ pairs with total spin S is proportional to the statistical weight $2S+1$. The predicted ratios, for example 3:1 for K*(890):K production, are in agreement with the data.

In the fragmentation region ($x \to \pm 1$) the situation is quite different. This is the region in which the produced particle has acquired a large fraction of the incident longitudinal momentum, and as expected the spectrum is dependent on the quantum numbers of the fragmenting particle.

6.1. Fragmentation versus recombination

To illustrate the application of parton ideas to low p_T fragmentation consider the π^+ inclusive cross section in a proton–proton collision; $pp \to \pi^+X$. A π^+ produced with a large fraction of the fragmenting proton's momentum, say $x \sim 0.8$, is expected to arise from a quark whose momentum fraction is also large. Such a quark is most likely to be a u valence quark of the initial proton moving in the same direction. We expect this fast quark to be unaffected by the hadron collision, and to be described by the same structure function, $f_p^u(x)$, found in deep inelastic lepton scattering (see § 3.2). Thus to predict $pp \to \pi^+X$ we need to understand the mechanism by which a π^+ can be formed from such a fast u quark. One possibility is that the u fragments into π^+ by the mechanism that we used for high p_T processes. But at low p_T there is the alternative possibility that the u combines with a slow $\bar{d}$ from the proton sea to form a π^+. These two mechanisms, known as fragmentation and recombination respectively, are sketched in figure 53. They will be discussed in turn.

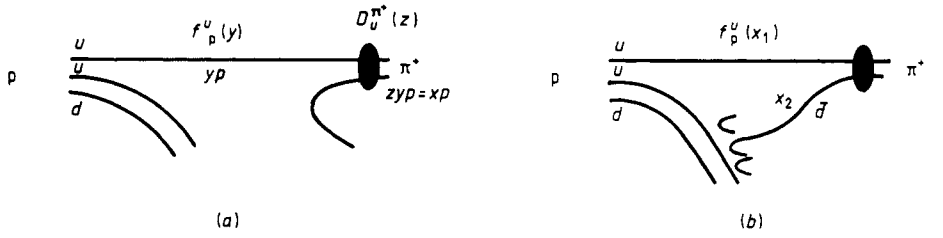

Figure 53. (*a*) The fragmentation and (*b*) the recombination mechanism for a proton fragmenting into a π^+ meson.

6.1.1. The fragmentation model. Using the fragmentation mechanism (figure 53(*a*)), the $pp \to \pi^+ X$ inclusive cross section takes the form

$$\frac{1}{\sigma}\frac{d\sigma^{(p\to\pi^+)}}{dx} = \int_x^1 f^u_p(y) D^{\pi^+}_u(x/y)\,dy/y. \tag{6.1}$$

But with the known structure and fragmentation functions (see § 3) this yields an answer more than an order of magnitude below the data (Das and Hwa 1977). The trouble is that the momentum is lost in two stages ($x = yz$); first, the quark carries only a fraction y of the incident proton's momentum, and second, it then fragments into a π^+ together with other particles which compete for the momentum.

We can look at this deficiency using the spectator quark counting rules, (3.14), which predict

$$f^u_p(y) \sim (1-y)^3 \qquad D^{\pi^+}_u(z) \sim (1-z). \tag{6.2}$$

Inserting this behaviour in (6.1) gives

$$\frac{d\sigma^{(p\to\pi^+)}}{dx} \sim (1-x)^{2n_s-1} \sim (1-x)^5 \tag{6.3}$$

where n_s is the total number of spectator quarks. In contrast, experiments reveal a π^+ momentum behaviour $(1-x)^\beta$ with β near 3.

The various models based on quark fragmentation avoid this difficulty by a mechanism known as the quark 'held-back' effect. For example, for the meson fragmentation process, $\pi^+ p \to hX$, one valence quark is held back in the central region ($x \simeq 0$) and the other valence quark (plus the gluons and sea) fragments as if it carried all the π^+ momentum. Since there are equal probabilities for the u or $\bar{d}$ to go forward and fragment

$$\frac{1}{\sigma}\frac{d\sigma^{(\pi^+\to h)}}{dx} = \tfrac{1}{2}[D^h_u(x) + D^h_{\bar{d}}(x)]. \tag{6.4}$$

Meson fragmentation data are found to compare well with the predictions obtained using the quark fragmentation functions determined from leptoproduction data (Andersson *et al* 1977). Indeed, the motivation for the fragmentation model is the surprising similarity between multiparticle production mechanisms in e^+e^- annihilation, in leptoproduction and in low p_T hadron–hadron interactions (see figures 49 and 50). We speak of 'jet universality'. In proton fragmentation a valence quark is held back and the remaining diquark system goes forward and fragments, and so, for

example we have

$$\frac{1}{\sigma}\frac{d\sigma^{(p\to\pi^{\pm})}}{dx}=\tfrac{2}{3}D_{ud}^{\pi^{\pm}}(x)+\tfrac{1}{3}D_{uu}^{\pi^{\pm}}(x). \tag{6.5}$$

Diquark fragmentation functions obtained from recent deep inelastic neutrino data appear to satisfy this equality (see, for example, Kittel 1981).

The 'held-back' effect is also operative in the quark chain approach of the Orsay group (Capella *et al* 1979, 1980). Although this fragmentation model is formulated in terms of parton concepts it is inspired by the dual topological unitarisation scheme. It assumes that the interaction separates the valence quarks of each incident proton into two coloured systems, one with the quantum numbers of a valence quark and the other those of a diquark. To neutralise these coloured systems, two multiparticle chains are formed stretching from one proton to the other, as in figure 54(*a*). It is

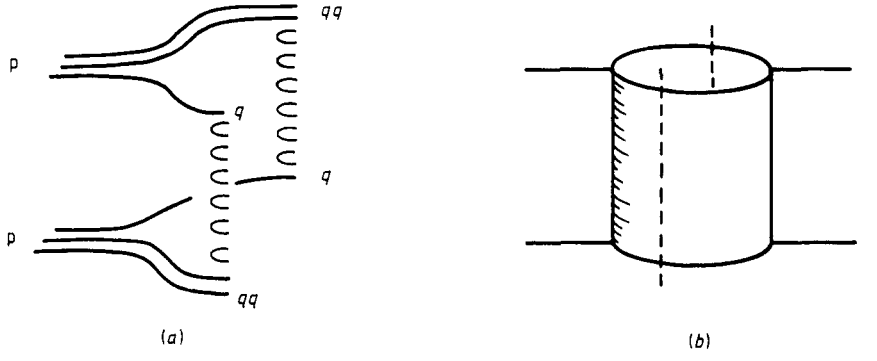

Figure 54. The cylinder topology of diagram (*b*) is formed by the 'back-to-back' product of amplitudes of diagram (*a*).

argued that the valence quarks are held back in the central region and that the diquarks carry most of the proton momenta. Squaring the diagram and summing over intermediate states to obtain the cross section, as required by unitarity, gives the cylinder topology of the Pomeron in the dual model (figure 54(*b*)). This provides some justification for the two-chain colour separation, at least in the central region.

Attempts have been made to put this held-back mechanism on a firmer theoretical basis by invoking the concept of stretching the colour flux tube (Andersson *et al* 1980), or through the dual model (Cohen-Tannoudji *et al* 1981).

It is clearly important to compare the rapidity distribution of the particles produced in pp interactions with that in e^+e^- annihilation which arises from a single multiparticle chain (see figure 55). Comparing data at 30 GeV, we find that the average charged-particle multiplicities and the central plateau heights satisfy

$$\langle n\rangle_{e^+e^-}\gtrsim\langle n\rangle_{pp} \qquad \frac{dn(e^+e^-)}{dy}>\frac{dn(pp)}{dy}.$$

At first sight this appears to rule out the two-chain model (figure 54) from which naively we would predict $\langle n\rangle_{pp}\simeq 2\langle n\rangle_{e^+e^-}$. However, the 'held-back' effect may restore agreement with the data. First, the plateaux from the two multiparticle chains are each moved away from $y=0$ so that they only partially overlap in rapidity. Secondly,

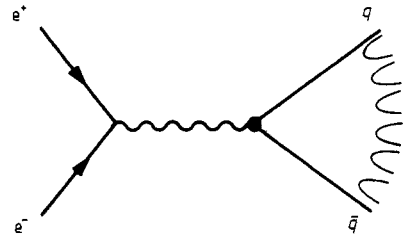

Figure 55. Schematic diagram of the process $e^+e^- \rightarrow$ hadrons.

only the sub-energy determines the plateau height rather than the full energy as in e^+e^-. Consistency with existing data is possible (Capella *et al* 1980) and it will be interesting to see if the two-chain model correctly predicts the development of the plateaux with increasing energy.

6.1.2. The recombination model

The recombination model (figure 53(*b*)) appears to be an entirely different approach to low p_T fragmentation. The basic idea is that the fast valence quark recombines with a slow ($x_2 \simeq 0$) antiquark from the sea. Now $x = x_1 + x_2 \simeq x_1$, and so for the example $pp \rightarrow \pi^+X$

$$\frac{d\sigma^{(p\rightarrow\pi^+)}}{dx} \sim f_p^u(x) \sim (1-x)^3 \tag{6.6}$$

in reasonable agreement with experiment, and in contrast to the prediction of (6.3). The original idea goes back several years (Goldberg 1972, Pokorski and Van Hove 1975), but the present impetus originates from the observation by Ochs (1977) that the ratio of π^+ to π^- inclusive production by protons satisfies

$$\frac{d\sigma^{(p\rightarrow\pi^+)}/dx}{d\sigma^{(p\rightarrow\pi^-)}/dx} \simeq \frac{f_p^u(x)}{f_p^d(x)}$$

with the quark structure functions determined from inelastic lepton scattering data (see § 3.2). This follows from (6.6) and the analogous relation for $p \rightarrow \pi^-$.

In detailed applications of the model, allowance is made of the momentum fraction x_2 carried by the sea quark (see figure 53(*b*)). A knowledge of the joint $q-\bar{q}$ momentum probability distribution and the $q-\bar{q}$ recombination function is required. There have been several applications to determine meson structure functions among which are Das and Hwa (1977), Duke and Taylor (1978), Hwa and Roberts (1979) and Aitkenhead *et al* (1980).

A recent theoretical development is the valon recombination model of Hwa (1980). In this approach hadron fragmentation proceeds as follows:

intitial hadron → valons → partons → valons → final hadron

where the valons are constituent or 'dressed' valence quarks surrounded by a sea of gluons and $q\bar{q}$ pairs. For example, a nucleon is made of just three valons, the detailed internal structure of which cannot be resolved at low Q^2. In deep inelastic lepton scattering the virtual photon can resolve the partons in a valon. Their structure

functions are assumed to be universal with an evolution in Q^2 given by lowest-order perturbative QCD with a δ function input at low Q^2. If this can be accepted, deep inelastic lepton scattering and lepton pair production data may be used to determine the valon structure function of an initial proton or pion, which in turn predicts the recombination of valons into the final hadron. The calculations have been carried out for $pp \to \pi^+ X$ (Hwa and Zahir 1981).

To summarise, the theoretical interpretation of low p_T fragmentation is still open to debate, and continues to attract a lot of controversy. We have seen that the existing parton models divide essentially into the quark fragmentation and the quark recombination approaches. Put simply, in fragmentation models a valence quark is 'held back' and the inclusive distribution is described by the fragmentation functions, $D_q^h(x)$, of the remaining fast forward-moving quark (or diquark) system. But in the recombination approach the inclusive distribution is given by the structure function, $f^q(x)$, of a fast forward-moving valence quark which recombines with a slow sea quark to produce the outgoing hadron. Although these seem to be contradictory viewpoints, there have been claims that from the standpoint of the dual topological unitarisation scheme they are essentially equivalent parton model interpretations of the same dual cylinder component (Cohen-Tannoudji *et al* 1980).

6.2. Counting rules for low p_T fragmentation

The inclusive distributions at high energy and low p_T are frequently fitted to the form $d\sigma/dx = A(1-x)^\beta$. Some of the observed values of β are listed in figure 56, which is taken from Bobbink *et al* (1980). Further results can be found in Denegri *et al* (1981).

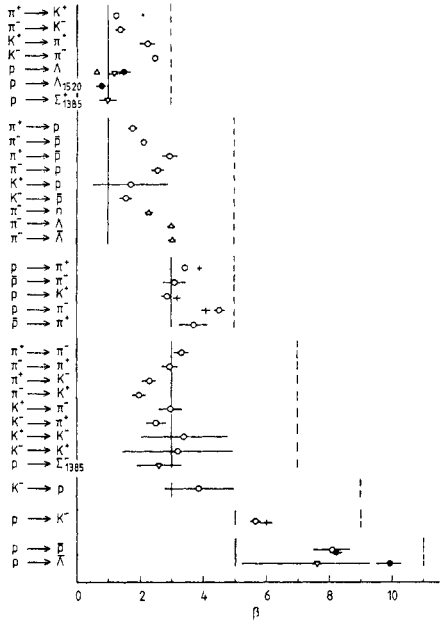

Figure 56. The exponents β obtained from fitting data for various reactions to the form $d\sigma/dx \sim (1-x)^\beta$. The lines are the counting rule predictions described in the text. The figure is from Bobbink *et al* (1980).

The quark counting rules (see, for example, Blankenbecler and Brodsky 1974) predict that as $x \to 1$ in the process $AB \to CX$

$$\frac{d\sigma^{(A\to C)}}{dx} \sim (1-x)^{2n_s-1} \tag{6.7}$$

where n_s is the minimum number of spectator quarks involved in the transition $A \to C$. An example was given in (6.3). The more spectators share the initial momentum the smaller is the chance of producing a hadron with a large fraction of the momentum.

The formulation of the counting rule has evolved in the light of experiment. The number of relevant spectators depends on whether the hadronic interaction $AB \to CX$ proceeds dominantly via quark or gluon exchange; on whether we count sea, as well as valence, quarks among the spectators; and, if so, how this is to be done. For example, consider $pp \to \pi^+X$; the lowest Fock state of the proton which fragments into a π^+ is $|uudd\bar{d}\rangle$. Figure 57 shows the fragmentation proceeding accompanied by either gluon exchange or quark exchange. In the former case there are three spectators yielding a $(1-x)^5$ behaviour, and in the latter two spectators giving a $(1-x)^3$ behaviour which is in better agreement with the data.

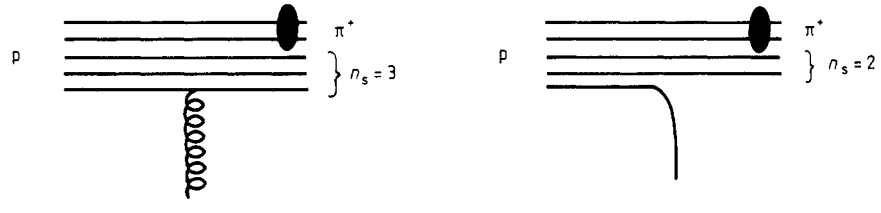

Figure 57. $p \to \pi^+$ fragmentation via gluon or quark exchange diagrams.

However, quark exchange leads to a dramatic long-range correlation between the fragmentation behaviour of the beam and target in a double inclusive reaction such as $pp \to \pi^+\pi^+X$. For example, for d quark exchange in figure 57 the lowest Fock state of the other incident proton is $|uudd\bar{d}d\bar{d}\rangle$ which fragments into a π^+ with four spectators. So with quark exchange the double inclusive cross section is

$$\frac{d^2\sigma(pp \to \pi_1^+\pi_2^+X)}{dx_1\,dx_2} \sim [(1-x_1)^3\,(1-x_2)^7 + 1 \leftrightarrow 2].$$

However, the recent ISR data for $pp \to \pi^+\pi^+X$ show a complete absence of such a correlation (Bobbink *et al* 1980).

Indeed, this lack of correlation is an essential feature of the models we discussed earlier for low p_T fragmentation. It is assumed that one incident hadron fragments independently of the other. An important test of this is that the ratio of $\pi^\pm$ inclusive production, $hp \to \pi^+X/hp \to \pi^-X$ in the proton fragmentation region should be independent of whether the beam hadron, h, is a p, π^+, π^-, K^+, etc. Experimentally this is found to be the case above about 200 GeV/c, but at lower momenta a component that vanishes as $s^{-1/2}$ is required (Kittel 1981), which may be due to quark exchange contributions.

Returning to the counting rule we see that for gluon exchange we expect $\beta = 5$ for $p \to \pi^+$ fragmentation. The predictions for other fragmentation processes are shown by the broken lines in figure 56 and clearly disagree with the observed exponents.

Prompted by this discrepancy, a physically reasonable suggestion is to count only valence quarks as spectators. This is motivated by the recombination model in which the role of sea quarks in sharing the momentum among spectators is reduced, relative to that of the valence quarks, by the peaking of the sea structure functions at small x. The full lines on figure 56 follow from this valence-quark-spectator counting rule, and are seen to be in better agreement with experiment.

Recently Gunion (1979) has reconsidered the counting rules from the viewpoint of lowest-order QCD. The reason why perturbative QCD may be applicable to low p_T fragmentation is illustrated by the fragmentation of a π into a valence quark (see figure 58). Initially the q and $\bar{q}$ have, on the average, equal fractions of the pion's

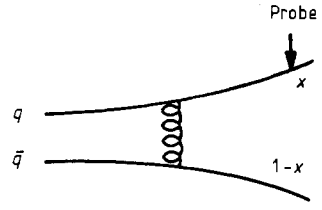

Figure 58. A π meson fragmenting into a valence quark, with one hard gluon leaving a single spectator.

momentum. In the lowest order, the way to obtain a quark with momentum fraction x near 1 is to transfer momentum from the $\bar{q}$ to the q via gluon exchange. With the pion and $\bar{q}$ on mass shell, the four-momentum squared of the quark q is

$$k^2 = -\frac{k_T^2 + m^2(x)}{1-x}$$

where m depends on the particle masses and is regular as $x \to 1$. Thus as $x \to 1$ the probed quark is far off mass shell and the momentum measurement acts as a short-distance probe. Neglecting spin, Gunion shows this contribution to the quark structure function of the pion is

$$f_\pi^v(x) \sim (1-x)$$

as $x \to 1$. Brodsky and Lepage (1979a,b) have considered the leading log QCD diagrams in this limit and shown that this lowest-order power law is not modified, although there are logarithmic modifications.

For the sea quark distribution of the pion, Gunion uses the lowest-order diagram of figure 59(a) which yields

$$f_\pi^s(x) \sim (1-x)^3$$

since two hard gluons are needed to transfer all the momentum to the sea quark.

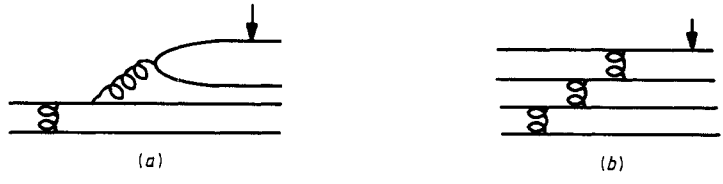

Figure 59. Possible diagrams for a π meson to fragment into a 'sea' quark, leaving three spectators.

This is to be compared with the hadronised four-quark diagram (figure 59(*b*)), which contains the q_s initially, which needs three hard gluons, and gives $(1-x)^5$ since there are three spectators. Applying this approach to $pp \to \pi^+ X$, the lowest-order diagram is figure 60 which yields

$$\frac{d\sigma^{(p\to\pi^+)}}{dx} \sim (1-x)^3.$$

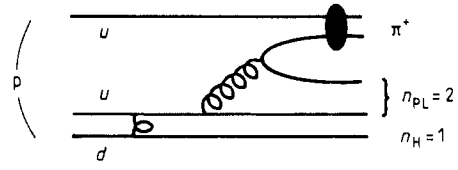

Figure 60. Pair creation diagram for $p \to \pi^+$ fragmentation, with two hard gluons.

The general rule, originally formulated for QED by Blankenbecler *et al* (1975), is that the $x \to 1$ behaviour of a diagram is

$$(1-x)^{2n_H+n_{PL}-1}$$

(where n_H is the number of spectators originating from the hadronic wavefunction and n_{PL} is the number of spectators associated with the point-like pair creation process) which corresponds to the count of hard gluons given above.

This rule agrees rather well with the data (see Gunion 1979). In particular exotic fragmentation processes are relatively weakly suppressed compared to the original spectator counting rule. For example, for $\pi^+ \to K^-$ fragmentation of figure 61 it gives $(1-x)^3$ as compared to $(1-x)^7$. In fact, the predictions of Gunion's rule are very similar to the suggestion of counting just the valence quark spectators of the hadronised state. For $\pi^+ \to K^-$ this also gives $\beta = 3$ (see figure 56).

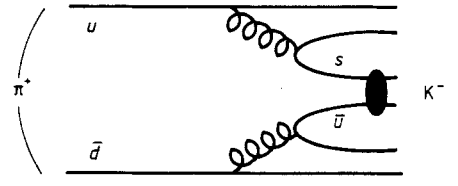

Figure 61. Pair creation diagram for $\pi^+ \to K^-$ fragmentation ($n_{PL}=4$, $n_H=0$).

Despite the empirical support for the use of these point-like pair creation QCD diagrams, with minimal suppression as $x \to 1$, their theoretical justification is far from clear. There appears to be no good reason why the created quarks should not interact with the other quarks so that the bound state momentum is redistributed, giving back the rule based on counting the spectators in the initial hadronised state.

Finally we note that the application of parton ideas to low p_T fragmentation should be restricted to $x \leqslant 0.8$. For larger x values triple-Regge phenomenology will dominate, as we shall discuss in § 8.

7. Exchange forces

7.1. Regge poles

In § 1.5 we remarked that the strong interaction between composite hadrons is a mutual colour polarisation effect, somewhat analogous to the interatomic forces which produce molecules. It involves the exchange of quarks and gluons between the hadrons, but to preserve the colour neutrality (whiteness) of the particles no net colour can be exchanged, only colourless clusters of partons. Hence the longest-range component of the force is provided by exchanging the lightest available hadron with the appropriate flavour quantum numbers, as in figure 8(*a*).

For the process $AB \to CD$ (figure 62) s, defined in (2.1), is the square of the centre-of-mass energy while t in (2.10) gives the scattering angle. However, the

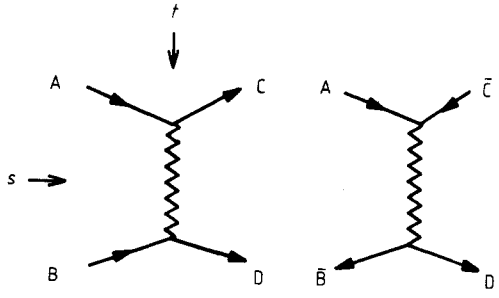

Figure 62. The s-channel ($AB \to CD$) and t-channel ($A\bar{C} \to \bar{B}D$) processes which are related by crossing. The particles which are interchanged (B, C) become their antiparticles in order to conserve quantum numbers. The particles exchanged in the process $AB \to CD$ must have the quantum numbers of $A\bar{C}$ and $\bar{B}D$.

exchanged particle is formed in the t-channel process $A\bar{C} \to \bar{B}D$ in which t gives the energy and s the scattering angle. Thus for the simplest case where $m_A = m_B = m_C = m_D \equiv m$, (2.10) with s and t interchanged gives

$$\cos \theta_t = 1 + \frac{2s}{t - 4m^2} \tag{7.1}$$

for the t channel. These s and t channels are related by crossing and share a common scattering amplitude, but involve different regions of the s and t variables (see, for example, Collins 1977).

The old-fashioned one-pion-exchange (OPE) approximation to the nuclear force consisted of representing the scattering amplitude by the t-channel pion propagator pole

$$A(s, t) \sim \frac{1}{m_\pi^2 - t}. \tag{7.2}$$

There are two related difficulties with this approach, however. First the pion is just the lightest of many particles with the required flavour quantum numbers, and to obtain the full nuclear interaction one must include the others, such as ρ, ω, f and A_2 as well as multiparticle exchange (2π, 3π, etc) which provide shorter-range contributions. Secondly, and more fundamentally, (7.2) is really just an approximation to the S wave ($l = 0$ partial wave) in the t channel (because it is independent of s and hence of $\cos \theta_t$, from (7.1)). This partial-wave decomposition is fine for the t-channel process

$A\bar{C} \to \bar{B}D$, but it will not do in the s-channel $AB \to CD$ where we want to use it. This is because any singularity in s gives rise to a divergence of the t-channel partial-wave series. For example, an s-channel particle pole

$$\frac{1}{m^2-s}=\frac{1}{m^2}\left[1+\frac{s}{m^2}+\left(\frac{s}{m^2}\right)^2+\ldots\right] \tag{7.3}$$

diverges as $s \to m^2$. Hence the t-channel partial-wave series

$$A(s,t)=\sum_{l=0}^{\infty}(2l+1)A_l(t)P_l(\cos\theta_t) \tag{7.4}$$

(where $A_l(t)$ is the partial-wave amplitude and P_l is a Legendre polynomial) will also diverge as $s \to m^2$ because of (7.1). There will certainly be many singularities in s (bound state and resonance poles, threshold branch points, etc) intervening between the t- and s-channel physical regions, and so the approximation (7.2) will break down before the s-channel region is reached. Instead we need a method of summing the full partial-wave series. This will not only enable us to overcome the divergence problem, but will also allow the simultaneous inclusion of all particles which lie on a given Regge trajectory like figure 9, and which occur in different t-channel partial waves.

A general way of achieving this was suggested by Sommerfeld (1949) (following Watson 1918) and is developed in detail in, for example, Collins (1977). For our purpose it will suffice to consider the particles lying on a single linear trajectory

$$\alpha(t)=\alpha_0+\alpha' t \tag{7.5}$$

such that $\alpha(t)$ passes through integer values of l at $t=m_l^2 (l=0, 1, 2, \ldots)$. The pole in the lth partial wave then takes the form

$$A_l(t)\simeq\frac{\beta(t)}{l-\alpha(t)}\simeq\frac{\beta(t)}{\alpha'(m_l^2-t)} \tag{7.6}$$

i.e. there is a 'Regge pole' in the partial-wave amplitude at $l=\alpha(t)$, and $\beta(t)$ is the residue function specifying the coupling of the pole to the external particles. The contribution of the trajectory to the amplitude is then, from (7.6) substituted in (7.4),

$$A(s,t)\simeq\sum_{l=0}^{\infty}(2l+1)\frac{\beta(t)}{l-\alpha(t)}P_l(\cos\theta_t). \tag{7.7}$$

Since the asymptotic form of $P_l(\cos\theta)\to(\cos\theta)^l$ as $\cos\theta\to\infty$, we find that (Perl 1974, p395)

$$A(s,t)\underset{s\to\infty}{\sim}\sum_{l=0}^{\infty}\frac{\beta(t)(\cos\theta_t)^l}{l-\alpha(t)}\sim\beta(t)(\cos\theta_t)^{\alpha(t)}\sim\beta(t)s^{\alpha(t)} \tag{7.8}$$

at fixed t, from (7.1).

Equation (7.8) is the characteristic Regge-pole asymptotic power behaviour of the scattering amplitude as a function of s at fixed t stemming from the exchange of a Regge trajectory of composite particles (Regge 1959, 1960). It predicts that in a two-body process

$$\frac{d\sigma}{dt}\sim\frac{1}{s^2}|A(s,t)|^2\sim F(t)\left(\frac{s}{s_0}\right)^{2\alpha(t)-2} \tag{7.9}$$

where $\alpha(t)$ is the leading Regge trajectory which can be exchanged, and $s_0 \simeq 1\ \text{GeV}^2$ is the hadron mass scale. This has been well verified in many processes (Collins 1977, Irving and Worden 1977).

The trajectory $\alpha(t)$ is readily determined by plotting $\log(\mathrm{d}\sigma/\mathrm{d}t)$ as a function of $\log s$ at each t value. For example, in $\pi^- p \to \pi^0 n$ the t-channel process $\pi^-\pi^0 \to \bar{p}n$ has the flavour quantum numbers $I = 1$, $P = G = +$, i.e. of the ρ meson in table 2, so the ρ trajectory of figure 9 can be exchanged. But in the s channel $-t$ is the square of the momentum transferred and so (7.8) gives us the continuation of this trajectory to negative values of t, as shown in figure 63.

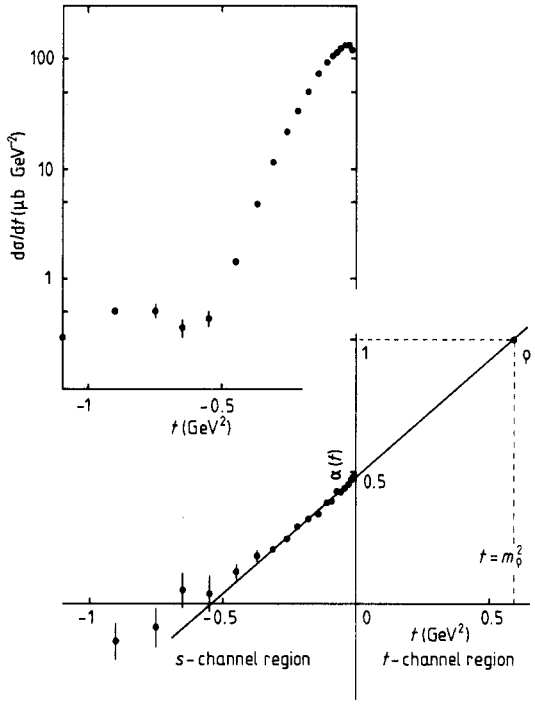

Figure 63. The $\pi^- p \to \pi^0 n$ differential cross section for beam momentum 20.8 GeV/c (Barnes *et al* 1976). The lower plot compares the values of $\alpha(t)$ (with $t \leq 0$) obtained by fitting to $\pi^- p \to \pi^0 n$ data in the momentum range 20–200 GeV/c with the extrapolation of the linear ρ trajectory of figure 9.

If (7.5) is substituted into (7.9) we find

$$\frac{\mathrm{d}\sigma}{\mathrm{d}t} \sim F(t)\left(\frac{s}{s_0}\right)^{2\alpha_0 - 2} \exp\left[2\alpha' \log(s/s_0)t\right] \tag{7.10}$$

and so the forward peak in $|t|$ becomes sharper ('shrinks') as $\log s$ increases. This shrinkage, which is due to the slope of the Regge trajectory, is a characteristic feature of Regge poles.

However, (7.8) only indicates the asymptotic s behaviour of a Regge pole. A more complete expression, which exhibits the principal features of Reggeon exchange, such as figure 62, is (Collins 1977)

$$A(s,t) = \gamma_{AC}(t)\gamma_{BD}(t)\frac{\exp\left[-i\pi\alpha(t)\right] + \mathscr{S}}{2\sin\pi\alpha(t)} \frac{1}{\Gamma(\alpha(t)+1)}\left(\frac{s}{s_0}\right)^{\alpha(t)}. \tag{7.11}$$

Here $\gamma_{AC}(t)$ represents the coupling of the trajectory to particles A and C at the upper vertex, and γ_{BD} is the lower vertex. This factorisation property of the coupling is well verified. The factor $[\sin \pi\alpha(t)]^{-1}$ is the Reggeon propagator and produces the required resonance poles in t whenever $\alpha(t)$ passes through an integer, as in (7.6). $\mathscr{S}$ is called the 'signature' and takes the values $\mathscr{S} = \pm 1$ for even/odd signature trajectories. It arises because the Reggeon is really the sum of two terms, as in figure 64, and we get

$$(-s)^{\alpha(t)} + \mathscr{S}(-u)^{\alpha(t)} \to s^{\alpha(t)} \{\exp[-i\pi\alpha(t)] + \mathscr{S}\} \tag{7.12}$$

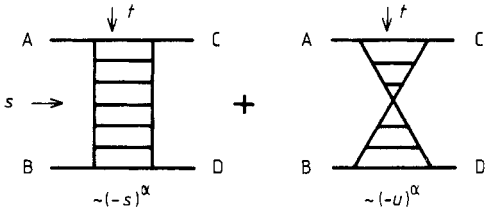

Figure 64. A Reggeon (of signature $\mathscr{S}$) is the sum, (7.12), of planar s–t and planar u–t contributions, respectively. Planar diagrams are ones in which the particle lines do not cross; the second diagram becomes planar in u, t if it is untwisted by interchanging B and D (see (2.1) and (2.11)). The rungs of the ladders represent the sum over all physical intermediate states in the $s(u)$ channel and, through unitarity, build up the imaginary part of the amplitude in $s(u)$.

as $s \to \infty$ at fixed t from (2.12). It means that (7.11) only has poles for even/odd integer values of $\alpha(t)$ respectively, and so even and odd partial waves (with their different symmetry properties under $\cos\theta_t \leftrightarrow -\cos\theta_t$, i.e. $s \leftrightarrow u$) have separate trajectories. This signature factor has the important consequence that, since $\gamma(t)$, $\alpha(t)$ are expected to be real functions of t for $t < 0$, the phase of (7.11) is given by

$$\rho \equiv \frac{\mathrm{Re}\{A\}}{\mathrm{Im}\{A\}} = -\frac{\cos\pi\alpha + \mathscr{S}}{\sin\pi\alpha}. \tag{7.13}$$

This phase is required for consistency with fixed-t dispersion relations, and is well verified experimentally. The Γ function is included in (7.11) to ensure that there are no unphysical resonance poles at negative values of $\alpha(t)$. Since

$$\frac{1}{\Gamma(\alpha+1)} = -\frac{\sin\pi\alpha}{\pi}\Gamma(-\alpha) \tag{7.14}$$

it is evident that this function vanishes for $\alpha = 0, -1, -2, \ldots$, and so cancels the 'nonsense' poles of the Reggeon propagator. The ρ meson has spin 1 and so its trajectory has $\mathscr{S} = -1$. Hence when $\alpha(t) \to 0$, which we see from figure 63 happens for $t \simeq -0.5$ GeV^2, (7.11) vanishes. The dip in the $\pi^- p \to \pi^0 n$ differential cross section is usually regarded as a verification of the nonsense decoupling at this point. (There are, however, alternative explanations involving cuts, see § 9.)

Despite the fact that the ρ and A_2 trajectories have opposite signature ($\mathscr{S} = -1$ and $+1$, respectively, giving leading particles with spin 1 and 2) these two trajectories look like a single trajectory in figure 9, with particles at every positive integer value of s. The observed trajectories are thus exchange-degenerate. If their couplings are equal too then in processes like $K^- p \to \bar{K}^0 n$ and $K^+ n \to K^0 p$ where we have $A_2 \pm \rho$ exchange (the sign change occurring because ρ has negative C), the respective phases

will be given by

$$\tfrac{1}{2}(\exp[-i\pi\alpha(t)]+1\pm\{\exp[-i\pi\alpha(t)]-1\})=\exp[-i\pi\alpha(t)],\ 1 \tag{7.15}$$

so the latter reaction should have a real phase, which is certainly experimentally confirmed (via the optical theorem), while the former has a phase which changes with $\alpha(t)$. But their differential cross sections, which depend on $|A|^2$ only, should be identical. The data are in reasonable agreement with these predictions (see, for example, Irving and Worden 1977).

The optical theorem illustrated in figure 65 (see Collins 1977) gives

$$\sigma_T(AB)\sim\frac{1}{s}\,\mathrm{Im}\,A(AB\to AB,\ s,\ t=0)\sim s^{\alpha(0)-1} \tag{7.16}$$

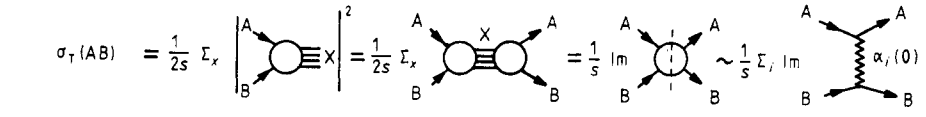

Figure 65. Pictorial representation of the optical theorem, which relates the AB total cross section to the imaginary part of the forward amplitude for elastic AB scattering. The third equality follows from unitarity.

where α is the leading trajectory which can be exchanged in elastic scattering. In figure 10 we see that at high energy all the total cross sections are nearly constant with energy, which implies that $\alpha(0)\simeq 1$ in (7.16). This is not true of the meson trajectories in figure 9, which have $\alpha(0)\simeq\frac{1}{2}$, nor of any others presently known. The leading trajectory exchanged in elastic scattering has the quantum numbers of the t-channel $A\bar{A}\to B\bar{B}$, which is flavourless and should be universal. It seems reasonable to suppose therefore that, unlike ordinary meson trajectories which contain valence quarks, the flavourless exchange in elastic scattering is made of gluons. Since no net colour can be transferred the minimum contribution is the two-gluon exchange box of figure 23. As we noted in § 2 this trajectory is called the Pomeron P. Its properties will be discussed in § 9.

In addition to the exchange of a single Reggeon, as in figure 62, it is also possible to exchange two or more Reggeons simultaneously. This gives rise to Regge cuts, which become important at large values of $-t$, as we shall see in § 9. For small $-t$ however, the Regge poles are dominant and are an indispensable tool for the analysis of hadron cross sections. By incorporating SU(3) flavour symmetry into the Regge residues, and assuming that the s dependence is given by extrapolations of Regge trajectories which are linear functions of t like (7.5) passing through the known resonances (like figure 63), and that the amplitude phase is given by the signature factor as in (7.13), one can predict quite well the behaviour of hadron scattering processes at low $|t|$ and high s. The scope of this success is summarised in, for example, Collins (1977) and Irving and Worden (1977).

We next want to look at the parton description of Regge exchanges.

7.2. Duality and quark line diagrams

In the parton model flavour is carried by the quarks and hence the exchange of flavour (e.g. the exchange of charge in $\pi^-p\to\pi^0n$ discussed above) can be represented by quark line diagrams showing just the valence quarks of the hadrons which are involved. Some examples are shown in figures 66(a) and (d).

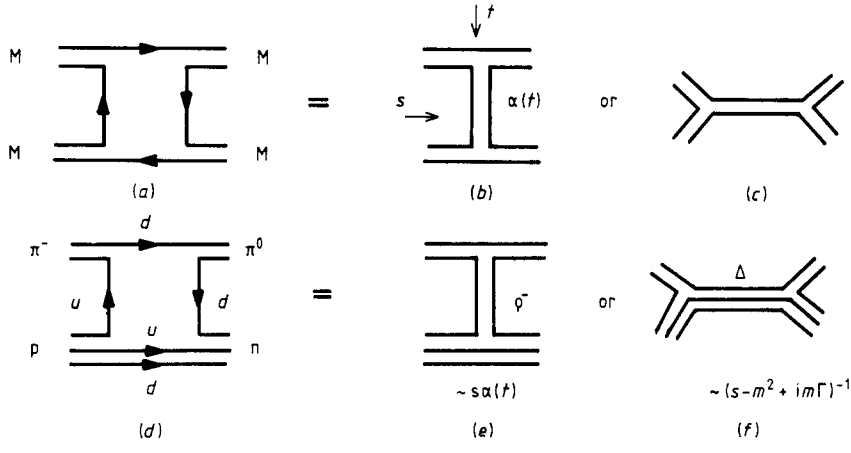

Figure 66. Duality diagrams for MM→MM and $\pi^-p \to \pi^0 n$, representing both Regge exchanges (*b*) and (*e*) and resonances (*c*) and (*f*).

These figures also illustrate the fact that the same diagram can be used to describe (i) the exchange of a Reggeon in the t channel, giving an amplitude behaving like $s^{\alpha(t)}$ as $s \to \infty$, and (ii) s-channel resonances which give Breit–Wigner poles in the amplitude

$$A \underset{s \to m^2}{\sim} \frac{1}{s - m^2 + im\Gamma} \tag{7.17}$$

where m is the resonance mass and Γ is its width. The diagram represents not just a single resonance, however, but all the (infinite number of?) resonances which can be formed with the same valence quarks, including both orbital and radial excitations.

The hypothesis of duality (see, for example, Collins (1977) for a review and references) is that these two types of diagrams ((*b*) and (*c*), or (*e*) and (*f*)) are in fact equivalent (dual to each other) and really represent just a single contribution to the scattering amplitude. A concrete mathematical realisation of this hypothesis is given by the Veneziano model (1968) for the scattering amplitude, viz

$$V(s, t) = \gamma^2 \frac{\Gamma(1-\alpha(s))\Gamma(1-\alpha(t))}{\Gamma(1-\alpha(s)-\alpha(t))}. \tag{7.18}$$

From the inverse of (7.14) it is evident that $\Gamma(1-\alpha(t))$ gives rise to resonance poles in s whenever $\alpha(s)$ passes through a positive integer, and similarly there are poles in t whenever $\alpha(t)$ is a positive integer, but the Γ function in the denominator ensures that there are no double poles when $\alpha(s)$ and $\alpha(t)$ are integers simultaneously.

From Stirling's formula (Magnus and Oberhettinger 1949 p4) we find that

$$\frac{\Gamma(x+a)}{\Gamma(x+b)} \xrightarrow[x \to \infty]{} x^{a-b} \tag{7.19}$$

(except in a wedge along the negative x axis where poles appear at integer x). So if we have a linear trajectory like (7.5)

$$V(s, t) \xrightarrow[\substack{s \to \infty \\ t \text{ fixed}}]{} \frac{\gamma^2 \pi(-\alpha' s)^{\alpha(t)}}{\Gamma[\alpha(t)] \sin \pi\alpha(t)} = \frac{\gamma^2 \pi(\alpha' s)^{\alpha(t)}}{\Gamma[\alpha(t)] \sin \pi\alpha(t)} \exp[-i\pi\alpha(t)] \tag{7.20}$$

which may be compared with (7.11).

The model (7.18) thus has the following properties. (*a*) It is manifestly crossing symmetric with resonance poles and Regge asymptotic behaviour in both s and t. (*b*) It has the nonsense Γ factor to remove the unphysical poles at negative integer values of α. (*c*) The scale factor s_0 in (7.11) has been replaced by $(\alpha')^{-1}$ in (7.20), and we note from figure 9 that $(\alpha')^{-1} \simeq 1\ \text{GeV}^2$, the hadron mass scale. (*d*) The asymptotic phase is $\exp[-i\pi\alpha(t)]$, which gives a positive imaginary part for $s > 0$. To reproduce the phase of (7.11) we need the sum of two terms, like figure 64, viz

$$\tfrac{1}{2}[V(s,t)+\mathscr{S}V(u,t)] \xrightarrow[t\ \text{fixed}]{s\to\infty} \frac{\gamma^2\pi(\alpha' s)^{\alpha(t)}}{\Gamma[\alpha(t)]\sin\pi\alpha(t)}\tfrac{1}{2}\{\exp[-i\pi\alpha(t)]+\mathscr{S}\}. \qquad (7.21)$$

(*e*) In an exotic process such as $\pi^+\pi^+ \to \pi^+\pi^+$, as there are no charge-two meson resonances there are no poles in s and hence only the second term of (7.21) appears and the phase is real. This is because the imaginary parts of the ρ and f exchanges cancel by exchange degeneracy, as in (7.15). The imaginary part of the amplitude, and hence from (7.16) $\sigma_T(\pi^+\pi^+)$, is given entirely by the gluon-exchange Pomeron (P). On the other hand, in $\pi^+\pi^- \to \pi^+\pi^-$, which does have s-channel resonances, the ρ and f contributions add (+ sign in (7.15)) and σ_T involves these trajectories as well as P. Similarly pp → pp is exotic but $\bar{\text{p}}\text{p} \to \bar{\text{p}}\text{p}$ is not and so the total cross sections are given by

$$\begin{aligned}\sigma_T(\text{pp}) &= \text{P}+\text{f}-\omega+\text{A}_2-\rho \sim As^{\alpha_P(0)-1}\\ \sigma_T(\bar{\text{p}}\text{p}) &= \text{P}+\text{f}+\omega+\text{A}_2+\rho \sim As^{\alpha_P(0)-1}+Bs^{\alpha_R(0)-1}\end{aligned} \qquad (7.22)$$

the sign changes stemming from the fact that ω and ρ are odd under charge conjugation (p ↔ $\bar{\text{p}}$). With exchange degeneracy $\text{f} = \omega$ and $\text{A}_2 = \rho$, and so only P contributes to pp, whereas the four (degenerate) trajectories of figure 9, with $\alpha_R(0) \simeq \frac{1}{2}$, do not cancel in $\bar{\text{p}}\text{p}$. This explains why $\sigma_T(\bar{\text{p}}\text{p})$ is higher than $\sigma_T(\text{pp})$ at low energies in figure 10, but falls to meet it like $s^{-1/2}$ at high s.

As reviewed in, for example, Jacob (1974) and Collins (1977), this duality idea, though it lacks any very fundamental justification at the present time, enables us to summarise conveniently many of the properties of Regge exchanges, including their flavour dependence, exchange degeneracy, etc. Because of this it is useful to formalise the rules for drawing duality quark line diagrams. These are generally called Zweig's rules (Rosner 1969) and are:

(i) The flavour of each particle is represented by its valence quarks, with a positive arrow for a quark and negative for a $\bar{q}$, so a meson is  and a baryon is  .

(ii) Each hadronic process is represented by a connected planar diagram which can be cut at any intermediate stage by lines representing just a single meson or baryon. This ensures flavour conservation, no exotic intermediate states and exchange degeneracy.

(iii) No quark line begins and ends on the same particle (this would be a sea quark).

The diagrams of figure 66 accord with these rules. An interesting example is provided by $\pi^-\text{p} \to \text{Vn}$ where V is a vector meson; ω, φ, ψ or Υ. We see in figure 67 that only the first has an allowed diagram, while the others require the creation of a sea $q\bar{q}$ pair, and these processes are highly suppressed. Similarly the decay $\psi^*(4415) \to \text{D}\bar{\text{D}}$ is allowed (figure 68), but $\psi(3100)$ is below the $\text{D}\bar{\text{D}}$ threshold so its hadronic decays violate Zweig's rules and are highly suppressed. This is why the latter is very narrow (long-lived) while the former is not. In the $\psi^*(4415)$ the excited $c\bar{c}$

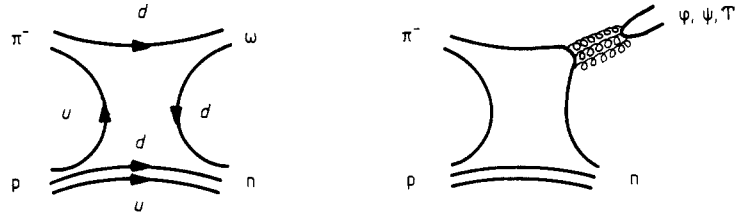

Figure 67. Allowed and 'forbidden' duality diagrams for $\pi^- p \to Vn$.

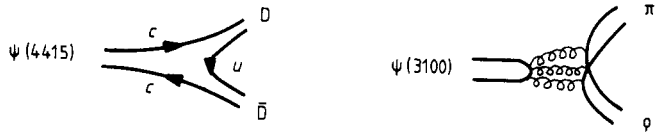

Figure 68. Allowed and 'forbidden' duality diagrams for $\psi(c\bar{c})$ decays.

pair can easily lose energy by creating a $u\bar{u}$ or $d\bar{d}$ pair in the vacuum to produce the lower-mass D and $\bar{D}$ mesons. But in the $c\bar{c}$ ground state, $\psi(3100)$, they do not have enough energy for this, and instead must first annihilate into at least three virtual gluons (to conserve colour and charge conjugation) which create the final-state hadrons when they attempt to escape confinement. The probability for this is proportional to $[\alpha_s(m_\psi^2)]^3$, and since α_s is quite small ($\simeq 0.3$) the decay is highly suppressed.

The representation of hadronic processes by these quark line diagrams is a useful way of summarising all the main phenomenological features such as resonance excitation and decay, Regge exchanges and the phases of amplitudes. They do not, however, include any threshold branch points, or Regge cuts. The Veneziano model is thus not unitary, and attempts to construct realistic dual models consistent with unitarity have not been very successful. Despite this the Veneziano model is a remarkably good first approximation to the scattering amplitude, incorporating all the resonance and exchange poles on Regge trajectories. It is thus essential to try and gain some understanding of how Reggeons may be generated dynamically in QCD.

7.3. The dynamics of Regge trajectories

The particles which lie on a meson Regge trajectory like figure 9 are $q\bar{q}$ bound states. To calculate a Regge trajectory from first principles would thus require a solution to the QCD confinement problem, which is far beyond our theoretical competence at the moment. We can, however, attempt an educated guess as to how the dynamics may work, based on experience with much simpler models.

In § 1.3 we remarked how non-relativistic potential models, with confining potentials which are increasing functions of the separation r at large r, can account for the charmonium (ψ) and beauty (Υ) states. The radial Schrödinger equation contains the effective potential (1.14), in which the first term is the attractive interaction potential and the second term is the centrifugal repulsion representing the difficulty of holding high-l states together. Usually this repulsion comes to dominate at large l and so high-l bound states cannot be formed. In states of large l the constituents spend much of their time at large r, where the potential is weak. However, confining potentials are an exception to this because $V(r)$ increases with r and so the bound state can still

be held together. High-l states are, of course, heavier because the constituents have greater internal kinetic energy.

A simple example is the three-dimensional harmonic oscillator potential, $V(r) = \lambda r^2$, whose energy eigenvalues are (Morse and Feshbach 1953 p1662)

$$E_{nl} = (2n_r + l + \tfrac{3}{2})\hbar\omega_c \tag{7.23}$$

where $n_r = 0, 1, 2, \ldots$, is the radial quantum number and $2\pi\omega_c = (\lambda/m)^{1/2}$, m being the quark mass. We thus find a linear trajectory for l against E. More generally it is found that for $V \sim r^n$ the asymptotic form of the trajectory is (Quigg and Rosner 1979)

$$l \sim E^{(n+2)/2n}. \tag{7.24}$$

Note that with $n = -1$ this gives $l \sim E^{-1/2}$, in agreement with the Rydberg formula for the hydrogen atom $E_{nl} \sim (n_r + l + 1)^{-2}$. The observed linearity of l with M^2 in figure 9 might suggest that $n = \frac{2}{3}$. However, as we discussed in § 1, it is only possible to take these potential models seriously when the system is non-relativistic ($E \ll mc^2$) so these high-E limits are probably of limited relevance. The important point is that the increase of l with M^2 is evidence for the increase of the interaction strength with r, and hence for at least partial confinement.

Another, somewhat more realistic, model which we can use for Regge trajectories is based on Feynman perturbation field theory (Eden *et al* 1966, Collins 1977, Polkinghorne 1980). The results for the interactions of scalar particles in φ^3 theory are very well known. The basic interaction amplitude (figure 69(a)) is single scalar exchange $(s - m^2)^{-1}$, where m is the mass, and so as $s \to \infty$ it behaves like s^{-1}. If we include further exchanges it is found that the leading $\log s$ form of the amplitude is given by the ladder diagrams, and that an n-rung ladder has the asymptotic form

$$\sim \frac{[K(t)\log s]^{n-1}}{s(n-1)!} \tag{7.25}$$

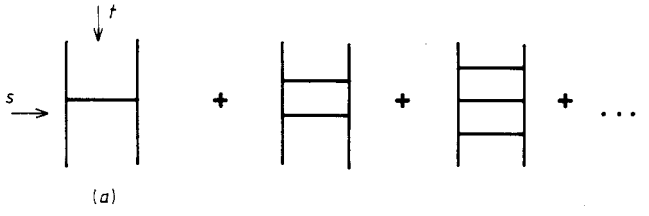

(a)

Figure 69. Ladder diagrams for scalar particles which sum to give $s^{\alpha(t)}$ behaviour.

where $K(t)$ arises from the box diagram loop integration. Summing the diagrams with all possible numbers of rungs gives

$$A(s,t) \sim \sum_{n=1}^{\infty} \frac{[K(t)\log s]^{n-1}}{s(n-1)!} \sim s^{\alpha(t)} \tag{7.26}$$

where $\alpha(t) \equiv -1 + K(t)$. It can be verified in perturbation theory that more complicated diagrams (including those in which the rungs cross over each other) either do not contribute to the leading $\log s$ behaviour, or constitute renormalisation effects. The leading behaviour always comes from ladder diagrams like figure 9 in which the rungs are coupled in the order of their rapidities (De Tar 1971). So if one is willing to assume that this set of diagrams is the correct one to obtain the leading behaviour,

we have generated a Regge trajectory by summing ladders. In this model $K(t)>0$ and $\to 0$ as $t\to-\infty$, so that $\alpha(t)\xrightarrow[-t\to\infty]{}-1$. This is because the Born approximation (figure 69(*a*)), which controls the large t limit, behaves like s^{-1}.

There are several problems with applying these ideas to QCD with gluon exchanges between quarks. First, we have a spin-1 gluon propagator with s dependence in the numerator. Secondly, the quarks have spin $\frac{1}{2}$ so the total angular momentum of the Born diagram is the vector sum of their spins and the orbital angular momentum. Thirdly, we are dealing with massless gluons in an IR-divergent perturbation theory. And finally, and perhaps most serious, we have a non-Abelian UV-divergent confining theory, so that the quarks and gluons in the intermediate states do not represent the unitarity structure properly. The intermediate states should really be physical particles. Some subtle cancellations are known to occur (Grisaru *et al* 1973, Bartels 1980) but the complete solution is not known.

We shall simply ignore most of these problems, and begin by observing that the basic Born diagram (figure 70(*a*)) has the scaling form $\sim t/s$ for s, $-t\to\infty$, s being the gluon propagator denominator (see table 3—the roles of s and t are interchanged). If we then assume that the multi-gluon exchanges of figure 70 Reggeise like those

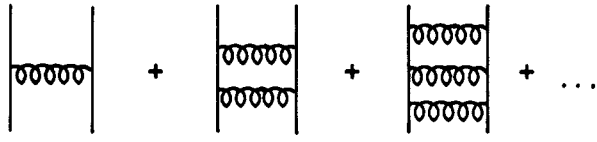

(*a*)

Figure 70. Quark–gluon ladder diagrams which are speculated to sum to give a $ts^{\alpha(t)}$ behaviour.

of figure 69 we may expect the behaviour $\sim ts^{\alpha(t)}$ with $\alpha(-\infty)=-1$, though, because of the cancellations noted above, it is certainly not obvious that the trajectory must end up at -1. Indeed, figure 63 indicates that it may continue straight down (see Collins *et al* 1968). The suggestion that the trajectory should eventually asymptote to a negative integer (Blankenbecler *et al* 1973, 1974) stems from the fact that hard scattering (2.24) controls the large-angle limit, as discussed in § 2.3, and it is hoped that this matches smoothly onto the Regge limit. (There is clearly a strong similarity between figure 66 and the constituent interchange model of figure 38.) If so, then for meson scattering, MM→MM, the amplitude may take the form (figure 71(*a*))

$$A(s,t)\underset{s\to\infty}{\sim}F_{\mathrm{M}}^{2}(t)ts^{\alpha(t)}\underset{|t|\gg m^{2}}{\sim}\frac{1}{t}s^{\alpha(t)} \tag{7.27}$$

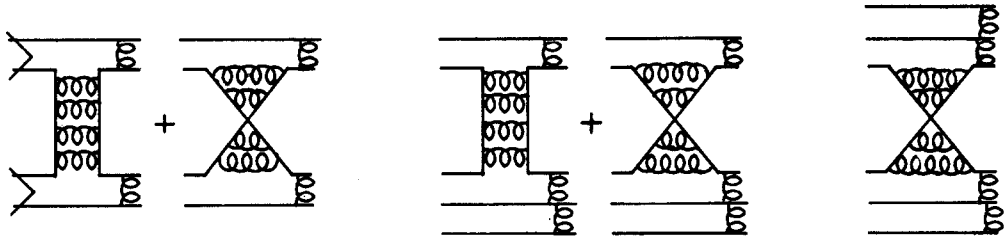

(*a*) (*b*) (*c*)

Figure 71. Quark line diagrams (with gluon insertions) which lead to the asymptotic behaviour for (*a*) MM, (*b*) MB and (*c*) BB hard scattering.

where, as described in § 2.3, the form factor $F_M(t)$ gives the probability of the meson re-forming after the hard scattering, and its asymptotic behaviour is given by (2.22). Then

$$\frac{d\sigma}{dt} \underset{s\to\infty}{\sim} \frac{1}{s^2}|A|^2 \sim \frac{1}{t^2}s^{2\alpha(t)-2}. \tag{7.28}$$

But in the fixed-angle limit, s, $-t\to\infty$, s/t fixed, we have $\alpha(t)\to -1$ and so $d\sigma/dt \sim s^{-6}f(t/s)$ in agreement with (2.26). Similarly for MB and BB scattering we find

$$\begin{aligned} A(\mathrm{MB}\to\mathrm{MB}) &\underset{s\to\infty}{\sim} F_M(t)F_B(t)ts^{\alpha(t)} \qquad \text{so} \qquad \frac{d\sigma}{dt} \underset{s,-t\to\infty}{\sim} s^{-8}f\left(\frac{t}{s}\right) \\ A(\mathrm{BB}\to\mathrm{BB}) &\underset{s\to\infty}{\sim} F_B^2(t)ts^{\alpha(t)} \qquad \text{so} \qquad \frac{d\sigma}{dt} \underset{s,-t\to\infty}{\sim} s^{-10}f\left(\frac{t}{s}\right) \end{aligned} \tag{7.29}$$

from (2.22), in accord with (2.27) and (2.28). Note that in BB scattering only the t–u planar diagram (figure 71(c)) is possible, giving the real phase of (7.15) rather than (7.12). Analyses of the data based on this sort of approach have been presented by Coon *et al* (1978) who discuss alternative trajectory end points ($\alpha(t)\to -2$ or -3) suggested by different ways of applying the dimensional counting rules. However, we should stress again that both the form of the Reggeisation in QCD and the overlap of the Regge and large-angle limits are plausible speculations, not proven results.

Figure 71 suggests a physical description of the Reggeon exchange process. As the hadrons approach each other the quarks are mutually attracted and slow down by radiating virtual gluons, as in figure 72(a). By absorbing the gluons emitted from the other quark, each quark can reverse its direction of motion, and thus they can be exchanged between the hadrons. If a q and a $\bar{q}$ attract each other, as in figure 72(b),

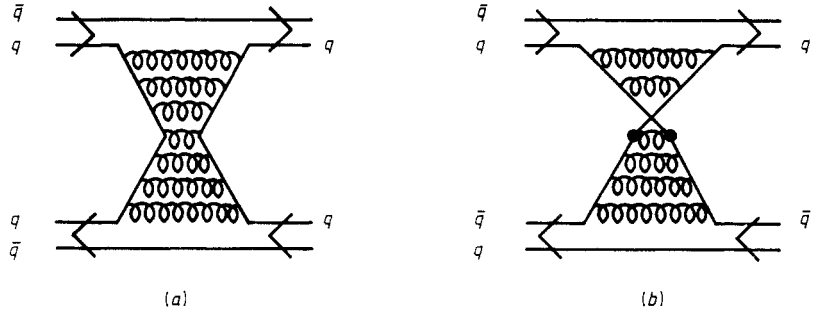

Figure 72. Parton description of Reggeon exchange. In (b) the dots show the annihilation and subsequent creation of $q\bar{q}$ pairs.

they can annihilate, but subsequently another $q\bar{q}$ pair must be created so that colourless hadrons can appear in the final state. Of course, the likelihood of just two outgoing hadrons mopping up all the virtual gluons in this way is rather small at high energies, which is presumably why the Reggeon exchange cross sections fall with s. Thus the dominant Reggeons (which are shown in figure 9) have $\alpha(t\simeq 0)\simeq 0.5$ and so $d\sigma/dt \sim s^{-1}$ at small $|t|$ from (7.9). Heavier quarks are obviously harder to 'turn round' and so the intercepts of the trajectories containing s, c or b quarks are lower than those in figure 9, giving a more rapidly decreasing cross section. It is more likely

that some of the gluons will hadronise independently of the forward-going quarks, as in figure 15, and so multiparticle final states are much more likely than two-particle ones as s increases.

This will form the subject of the next section.

8. Inclusive reactions

In the early 1970s the study of inclusive processes dominated hadronic-interaction physics. In a typical ISR collision about 18 hadrons are produced and we are clearly forced to be selective about the information obtained and studied. A useful choice is to study inclusive processes of the type

$$A+B\rightarrow C+X$$

where C is the observed particle and X represents everything else produced. Such reactions are described by three independent kinematic variables, for example, s, t of (2.1), (2.10) together with the missing mass squared:

$$M^2\equiv(p_A+p_B-p_C)^2 \tag{8.1}$$

see figure 73. Alternatively we may use s with p_L, p_T the longitudinal, transverse components of $\boldsymbol{p}_C$. As noted in § 2.1 the p_L dependence is usually expressed in terms of x ($\equiv p_L/p$ in the CM frame) or the rapidity y of (2.9). In the CM frame, $\boldsymbol{p}_A+\boldsymbol{p}_B=0$, we see from (8.1) that

$$M^2/s\simeq(1-x) \tag{8.2}$$

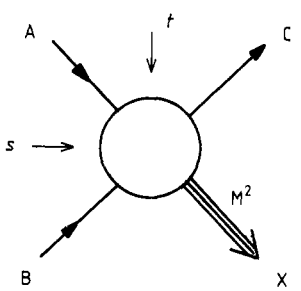

Figure 73. Kinematic variables for AB → CX where X represents all the other particles produced.

for $p_L\gg p_T$ and large s. For a fixed s the extremities of the x plot are populated by low missing mass.

8.1. Mueller's theorem

A major stimulus for the study of inclusive reactions was the prediction by Feynman (1969) (and also by Yang and collaborators: Benecke *et al* (1969)) that the cross section would scale at high energies, i.e. the cross section would be a function of two variables x and p_T, and not of the energy $\sqrt{s}$ directly. The arguments for 'Feynman' scaling were based mainly on physical intuition. (We have already encountered an analogous, but distinct, scaling prediction by Bjorken for deep inelastic lepton scatter-

ing $e+p\to e+X$.) However, it was soon shown that these results follow from a generalisation of the application of Regge theory to the optical theorem.

To introduce this idea it is useful to recall the ordinary optical theorem (7.16) which relates, via unitarity, the total cross section $(A+B\to X)$ to the imaginary part of the forward elastic scattering amplitude

$$\sigma_T(AB)\simeq\frac{1}{s}\,\mathrm{Im}\,A(AB\to AB)|_{t=0}. \tag{8.3}$$

This was represented pictorially in figure 65. The total cross section is very complicated, being the sum of the cross sections of many multiparticle reactions, each with their own energy dependence. Yet, through the magic of the optical theorem, it is given by a single two-body elastic scattering amplitude. Thus the properties of the latter (Regge asymptotic behaviour, duality properties, factorisation, etc) can be used to determine the behaviour of the total cross section as in (7.22).

Mueller (1970) extended the optical theorem to relate the inclusive cross section for $A+B\to C+X$ to an elastic three-body forward amplitude

$$f\equiv E_C\frac{d\sigma}{d^3p_C}(A+B\to C+X)\simeq\frac{1}{s}\,\mathrm{Disc}_{M^2}A(AB\bar{C}\to AB\bar{C}) \tag{8.4}$$

where the discontinuity is to be taken only across the M^2 cut of the elastic amplitude. This is represented pictorially in figure 74. The generalisation is not as straightforward as it looks, however. Since C is an outgoing particle we are not in the physical region of the elastic process $AB\bar{C}\to AB\bar{C}$. We need to make a delicate analytic continuation of the (many-variable) three-body amplitude from the physical region of $A+B\to C+X$.

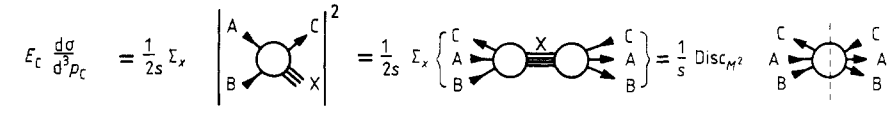

Figure 74. Pictorial representation of Mueller's optical theorem.

(This continuation has been justified for field theoretic models.) The importance of Mueller's optical theorem is that the behaviour of the inclusive reaction can be obtained from that of the, theoretically much simpler, elastic three-body amplitude.

To predict the inclusive cross section for $A+B\to C+X$ we shall assume Regge behaviour for the three-body amplitude. The predictions are therefore relevant to large s and small p_T. It is necessary to distinguish between three kinematical regions for particle C. The beam and target fragmentation regions correspond to finite $t\equiv(p_A-p_C)^2$ and $u\equiv(p_B-p_C)^2$, respectively. Intuitively C can be regarded as a fragment of A (or B) if, as in figure 15, the momentum difference between the two remains finite at large s. The third region is the central region where t and u are both large and C is not closely associated with either incoming particle.

A general criterion for a Regge expansion of a multiparticle amplitude, such as $AB\bar{C}\to AB\bar{C}$, is that the kinematic invariant spanning the Regge exchange should be large (say $\gtrsim 5\ \mathrm{GeV}^2$). In the central region, where t and u are both large, we have the double Regge limit. On the other hand, in the beam fragmentation region ($s\to\infty$, t finite) there are three different Regge limits when different combinations of the invariants M^2 and s/M^2 become large. We discuss these first.

8.2. The fragmentation region

Typical Regge contributions for the three different limits are shown in figure 75. We shall discuss these in turn.

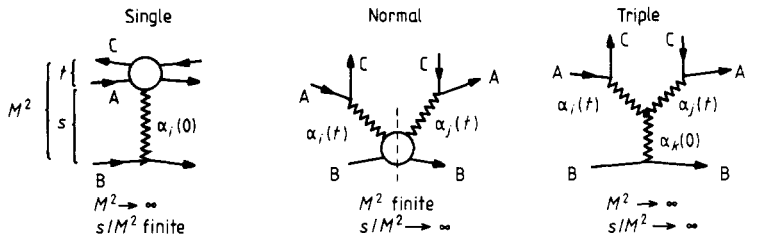

Figure 75. Regge limits in the beam fragmentation region $A \overset{B}{\to} C$.

(i) The single Regge limit ($M^2 \to \infty$, s/M^2 fixed). Here the Regge expansion of the forward elastic $AB\bar{C}$ amplitude in (8.4) gives an inclusive cross section (2.5) of the form

$$f = \sum_i \beta_i\left(\frac{s}{M^2}, t\right)(M^2)^{\alpha_i(0)-1}. \tag{8.5}$$

Assuming the leading singularity, the Pomeron, has $\alpha_P(0) = 1$ and the leading meson exchanges have $\alpha_R(0) = \frac{1}{2}$ we have scaling of the inclusive cross section as $s \to \infty$ and a $s^{-1/2}$ approach to the scaling form.

(ii) The normal Regge limit (M^2 finite, $s/M^2 \to \infty$). In this case (8.4) yields an inclusive cross section:

$$f = \frac{1}{s}\sum_{ij} \beta^i_{AC}(t)\beta^j_{AC}(t)s^{\alpha_i(t)+\alpha_j(t)} \operatorname{Disc}_{M^2} A(\alpha_i B \to \alpha_j B) \tag{8.6}$$

which contains the Reggeon-particle forward-scattering amplitude with maximal helicity flip of the Reggeon.

(iii) The triple Regge limit ($M^2 \to \infty$, $s/M^2 \to \infty$). This kinematic region is the overlap of the above two regions. For large M^2 we can expand the Reggeon-particle amplitude of (8.6) in terms of Regge exchanges in the $B\bar{B}$ channel:

$$f = \frac{1}{s}\sum_{ijk} \beta_{ijk}(t)s^{\alpha_i(t)+\alpha_j(t)}(M^2)^{\alpha_k(0)-\alpha_i(t)-\alpha_j(t)}. \tag{8.7}$$

Although applicable only in a very limited kinematic domain, triple Regge analyses of the data have been very successful. Many tests, some involving dual model arguments, have been performed. A recent review has been given by Ganguli and Roy (1980).

As an illustration consider the determination of the ρ trajectory from $\pi^{\pm}p \to \pi^0 X$ data at 100 GeV/c (Barnes *et al* 1978). The dominant triple Regge contribution has $\alpha_i = \alpha_j = \alpha_\rho$ together with a Pomeron, assumed to be $\alpha_k(0) = 1$. Thus, using (8.2), the inclusive cross section is

$$f = \beta_\rho(t)(1-x)^{1-2\alpha_\rho(t)}. \tag{8.8}$$

The x dependence of the data in the triple Regge region ($0.8 < x < 0.98$), for fixed values of t, is found to give a reasonable ρ trajectory, $\alpha_\rho(t)$, for $-t \leqslant 1.5$ (GeV/c)^2.

At higher values of $-t$ the trajectory levels off at about -0.5. This may be attributed to the hard scattering effects discussed in the previous section. The trajectories approach negative integers if the Regge exchanges become hard scattering terms as $t \to -\infty$. The idea is that for large angle $AB \to CX$, for example figure 76, only the most elementary constituent interchange (CIM) processes such as $Aq \to Cq$ contribute (Sivers *et al* 1976). Then $\alpha_{AC}(-\infty)$ is determined by the requirement that the dimensional counting rule (6.7) should agree with (8.8), i.e. we need

$$\alpha_{AC}(-\infty) = 1 - n_s$$

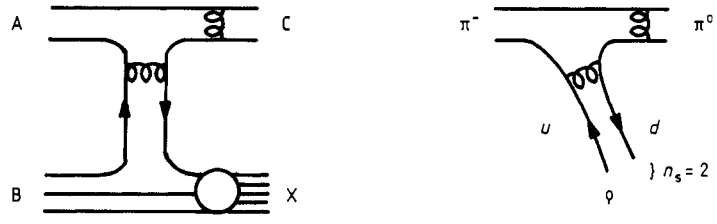

Figure 76. The CIM contribution $Aq \to Cq(\pi^- u \to \pi^0 d)$ to $AB \to CX(\pi^- p \to \pi^0 X)$.

where n_s is the minimum number of effective spectators in the transition $A \to C$. In the low-t region the trajectory is lifted above this value by gluon bremsstrahlung, as described in § 7.3. Thus, for our example $\pi^- p \to \pi^0 X$ the typical CIM process is $\pi^- u \to \pi^0 d$, shown in figure 76(*b*), and there are two spectators, and two hard gluons are needed for large-angle scattering. Hence we expect $\alpha_\rho(-\infty) = -1$. However, estimates of the magnitude of this CIM contribution are well below the data (Barnes *et al* 1978).

An alternative interpretation of the data is that one should add the triple Regge contribution to the recombination model of § 6 (Van Hove 1979), the former dominating for $x \gtrsim 0.8$ and the latter for smaller x.

The triple Regge analysis of diffractive data, particularly $pp \to pX$, allows a study of the, theoretically important, triple Pomeron, PPP, and PPR couplings. There were discrepancies between the original analyses (Field and Fox 1974, Roberts and Roy 1974) which were due to the use of different data compilations. Recent data support the results of the latter analysis and give a non-vanishing triple Pomeron coupling at $t = 0$ and also a dominant triple Pomeron component to diffractive processes, i.e. $G_{PPP} \gg G_{PPR}$ (see Ganguli and Roy 1980).

8.3. The central region

In the central region for $A + B \to C + X$ the invariants s, t, u are all large:

$$t = -\sqrt{s}(E - p_L) \qquad u = -\sqrt{s}(E + p_L). \tag{8.9}$$

However

$$\kappa^2 \equiv ut/s = E^2 - p_L^2 = m_C^2 + p_T^2 \tag{8.10}$$

is finite.

In this region the double Regge limit (figure 77) is appropriate for the $AB\bar{C} \to AB\bar{C}$ amplitude. The inclusive cross section is then of the form

$$f = \sum_{ij} \beta_{ij}(\kappa) |t|^{\alpha_i(0)-1} |u|^{\alpha_j(0)-1}. \tag{8.11}$$

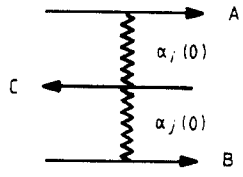

Figure 77. Double Regge limit in the central region.

With the canonical choice $\alpha_P(0) = 1$ and $\alpha_R(0) = \frac{1}{2}$ this becomes

$$f = \beta_{PP}(\kappa) + \kappa^{-1/2} s^{-1/4} \sum_R [\beta_{PR}(\kappa) \exp(-y/2) + \beta_{RP}(\kappa) \exp(y/2)] + O(s^{-1/2})$$

where here y is the centre-of-mass rapidity, see (2.9). Thus asymptotically we expect the inclusive cross section to scale, and also to be independent of y with a central plateau. An $s^{-1/4}$ approach to scaling is predicted. From duality arguments the leading non-scaling terms are found to be positive and so the approach to scaling in the central region should be from above. Experimentally, however, all the central cross sections are found to rise with energy. This was suspected from the beginning, but is now confirmed by recent ISR data, which have shown a rise of as much as 40% in the $pp \to \pi^- X$ central cross section over the ISR energy range. There have been many models attempting to explain this effect, and also the shape of the y distribution and the shrinkage of the p_T distribution with increasing energy. They are discussed in the review of Ganguli and Roy (1980). Most anticipate that scaling will occur when high enough energies have been achieved.

We should stress that the Mueller–Regge formalism, though extremely powerful for inclusive phenomenology, is not a substitute for a dynamical model for multiparticle production. For instance, it does not explain the nature of the Pomeron singularity. This will be the subject of the next section.

9. The Pomeron and Regge cuts

9.1. The Pomeron pole

The approximate constancy with s of all the high-energy forward elastic hadron differential cross sections, and of the hadron scattering total cross sections, implies that the elastic scattering amplitude $A(s, t \simeq 0) \sim s$, and hence, if a Regge pole exchange is the dominant mechanism, that there is a trajectory (called the Pomeron, P) with $\alpha_P(0) \simeq 1$ (see (7.8), (7.9) and (7.16)). Since this behaviour seems to be independent of the flavour of the hadrons (and hence of their quark structure) and since the known trajectories involving quark exchange all have $\alpha_R(0) \leqslant \frac{1}{2}$, it is generally supposed that the P represents gluon exchanges.

A physical picture of how this may happen was given by Low (1975) (see also Nussinov 1976). As the colour singlet hadrons approach near each other a colour octet gluon may be exchanged between them (figure 78(*a*)). But as a result each

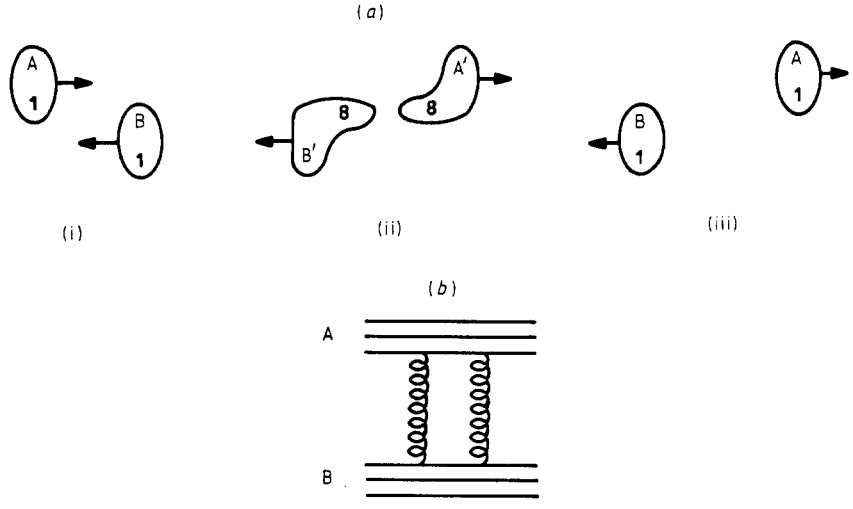

Figure 78. Two-gluon exchange in AB elastic scattering. After single-gluon exchange the colour singlets A, B become colour octets A′, B′, and a further gluon exchange is necessary to produce outgoing singlets.

hadronic cluster then becomes an octet, and as they attempt to move apart the colour lines of force connecting them get stretched. Only by the exchange of another gluon can the clusters become colourless, and hence be free to separate. Thus the fundamental diagram for the elastic scattering amplitude should be two-gluon exchange (figure 78(*b*)). Since the gluon has spin 1, the single-gluon exchange amplitude $\sim s$ at fixed t (see table 3) and the two-gluon box like $\sim(\mathrm{i}/s)ss = \mathrm{i}s$ (the i/s arising from the phase-space integration) which is just the phase and energy dependence of (7.11) with $\alpha = 1$ and even signature ($\mathscr{S} = +1$). (We assume that the IR divergences of massless gluon exchange cancel for composite systems.)

Inserting gluons and/or $q\bar{q}$ pairs to make ladders like figure 79 may be expected to produce a Pomeron trajectory, perhaps with $\alpha(0) > 1$, somewhat like the mechanism discussed in § 7.3. Indeed the slow rise of σ_T with s at the highest energies in figure

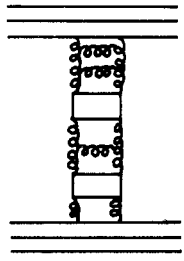

Figure 79. Gluon ladders (with possible quark loop insertions) which may sum to produce a Pomeron trajectory.

10 can be explained if $\alpha_P(0) = 1.068$ (Collins *et al* 1974). Such a rising power behaviour should not continue indefinitely, however (Froissart 1961, Martin 1963, 1966).

The finite range of the hadronic interaction, R (given by the exchange of the lightest hadron, the pion—see § 1.5), means that only in low angular momentum states l such that $l \leqslant l_{\max} \simeq R\sqrt{s}\log s$ can scattering occur. If the hadrons pass each other

at higher l their impact parameter is greater than R and so they miss each other. Partial-wave unitarity (i.e. conservation of probability) demands that each partial-wave amplitude obeys $\operatorname{Im} A_l(s) \leqslant 1$. Hence from the optical theorem (7.16)

$$\sigma_T(s) = \frac{1}{s} \operatorname{Im} A(s, 0) = \frac{1}{s} \sum_{l=0}^{\infty} (2l+1) \operatorname{Im} A_l(s)$$

$$\leqslant \frac{1}{s} \sum_{l=0}^{l_{max}} (2l+1) \leqslant R^2 \log^2 s \simeq \frac{1}{m_\pi^2} \log^2 s. \tag{9.1}$$

Thus the total cross section can grow no more rapidly with s than $\log^2 s$, and not like $s^{\alpha_P(0)-1}$ with $\alpha_P(0) > 1$. This is called the 'Froissart bound'. However, even at ISR energies where $\log s \simeq 8$ we find that $\sigma_T(pp)$ is only of the order of $1/m_\pi^2$ (figure 10) and hence the cross section is still about two orders of magnitude below the Froissart bound. Only at astronomically high energies does the observed $s^{0.068}$ behaviour exceed (9.1), so it is not clear that the mechanisms which will ultimately restore $\alpha \leqslant 1$ for the leading Regge singularity are operative at attainable energies. Other explanations for the rise of $\sigma_T(s)$ involving multiple P exchanges are discussed below. But there is good experimental evidence that the Pomeron coupling factorises (see, for example, Cool *et al* 1981) as one would expect for a pole, but not necessarily for a cut.

We have seen that quark exchange ladders (figure 70) result in Regge trajectories. The particles on these trajectories arise through the binding of the quarks. Figure 79 might similarly be interpreted as the exchange of flavourless particles made just from gluons. The existence of such 'glueballs' (Jaffe and Johnson 1975) has often been conjectured, but so far there is no definitive proof that any observed particle is a glueball rather than an ordinary $q\bar{q}$ state (Donoghue 1980). It is, of course, perfectly possible that some of the known flavourless particles are mixtures of glueballs and $q\bar{q}$ resonances, exemplified by the insertion of quark boxes in figure 79. However, the success of Zweig's rules (see § 7.2) suggests that such mixing may be small for high-mass states, and the occurrence of a spin-2 glueball at a mass m_g such that $\alpha_P(m_g^2) = 2$ cannot be ruled out. Such a weakly-coupled meson is very difficult to isolate, particularly since the small slope of the Pomeron trajectory ($\alpha'_P \simeq 0.1\ \mathrm{GeV}^{-2}$) suggests $m_g^2 \simeq 10\ \mathrm{GeV}^2$.

The final-state hadrons of figure 78 do not have to be identical to the incoming ones. The gluon exchanges may result in excitation of the quarks, so that the outgoing particle has the same flavour content, but higher mass and possibly angular momentum. This is known as 'diffractive excitation'. Examples are $\pi p \to \pi N^*$ (where N^* is an excited $I = \frac{1}{2}$ nucleon state) and $\pi p \to A_2 p$, since the A_2 has the same quark content as π but higher spin (see table 2). In all such cases it is found that at high energy the cross section is essentially independent of energy, unlike the flavour exchange processes discussed in § 7. Likewise in the Mueller–Regge approach to inclusive processes of § 8 we have observed the need for P exchange in the elastic amplitude for $AB\bar{C} \to AB\bar{C}$.

Naively one might regard figure 79 as qq scattering, the remaining quarks in the hadrons being simply spectators. If so, for particles containing identical quarks, one has (Kokkedee 1969) $\sigma_T(MM) = 4\sigma_T(qq)$, $\sigma_T(MB) = 6\sigma_T(qq)$ and $\sigma_T(BB) = 9\sigma_T(qq)$, the coefficients being the number of ways of pairing the valence quarks. Hence, one predicts that, for example, $\sigma_T(pp)/\sigma_T(\pi p) = 1.5$ (since π and p are made of identical u and d quarks) in fair agreement with the ratio 1.7 found at the highest energies in figure 10. From this viewpoint one might also expect that the pp elastic differential cross section would fall more rapidly with increasing $-t$ than that for πp, in the ratio

$(F_B(t)/F_M(t))^2 \sim t^{-2}$, because of the greater difficulty of reforming the $3q$ particle in the final state, as discussed in § 2.3. This is also in accord with experiment (Collins and Wright 1979).

Further confirmation that P exchange often involves essentially just a single quark from each hadron, as in figure 79, comes from the success of the hypothesis of f dominance of the P coupling (Carlitz *et al* 1971). The Pomeron has the same quantum numbers as the f meson and hence one may expect that the longest-range part of the coupling at small $|t|$ will stem from the formation of a virtual f meson as in figure 80.

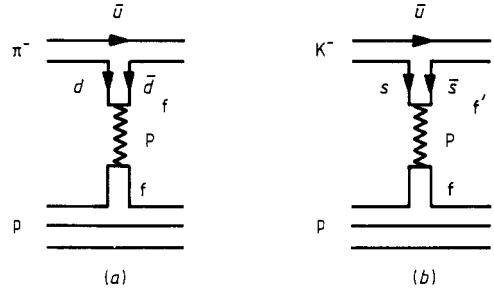

Figure 80. f(f′) dominance of the Pomeron coupling in π^-p and K^-p elastic scattering.

(This is analogous to the vector dominance hypothesis that the photon couples to a hadron via the lightest available vector mesons—see § 2.3 and (2.20).) Hence the P-exchange amplitude involves the inverse propagator $(\alpha_P(t)-\alpha_f(t))^{-1}$ representing the amount by which the f is off its 'mass shell'. For example, in πp both the valence quarks of the π are capable of forming an f, so there are two diagrams like figure 80(a). But in Kp scattering only one of the K quarks can form an f, the other giving rise to the heavier f′($s\bar{s}$) state as in figure 80(b) (see table 2) which takes the coupling further off its mass shell. It is thus predicted that at high energies

$$\frac{\sigma_T(Kp)}{\sigma_T(\pi p)} = \frac{(\alpha_P(0)-\alpha_f(0))^{-1}+(\alpha_P(0)-\alpha_{f'}(0))^{-1}}{2/(\alpha_P(0)-\alpha_f(0))} \simeq 0.8 \tag{9.2}$$

in good agreement with figure 10.

9.2. Regge cuts

It is possible for more than one Reggeon to be exchanged, as in figure 81(a). It will be noted that the two Reggeons are coupled to different constituents of the hadron. This is because at high energies the hadrons pass each other very rapidly and the chance of the same pair of constituents interacting twice (as in figure 81(b)) falls rapidly with s. This is verified in field theory models in which the Reggeons are represented by sums of ladders, as discussed in § 7. It can be shown that the exchange of two or more Reggeons will give rise to a branch cut in the t-channel angular momentum plane, at $l = \alpha_c(t)$, called a Regge cut (see Collins (1977 chap 8) for a detailed discussion).

Schematically, a two-Reggeon cut amplitude, like $R_1 \otimes R_2$ of figure 81(a), is given by

$$A^c(s,t) \sim \frac{i}{|s|}\int d\Phi_{12} A^{R_1}(s,t_1) A^{R_2}(s,t_2) \tag{9.3}$$

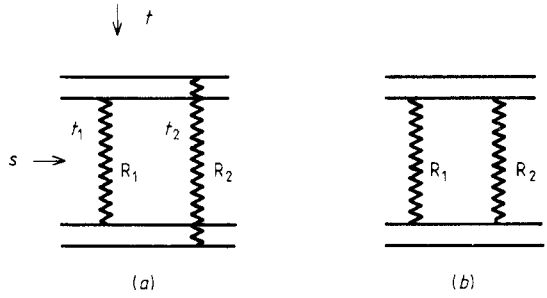

Figure 81. (*a*) Two-Reggeon exchange, denoted $R_1 \otimes R_2$, with momentum transfers given by t_1, t_2, respectively, gives rise to a cut in the complex l plane. Planar diagram (*b*) gives a negligible contribution at high s.

where the integral is over the two-Reggeon phase space (see equation (8.4.1) of Collins (1977) for a more exact expression). The position of the branch point trajectory is given by

$$\alpha_c(t) = \max\{\alpha_1(t_1) + \alpha_2(t_2) - 1\} \tag{9.4}$$

the maximum being taken over the available phase space, and the asymptotic form of the cut amplitude is

$$A^c(s, t) \underset{s\to\infty}{\sim} \frac{s^{\alpha_c(t)}}{\log s} \tag{9.5}$$

the $\log s$ arising from the integration.

Cuts involving P exchange have particularly interesting properties. For a linear P trajectory, $\alpha_P(t) = 1 + \alpha'_P t$, (9.4) gives a $P \otimes P$ cut at

$$\alpha_c(t) = 1 + \frac{\alpha'_P}{2} t \tag{9.6}$$

so that the pole and cut coincide at $t = 0$, and the cut lies above the pole for $t < 0$. Since the P amplitude is almost pure imaginary for $t \simeq 0$, $A^P \sim is$, (9.3) gives a cut amplitude of the form $(i/s)is\, is/\log s = -is/\log s$, i.e. modulo $\log s$, it has the same energy dependence as the pole but the opposite phase. It may be anticipated that the P pole will dominate at small $|t|$, but that the cut with its flatter t dependence will take over at larger $|t|$, and that there will be an intermediate region where the amplitude is very small because of the destructive interference between the pole and the cut, with their opposed phases. The pp (and $\bar{p}p$) differential cross sections exhibit a sharp dip at $|t| = 1.4\ \text{GeV}^2$ (figure 82) which is readily interpreted in this way (Collins and Gault 1978). If $\alpha_P(0)$ is above 1 the cuts will also be above 1 and the asymptotic behaviour is controlled by a superposition of multi-P cuts which obeys the bound (9.1) (see, for example, White 1980). A similar destructive interference between the ρ pole and a $\rho \otimes P$ cut can be used as an alternative explanation for the dip at $|t| = 0.5\ \text{GeV}^2$ in figure 63 to the nonsense decoupling mechanism discussed in § 7.1. A comprehensive analysis of flavour-exchange processes with Regge cuts along these lines has been presented by Kane and Seidl (1976).

Equation (9.3) may be generalised to include the exchange of any number of Reggeons (see, for example, Collins 1977 chap 8) and it is found that the more Reggeons are exchanged the flatter is the branch point trajectory as a function of t.

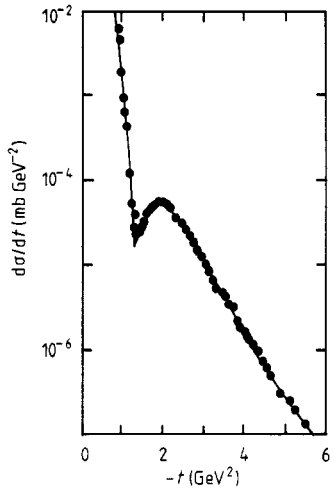

Figure 82. The differential cross section for pp elastic scattering at $\sqrt{s} = 53$ GeV measured at the ISR. The fit is from Collins and Gault (1978).

So from the Regge theory standpoint scattering processes seem to become more and more complicated as $-t$ increases; with the dominance of multi-Reggeon exchange. This is to be contrasted with the parton viewpoint, that only simple parton diagrams (like, for example, figure 71(a)) determine the scattering process at large t.

The resolution of this conflict is straightforward if the Regge trajectories depart from linearity at large $|t|$ and asymptote to negative integers (probably -1 for the dominant exchange?) as discussed in § 7.3. In this case (9.4) gives

$$\alpha_c(-\infty) = \alpha_1(-\infty) + \alpha_2(-\infty) - 1$$

and so the cut ends up below the poles. We are thus left with the possibility that Regge poles dominate at small $|t|$, and, through the bending of the trajectories, as $t \to -\infty$, with an intermediate $|t|$ region (typically 0.5–2 GeV^2) where cuts are also important (see Collins and Wilkie 1981). This seems much more attractive than the supposition that the large-angle hard scattering mechanisms are quite distinct from the small-angle Regge exchange dynamics, with no simple way of interpolating between them.

9.3. Trajectory dynamics and particle production

In figures 71 and 79 we have drawn ladder diagrams to suggest how Reggeons may be built up in QCD from multi-parton intermediate states in the s channel. In fact, of course, since the partons are confined such diagrams do not represent possible physical states, and hence cannot properly display the unitarity structure of the theory. Instead we should include only multiparticle intermediate states as in figure 83(a) for which the QCD interpretation is something like figure 83(b). Only that subset of parton states in which the coloured partons are gathered into colourless hadronic clusters are to be allowed as intermediate states in these diagrams (Nussinov 1976). The optical theorem equates the sum of multiparticle cross sections for processes like figure 84 (the total cross section) to the imaginary part of the elastic amplitude of figure 83(b) (cf figure 65).

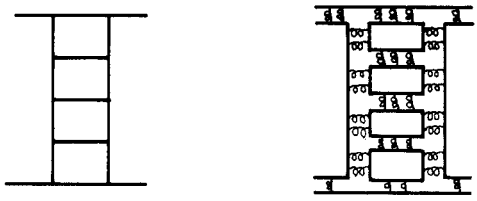

(*a*) (*b*)

Figure 83. Ladder diagrams which sum to give Regge behaviour. In (*a*) we show the physical particle intermediate states, and in (*b*) we symbolically sketch their parton composition.

The central region of figure 84 (x near 0) in which a quark from one particle and an antiquark from the other attract each other, slow down by the bremsstrahlung of gluons and hence ultimately hadrons, and finally annihilate each other, looks just like the inverse of figure 41(*c*) in which the $q\bar{q}$ pair separate and lose energy radiating hadrons. We might thus expect that the average particle multiplicity in hadron scattering $\langle n\rangle_h$ would be very similar to that in e^+e^- annihilation $\langle n\rangle_{e^+e^-}$ at the same energy, if allowance is made for the fact that some of the energy is carried by the spectator quarks (the top and bottom lines of figure 84) which populate the fragmentation regions, $|x|$ near 1, and which we discussed in § 6.1. In particular, for collisions involving protons the spectator system is a diquark which may produce a jet with a quite different multiplicity structure to those of the quarks or gluons (see, for example, Gunion 1980). An attempt has been made to allow for these effects (Basile *et al* 1980, 1981) by taking the energy available for hadron production to be

$$E_{\text{hadron}} = E_{\text{beam}} - E_{\text{fastest proton}}$$

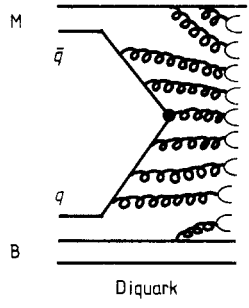

Figure 84. A multiparticle production process.

and comparing the pp multiplicity at this lower energy with that in e^+e^-. This shift of the pp curve in figure 11(*a*) results in quite good agreement with the e^+e^- multiplicity.

However, the dominant mechanism in high-energy hadron scattering is presumably not quark exchange (which gives the normal Regge trajectories with $\alpha_R(0) \leqslant \frac{1}{2}$) but gluon exchange, which we have identified with the Pomeron. If the f dominates the P coupling as in figure 80, this need not necessarily make much difference (see figure 85(*a*)). A simple physical interpretation of the diagram is that it is the slow sea quarks from the hadrons which interact via the exchange of two (or more) gluons. But the Low–Nussinov mechanism of gluon exchange followed by hadronisation in the colour field produced by the separating colour octets suggests bremsstrahlung through a

gluon jet, as in figure 85(*b*). Naively this would lead one to expect that $\langle n\rangle_h = \frac{9}{4}\langle n\rangle_{e^+e^-}$ due to the fact that the gluon–gluon vertex coupling is stronger than the quark–gluon vertex (Brodsky and Gunion 1976).

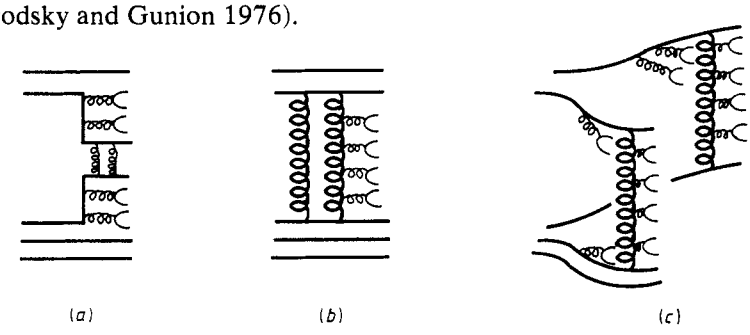

Figure 85. Multiparticle production by Pomeron exchange assuming (*a*) f dominance; (*b*) hadronisation direct from gluon exchange; (*c*) a valence quark from each hadron is 'held back' so that two independent chains of hadrons are formed.

Alternatively, if the 'held-back' effect discussed in § 6.1, in which one valence quark from each hadron interacts with (is held back by) the remaining quarks of the other hadron, is correct, then two independent chains of hadrons are produced, as in figure 85(*c*). These may be quark chains, gluon chains or some mixture of the two, as shown. Via the optical theorem (cf figure 65) these two chains produce the cylinder of figure 54, and give the Pomeron its distinctive topological structure expected in dual models. This leads one to expect that $\langle n\rangle_h \geqslant 2\langle n\rangle_{e^+e^-}$ (Capella 1981), contrary to the data of figure 11(*a*). However, consistency with these data is still possible if allowance is made for the diquark fragmentation and the fact the two chains have to share the incident energy. Only at very high energies when central region production dominates should $\langle n\rangle_{pp} \to 2\langle n\rangle_{e^+e^-}$. But as spin-1 gluon exchange is not the dominant mechanism here it is not obvious that the total cross section must be constant with s. A detailed discussion of these approaches has been given by Gunion (1980) (see also Capella 1981).

Clearly much remains to be understood about the precise mechanisms of particle production which build up the total cross section. As mentioned in § 5 we still do not have definite experimental evidence that gluons are more effective than quarks at radiating hadrons and so produce jets of higher multiplicity, as the naive colour coupling arguments suggest. Even more important, there is no obvious reason why these soft scattering processes should have any simple parton description. Since α_s is of the order of 1, parton interactions of arbitrary complexity all seem equally probable. However, the approximate scale invariance of hadron cross sections, and the similarity of the hadron multiplicities, etc, in forward scattering, and in hard processes like large p_T jets, deep inelastic scattering and e^+e^- annihilation, permits some optimism that a better understanding of the Pomeron in terms of QCD may emerge.

10. Conclusions

It should be evident from the preceding sections that our understanding of the theory of hadron reaction mechanisms is tantalisingly incomplete. We now have seemingly incontrovertible evidence that hadrons are made of more fundamental, point-like,

constituents. But these constituent partons (i.e. quarks and gluons) seem to be confined within the hadrons. Not only does this hypothesis enable us to understand most features of the spectrum of hadrons, but the constituents are actually 'seen', almost directly, in deep inelastic scattering experiments, and often the outcome of a scattering process is the production of jets of hadrons which appear to reflect the motions of the underlying partons.

Most particle physicists are optimistic that the SU(3) symmetric colour gauge theory, quantum chromodynamics (QCD), correctly describes the interactions of these partons. This is not only because some features of the scattering data, such as the scaling violations at large momentum transfers, where the running coupling constant has become small, appear to be satisfactorily (if not uniquely) explained by QCD perturbation theory, nor because QCD motivated potential models can be used to calculate the spectrum of heavy-quark states in impressive detail. It is also because QCD provides a self-consistent, renormalisable field theory which apparently leads both to asymptotic freedom (scaling) and to infrared slavery (the confinement of the partons). But unfortunately, being able to write down the QCD Lagrangian does not yet enable one to deduce very much about the properties of hadrons and their interactions. Some pessimists may wonder if we shall ever reach that point. After all, even though we now possess a good basic understanding of atomic theory it is still very hard to achieve accurate calculations of atomic structures, and to predict atom–atom scattering cross sections, with their complicated exchange mechanisms, is out of the question for all but the very simplest atoms.

Fortunately it is also true that a rather good understanding of hadron interactions has already been achieved through the exchange of particles which lie on Regge trajectories. Regge theory has successfully accounted for the bulk of high-energy hadron scattering data at small momentum transfers, for both exclusive and inclusive processes. In particular, simple Regge pole exchange models, with exchange-degenerate, linear trajectories, and couplings which obey an SU(3) flavour symmetry, give a very good overall description of these data with very few parameters. Of course, exchange degeneracy and SU(3) are not exact, we are not quite sure what the Pomeron trajectory really represents, and at larger momentum transfers Regge cuts become important. So to obtain a really detailed quantitative account of the data requires rather more parameters, but still remarkably few given the vast quantity of data to be explained (Kane and Seidl 1976, Irving and Worden 1977). It thus seems clear that the strong interaction colour force between hadrons manifests itself principally through the exchange of colourless hadrons which lie on Regge trajectories. Regge theory had therefore already provided us, even before we were aware of it, with a phenomenological description of the underlying QCD processes.

Clearly much remains to be understood. We urgently require to show that QCD does indeed confine the partons (at least partially), and to get some idea of what these confining solutions are like, and the nature of their interactions. Going beyond this, the fact that the QCD $SU(3)_{colour}$ and the electroweak $SU(2) \times U(1)$ are both non-Abelian gauge theories and the similar properties of quarks and leptons, suggests that a more fundamental unification may be possible. This could perhaps be achieved through a unified gauge theory (Ross 1981) or through the revelation of a common composite structure for quarks and leptons (Harari 1980). Only the expenditure of much time, energy and money will tell. But it is important that in pursuit of these fascinating questions the interactions between the hadrons themselves should not be overlooked.

In this review we have tried to provide a fairly simple survey of hadronic processes from a modern, parton viewpoint, stressing the relationship between the parton model and Regge theory. The key to the understanding of hadron reaction mechanisms lies, it would seem, in the marriage of these two approaches.

References

Abers E and Lee B W 1973 *Phys. Rep.* **9C** 1
Aitkenhead W *et al* 1980 *Phys. Rev. Lett.* **45** 157
Albrow M G *et al* 1978 *Nucl. Phys.* B **145** 305
Altarelli G and Parisi G 1977 *Nucl. Phys.* B **126** 298
Amaldi U 1979 *CERN Yellow Rep.* 79–06
Amati D and Veneziano G 1979 *Phys. Lett.* **83B** 87
Andersson B, Gustafson G and Peterson C P 1977 *Phys. Lett.* **69B** 221, **71B** 337
Andersson B, Gustafson G and Sjöstrand T 1980 *Z. Phys.* C **6** 235
Anisovich V V and Shekhter V M 1973 *Nucl. Phys.* B **55** 455
Barger V 1974 *Proc. 17th Conf. on High Energy Physics, London* ed J R Smith (Didcot: Rutherford Laboratory) I-193
Barger V and Phillips R J N 1974 *Nucl. Phys.* B **73** 269
Barnes A V *et al* 1976 *Phys. Rev. Lett.* **37** 76
—— 1978 *Nucl. Phys.* B **145** 67
Bartels J 1980 *Nucl. Phys.* B **175** 365
Basile M *et al* 1980 *Phys. Lett.* **92B** 367
—— 1981 *Phys. Lett.* **99B** 247
Benecke J, Chou T T, Yang C N and Yen E 1969 *Phys. Rev.* **188** 2159
Berge J P *et al* 1980 *Phys. Lett.* **91B** 311
Berger Ch *et al* 1980 *Pluto Collaboration* DESY 80/69
Bjorken J D 1973 *Proc. 1973 SLAC Summer Inst.* SLAC-167
Bjorken J D and Brodsky S J 1970 *Phys. Rev.* D **1** 1416
Bjorken J D and Drell S D 1964 *Relativistic Quantum Mechanics* (McGraw-Hill)
Blankenbecler R and Brodsky S J 1974 *Phys. Rev.* D **10** 2973
Blankenbecler R, Brodsky S J and Gunion J 1975 *Phys. Rev.* D **12** 3469
Blankenbecler R, Brodsky S J, Gunion J F and Savit R 1973 *Phys. Rev.* D **8** 4117
—— 1974 *Phys. Rev.* D **10** 2153
Bobbink G J *et al* 1980 *Phys. Rev. Lett.* **44** 118
Bohm A 1980 *Proc. 20th Int. Conf. on High Energy Physics, Madison* ed L Durand and L G Pondrom *AIP Conf. Proc.* **68** 551
Brodsky S J 1979a *Phys. Scr.* **19** 154
—— 1979b *Proc. 1979 SLAC Summer Inst. on Quantum Chromodynamics* ed A Mosher, p 133
Brodsky S J and Drell S D 1980 *Phys. Rev.* D **22** 2236
Brodsky S J and Farrar G 1973 *Phys. Rev. Lett.* **31** 1153
Brodsky S J and Gunion J F 1976 *Phys. Rev. Lett.* **37** 402
Brodsky S J and Lepage P 1979a *Phys. Rev. Lett.* **43** 545
—— 1979b *Phys. Lett.* **87B** 359
Brodsky S J and Weiss N 1977 *Phys. Rev.* D **16** 2325
Buras A J 1980 *Rev. Mod. Phys.* **52** 199
Buras A J and Gaemers K J F 1978 *Nucl. Phys.* B **132** 249
Capella A 1981 *Proc. Europhysics Study Conf. on Partons in Soft Hadronic Processes, Erice*
Capella A, Sukhatme U, Tan C I and Tran Thanh Van J 1979 *Phys. Lett.* **81B** 68, **93B** 146
Capella A, Sukhatme U and Tran Thanh Van J 1980 *Z. Phys.* C **3** 329
Carlitz R, Green M B and Zee A 1971 *Phys. Rev.* D **4** 3439
Carroll A S *et al* 1976 *Phys. Lett.* **61B** 303
CHARM 1981 *Phys. Lett.* **99B** 265
Close F 1979 *An Introduction to Quarks and Partons* (New York: Academic)
—— 1982 *Phys. Scr.* **25** 86
Cohen-Tannoudji G *et al* 1980 *Phys. Rev.* D **21** 2699

—— 1981 to be published
Collins P D B 1977 *Regge Theory and High Energy Physics* (Cambridge: Cambridge University Press)
Collins P D B and Gault F D 1978 *Phys. Lett.* **73B** 330
Collins P D B, Gault F D and Martin A 1974 *Nucl. Phys.* B **83** 241
Collins P D B, Johnson R C and Squires E J 1968 *Phys. Lett.* **26B** 223
Collins P D B and Wilkie T D B 1981 *Z. Phys.* C **7** 357
Collins P D B and Wright A D M 1979 *J. Phys. G: Nucl. Phys.* **5** 1461
Combridge B L, Kripfganz J and Ranft J 1977 *Phys. Lett.* **70B** 234
Cool R L *et al* 1981 *Phys. Rev. Lett.* **47** 701
Coon D D, Gunion J F, Tran Thanh Van J and Blankenbecler R 1978 *Phys. Rev.* D **18** 1451
Cords D 1980 *Proc. 20th Int. Conf. on High Energy Physics, Madison* ed L Durand and L G Pondrom *AIP Conf. Proc.* **68** 590
Cutler R and Sivers D 1978 *Phys. Rev.* D **17** 196
Darriulat P 1980 *Ann. Rev. Nucl. Particle Sci.* **30** 159
Das K P and Hwa R C 1977 *Phys. Lett.* **68B** 459
De Rujula A, Ellis J, Floratos E G and Gaillard M K 1978 *Nucl. Phys.* B **138** 387
De Tar C E 1971 *Phys. Rev.* D **3** 128
Denegri D *et al* 1981 *Phys. Lett.* **98B** 127
Di Lella L 1979 *Proc. 10th Symp. on Multiparticle Dynamics*
Dokshitzer Y L, D'Yakonov D I and Troyan S I 1980 *Phys. Rep.* **58** 271
Donoghue J F 1980 *Proc. 20th Int. Conf. on High Energy Physics, Madison* ed L Durand and L G Pondrom *AIP Conf. Proc.* **68** 35
Drell S D and Yan T M 1971 *Ann. Phys., NY* **66** 578
Duke D W and Taylor F E 1978 *Phys. Rev.* D **17** 1788
Eden R J, Landshoff P V, Olive D I and Polkinghorne J C 1966 *The Analytic S Matrix* (Cambridge: Cambridge University Press)
Eichten E *et al* 1980 *Phys. Rev.* D **21** 203
Ellis J, Gaillard M K and Ross G G 1976 *Nucl. Phys.* B **111** 253
Ellis J and Sachrajda C T 1979 *Quarks and Leptons, Cargese 1979. NATO Advanced Study Institutes* B **61** 285
Farhi E 1977 *Phys. Rev. Lett.* **39** 1587
Feynman R P 1969 *Phys. Rev. Lett.* **23** 1415
—— 1972 *Photon–Hadron Interactions* (New York: Benjamin)
Feynman R P and Field R D 1977 *Phys. Rev.* D **15** 2590
Feynman R P, Field R D and Fox G C 1978 *Phys. Rev.* D **18** 3320
Field R D 1979a *Phys. Scr.* **19** 131
—— 1979b *AIP Conf. Proc.* **55** 97
Field R D and Fox G C 1974 *Nucl. Phys.* B **80** 367
Fox G C 1977 *Nucl. Phys.* B **131** 107
Froissart M 1961 *Phys. Rev.* **123** 1053
Ganguli S N and Roy D P 1980 *Phys. Rep.* **67** 201
Gell-Mann M 1961 *Cal. Tech. Rep.*
—— 1964 *Phys. Lett.* **8** 214
Giacomelli G and Jacob M 1980 *Phys. Rep.* **55** 1
Gilman F J 1972 *Phys. Rep.* **4C** 95
Goldberg H 1972 *Nucl. Phys.* B **44** 149
Gourdin M 1974 *Phys. Rep.* **11C** 29
Greenberg O W and Nelson C A 1977 *Phys. Rep.* **32C** 1
Grisaru M T, Schnitzer H J and Tsao H S 1973 *Phys. Rev.* D **8** 4498
Gross D J and Wilczek F 1973 *Phys. Rev.* D **8** 3633
Gunion J F 1979 *Phys. Lett.* **88B** 150
—— 1980 *Proc. 11th Int. Symp. on Multi-Particle Dynamics, Bruges, Belgium*
Harari H 1978 *Phys. Rep.* **42C** 235
—— 1980 *Proc. 1980 Summer Inst.* ed A Mosher (Stanford: SLAC) p 141
Hey A J G and Morgan D 1978 *Rep. Prog. Phys.* **41** 675
Hwa R C 1980 *Phys. Rev.* D **22** 759, 1593
Hwa R C and Roberts R G 1979 *Z. Phys.* C **1** 81
Hwa R C and Zahir M S 1981 *Phys. Rev.* to be published
Iliopolous J 1976 *CERN Yellow Rep.* 76-11

Irving A C and Worden R 1977 *Phys. Rep.* **34C** 117
Isgur N and Karl G 1979 *Phys. Rev.* D **20** 1191
Itzykson C and Zuber J-B 1980 *Quantum Field Theory* (New York: McGraw-Hill)
Jacob M (ed) 1974 *Dual Theory* (Amsterdam: North-Holland)
Jacob M and Landshoff P V 1978 *Phys. Rep.* **48** 285
Jaffe R and Johnson K 1975 *Phys. Lett.* **60B** 201
Jauch J M and Rohrlich F 1955 *Theory of Photons and Electrons* (New York: Academic)
Jones D and Gunion J F 1979 *Phys. Rev.* D **19** 867
Kane G L and Seidl A 1976 *Rev. Mod. Phys.* **48** 309
Kittel W 1981 *Proc. Europhysics Study Conf. on Partons in Soft Hadronic Processes, Erice*
Kogut J and Susskind L 1974 *Phys. Rev.* D **9** 697, 3391
Kokkedee J J J 1969 *The Quark Model* (New York: Benjamin)
Konishi K, Ukawa A and Veneziano G 1979 *Nucl. Phys.* B **157** 45
Llewellyn-Smith C H 1972 *Phys. Rep.* **3C** 264
Low F E 1975 *Phys. Rev.* D **12** 163
McCubbin N A 1981 *Rep. Prog. Phys.* **44** 1027–76
Magnus W and Oberhettinger F 1949 *Functions of Mathematical Physics* (New York: Chelsea) p 4
Mandelstam S 1980 *Proc. 1979 Int. Symp. on Lepton and Photon Interactions*
Marciano W and Pagels H 1978 *Phys. Rep.* **36C** 1
Martin A 1963 *Strong Interactions and High Energy Physics* ed R G Moorhouse (Edinburgh: Oliver and Boyd)
—— 1966 *Nuovo Cim.* **42** 930, **44** 1219
Morse P M and Feshbach H 1953 *Methods of Theoretical Physics* (New York: McGraw-Hill)
Mueller A H 1970 *Phys. Rev.* D **2** 2963
Ne'eman Y 1961 *Nucl. Phys.* **26** 222
Nussinov S 1976 *Phys. Rev. Lett.* **34** 1286
Ochs W 1977 *Nucl. Phys.* B **118** 397
Owens J F, Reya E and Gluck M 1978 *Phys. Rev.* D **18** 1501
Particle Data Group 1980 *Rev. Mod. Phys.* **52** no. 2, part II
Perl M L 1974 *High Energy Hadron Physics* (New York: Wiley)
Perl M L *et al* 1975 *Phys. Rev. Lett.* **35** 1489
Pokorski S and Van Hove L 1975 *Nucl. Phys.* B **86** 243
Politzer H D 1973 *Phys. Rev. Lett.* **30** 1346
—— 1974 *Phys. Rep.* **14C** 130
Polkinghorne J C 1980 *Models of High Energy Processes* (Cambridge: Cambridge University Press)
Pomeranchuk I Y 1958 *Sov. Phys.-JETP* **7** 499
Quigg C and Rosner J L 1979 *Phys. Rep.* **56C** 167
Regge T 1959 *Nuovo Cim.* **14** 951
—— 1960 *Nuovo Cim.* **18** 947
Reya E 1981 *Phys. Rep.* **69** 195
Roberts R G and Roy D P 1974 *Nucl. Phys.* B **77** 240
Rosner J L 1969 *Phys. Rev. Lett.* **22** 689
Ross G G 1981 *Rep. Prog. Phys.* **44** 655
Rushbrooke J G and Webber B R 1978 *Phys. Rep.* **44** 1
Sivers D, Brodsky S J and Blankenbecler R 1976 *Phys. Rep.* **23C** 1
Sommerfeld A 1949 *Partial Differential Equations in Physics* (New York: Academic)
Sterman G and Weinberg S 1977 *Phys. Rev. Lett.* **39** 1436
Stroynowski R 1981 *Phys. Rep.* **71** 1
Van Hove L 1979 *Proc. 18th Int. Universitätswochen für Kernphysik, Schladming*
Veneziano G 1968 *Nuovo Cim.* A **57** 190
Watson G N 1918 *Proc. R. Soc.* **95** 83
Webber B R 1982 *Phys. Scr.* **25** 198
Weinberg S 1977 *NY Acad. Sci. Festschrift for I I Rabi* ed L Motz
White A 1980 *CERN Preprint* TH 2976
Wiik B H 1980 *Proc. 20th Int. Conf. on High Energy Physics, Madison* ed L Durand and L G Pondrom *AIP Conf. Proc.* **68** 1379
Wiik B H and Wolf G 1979 *Electron–Positron Interactions. Springer Tracts in Modern Physics* vol 86 (Berlin: Springer-Verlag)
Wolf G 1980 *Proc. 11th Int. Symp. on Multiparticle Dynamics, Bruges*
Zweig G 1964 *CERN Rep.* unpublished